ДОКЛАДЫ
АКАДЕМИИ НАУК СССР

PROCEEDINGS OF THE ACADEMY OF SCIENCES

OF THE USSR

Physical Chemistry Section

(DOKLADY AKADEMII NAUK SSSR)

IN ENGLISH TRANSLATION

VOL. 113 NOS. 1-6

CONSULTANTS BUREAU, INC.
227 WEST 17TH STREET, NEW YORK 11, N. Y.

an agency for the interpretation of international knowledge

PROCEEDINGS OF THE ACADEMY OF SCIENCES OF THE USSR

(DOKLADY AKADEMII NAUK SSSR)

Section: PHYSICAL CHEMISTRY

Volume 113, Issues 1-6

March-April, 1957

(A Publication of the Academy of Sciences of the USSR)

IN ENGLISH TRANSLATION

CONSULTANTS BUREAU, INC.

227 West 17th Street

New York 11, N. Y.

Printed in the United States

Annual Subscription	$160.00
Single Issue	35.00

SIGNIFICANCE OF ABBREVIATIONS MOST FREQUENTLY ENCOUNTERED IN SOVIET PERIODICALS

FIAN	Phys. Inst. Acad. Sci. USSR.
GDI	Water Power Inst.
GITI	State Sci.-Tech. Press
GITTL	State Tech. and Theor. Lit. Press
GONTI	State United Sci.-Tech. Press
Gosenergoizdat	State Power Press
Goskhimizdat	State Chem. Press
GOST	All-Union State Standard
GTTI	State Tech. and Theor. Lit. Press
IL	Foreign Lit. Press
ISN (Izd. Sov. Nauk)	Soviet Science Press
Izd. AN SSSR	Acad. Sci. USSR Press
Izd. MGU	Moscow State Univ. Press
LEIIZhT	Leningrad Power Inst. of Railroad Engineering
LET	Leningrad Elec. Engr. School
LETI	Leningrad Electrotechnical Inst.
LETIIZhT	Leningrad Electrical Engineering Research Inst. of Railroad Engr.
Mashgiz	State Sci.-Tech. Press for Machine Construction Lit.
MEP	Ministry of Electrical Industry
MES	Ministry of Electrical Power Plants
MESEP	Ministry of Electrical Power Plants and the Electrical Industry
MGU	Moscow State Univ.
MKhTI	Moscow Inst. Chem. Tech.
MOPI	Moscow Regional Pedagogical Inst.
MSP	Ministry of Industrial Construction
NII ZVUKSZAPIOI	Scientific Research Inst. of Sound Recording
NIKFI	Sci. Inst. of Modern Motion Picture Photography
ONTI	United Sci.-Tech. Press
OTI	Division of Technical Information
OTN	Div. Tech. Sci.
Stroiizdat	Construction Press
TOE	Association of Power Engineers
TsKTI	Central Research Inst. for Boilers and Turbines
TsNIEL	Central Scientific Research Elec. Engr. Lab.
TsNIEL-MES	Central Scientific Research Elec. Engr. Lab.–Ministry of Electric Power Plants
TsVTI	Central Office of Economic Information
UF	Ural Branch
VIESKh	All-Union Inst. of Rural Elec. Power Stations
VNIIM	All-Union Scientific Research Inst. of Meteorology
VNIIZhDT	All-Union Scientific Research Inst. of Railroad Engineering
VTI	All-Union Thermotech. Inst.
VZEI	All-Union Power Correspondence Inst.

Note: Abbreviations not on this list and not explained in the translation have been transliterated, no further information about their significance being available to us. – Publisher.

STUDY OF THE POLYMERIZATIONS OF 2,3-DIMETHYL-2-BUTENE, 2,3-DIMETHYL-1-BUTENE AND 3,3-DIMETHYL-1-BUTENE AT PRESSURES UP TO 4000 ATM

M. G. Gonikberg, V. M. Zhulin, V. T. Aleksanyan and Kh. E. Sterin

(Presented by Academician B. A. Kazansky, October 1, 1956)

In our previous paper [1] it was shown that high pressures increase the rate of polymerization of 2,3-dimethyl-2-butene very considerably. For example, at 300° and 200 atm some 20% of this olefin polymerizes in 50 hours, while at 23000 atm the whole of the monomer polymerized in 3 hours.

The present paper deals with the study of the kinetics in the polymerization of 2,3-dimethyl-2-butene at high pressure, as well as with the properties and composition of the polymers obtained. The polymers of 2,3-dimethyl-1-butene and 3,3-dimethyl-1-butene were also studied, these being obtained under analogous conditions.

The olefins used were redistilled in a rectifying column of 30 theoretical plate effectiveness immediately before the experiment, and had the following constants: 2,3-dimethyl 2-butene; B.p. 72.8–73.1° (760), d_4^{20} 0.7084, n_D^{20} 1.4122; 2,3-dimethyl-1-butene: B.p. 55.2–55.3°(760), d_4^{20} 0.6775, n_D^{20} 1.3900; 3,3-dimethyl-1-butene; B.p. 41.0-41.2° (760), d_4^{20} 0.6530, n_D^{20} 1.3760. These values are close to those given in the literature [2].

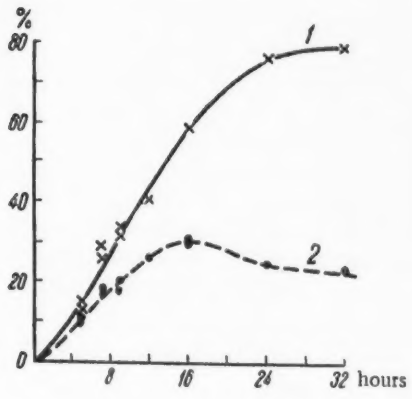

Fig. 1. Polymerization of 2,3-dimethyl-2-butene at 290° C and 3660-3870 atm.; 1) total polymer yield 2) dimer fraction yield.

The experiments were carried out in lead ampules of capacity 14-15 ml, placed in a steel reaction vessel type 40 Kh. The pressure was applied via oil and was measured with a spring gage reading up to 10000 kg/cm^2. The temperature in all experiments was 290 ± 2°C, this being measured with a thermocouple inserted in the center of the reaction vessel via a long steel jacket. The duration of the experiment was taken to be the time from attaining the set temperature to switching off the electric heater around the reaction vessel. After the ampule had been opened the monomer fraction was distilled off from the reaction product via the rectifying column, the dimer and higher fractions being distilled off in vacuo from a Claisen flask. The polymer fractions were transparent liquids.

Figure 1 gives the results from the experiments on the polymerization of 2,3-dimethyl-1-butene at 3660-3870 atm, τ being from 2 to 32 hours. It is clear from a consideration of Figure 1 that the yield of the dimer fraction passes through a maximum when τ is about 16 hours, which implies that the polymerization occurs, at least in part, in a stepwise fashion, via the intermediate formation of the dimer. Special experiments showed that the dimer fraction can in fact polymerize further. Under the conditions studied the mean degree of polymerization $\underline{n}$ is small (polymerization of 2,3-dimethyl-2-butene at 290°, τ = 6 hours):

P, atm.	Polymer Yield, as % of Product	n
1900	9.1	2.3
2700	11.7	2.3
3820	17.7	2.5

It was found that 2,3-dimethyl-1-butene was present in the main monomer fraction distilled off from the products of polymerization with 2,3-dimethyl-2-butene (this being found from the Raman spectrum); no structural isomers of 2,3-dimethyl-2-butene were found. See below for the composition of the dimer fractions.

TABLE 1

Polymerization of 2,3-Dimethyl-2-butene, 2,3-Dimethyl-1-butene and 3,3-Dimethyl-1-butene at 290°C

Olefin used	τ in hrs.	P, in atm.	Amount of starting material reacted, as % of the product	Fraction of product having n > 3, as % of total polymer
2,3-dimethyl-2-butene	5	3700—3780	11.6	—
Ditto	32	3740—3860	79.4	26.8
2,3-dimethyl-1-butene	4	3410—3590	75.0	45.5
3,3-dimethyl-1-butene	3	3500—3640	61.0	34.1

Under the same conditions of temperature and pressure 2,3-dimethyl-1-butene and 3,3-dimethyl-1-butene polymerize considerably more rapidly than 2,3-dimethyl-2-butene and form polymers of higher molecular weight (Table 1). The properties of some fractions of the polymerizates from the three hexenes used which fall close together in molecular weight are given in Table 2. The data of Table 2 show that the three polymerizates which are closely similar as regards molecular weight derived from the three hexenes studied differ materially in properties from one another and from the product of ionic polymerization.

Since 2,3-dimethyl-1-butene was found to be present in the monomer fraction of the polymerization product from 2,3-dimethyl-2-butene, we carried out some experiments in which mixtures of these two olefins were polymerized. It was found that the addition of small amounts of 2,3-dimethyl-1-butene (about 4%) did not materially influence the rate of polymerization of 2,3-dimethyl-2-butene. When both isomers were polymerized in a 1:1 ratio under pressure 2,3-dimethyl-2-butene reacted much faster, and 2,3-dimethyl-1-butene somewhat more slowly, than when the isomers were polymerized separately under the same conditions. This implies that copolymerization occurs. The refractive index and specific gravity of the dimer fraction from the polymerization of a mixture of 2,3-dimethyl-1-butene and 2,3-dimethyl-2-butene also show that this fraction is not a simple mixture of the corresponding fractions from polymerizates of the pure olefins (See Table 2). The difference between the properties of the dimer fraction from the polymerizate of 2,3-dimethyl-2-butene from those of the dimer fractions from polymerizates of 2,3-dimethyl-1-butene and the copolymerizate of the two olefins confirms the conclusion earlier drawn [1] that polymerization of 2,3-dimethyl-2-butene does not involve the intermediate step of its isomerization to 2,3-dimethyl-1-butene.

We also studied the compositions of the dimer fractions from the three hexenes by Raman scattering. The methods used in taking the spectra and making the measurements have already been described [4]. In view of the fact that data on the spectra of the majority of the olefins $C_{12}H_{24}$, cannot be found in the literature, we used the empirical rules discovered by Goubeau [5] when studying the dimer fractions, using the lines in the 1640-1680 cm^{-1} region first of all. According to Goubeau there is, for each of the olefins, one line in this spectral region of which the position depends on the nature of the substituent in the ethylene group. Our spectrometer enabled us to observe three lines in this region in mixtures of olefins: these were at 1640-1645, 1650-1660 and 1665-1680 cm^{-1}. The first belongs to mono-substituted ethylene, the second to cis-and unsymmetrical disubsti-

• The difference between the weights of the starting material and the product did not exceed 0.2 g (2%) in all the experiments.

tuted ethylenes and the third to the trans-disubstituted, tri-substituted and tetra-substituted ethylenes. It was not always possible to deduce the olefin structures more exactly by using other lines.

The results on the compositions of the dimer fractions, which in every case were mixtures of not less than two olefins, are given in Table 3.

TABLE 2

Properties of the Polymer Fractions Obtained from 2,3-Dimethyl-2-Butene, 2,3-Dimethyl-1-Butene and 3,3-Dimethyl-1-Butene

Polymer	B.p. °C (mm)	Mol. wt.	n_D^{20}	d_4^{20}	Bromine No.	Unsaturates
Dimer fraction from 2,3-dimethyl 2-butene;	68—70 (9)	162	1.4496	0.7963	102	103
Dimer fraction from 2,3-dimethyl 1-butene	51—125 (6)	164	1.4441	0.7906	70.5	72.3
Ditto	68.8—70.5 (10)	164	1.4417	—	69.5	71.3
1st dimer fraction from 3,3-dimethyl-1-butene	69—73 (20)	153	1.4229	0.7443	79.6	76.0
2nd dimer fraction from 3,3-dimethyl-1-butene	75—140 (20)	177	1.4316	0.7620	—	—
Polymer fraction from 2,3-dimethyl-2-butene	120—147 (5)	242	1.4652	0.8303	62.0	93.0
Polymer fraction from 2,3-dimethyl-1-butene	125—159 (6)	234	1.4590	0.8232	60.4	88.5
Polymer fraction from 3,3-dimethyl-1-butene	200—232 (20)	348	1.4578	0.8231	50.0	109
Polymer fraction from 2,3-dimethyl-2-butene	147—191 (5)	285	1.4729	0.8476	55.5	99.0
Polymer fraction from 2,3-dimethyl-1-butene	Residue above 149°C (5)	345	1.4706	0.8470	49.5	107
Dimer fraction from the polymerizate of a mixture of 2,3-dimethyl-2-butene and 2,3-dimethyl-1-butene (1 : 1)	58—125 (6)	—	1.4441	0.7997	87.3	—
Dimer fraction from ionic polymerization of 2,3-dimethyl-2-butene [3]	70—110 (100)	—	1.4280—1.4351	—	—	—
Dimer fraction from ionic polymerization of 2,3-dimethyl-1-butene [3]	70—111 (100)	—	1.4257—1.4353	—	—	—

A consideration of the data given in Table 3 leads one to conclude that the polymerization processes in the three hexenes studied involve structural isomerization. In fact, if structural isomerization did not occur, it would be impossible to expect to get cis-dialkylethylenes from the polymerization of 2,3-dimethyl-2-butene; but in actual fact the cis-dialkylethylenes predominate in amount in the dimer fraction. It is not possible to explain this without assuming that the structure isomerizes, a monoalkyl ethylene being formed from 2,3-dimethyl-1-butene when it dimerizes. It might be supposed that the parent monomer first isomerizes, and that the structural isomer so formed later polymerizes and copolymerizes with the parent olefin. But the monomer fraction from the polymerizates of 2,3-dimethyl-2-butene yields none of its structural isomers. This fact enables us to assume that neither the parent compound nor radicals from the monomer undergo structural isomerization, but that dimer molecules or $C_{12}H_{23}$ radicals must do this when this olefin polymerizes.

TABLE 3

Compositions of the Dimer Fractions from 2,3-Dimethyl-2-butene, 2,3-Dimethyl-1-butene and 3,3-Dimethyl-1-butene

Structural groups in the dimer fraction	2,3-dimethyl 2-butene	2,3-dimethyl 1-butene	3,3-dimethyl 1-butene
$H_2C=CH-R$	—	+	—
$H_2C=C(R)-R$	—	?	?
RHC = CHR (cis)	+ (predominates)	?	+
RHC = CHR (trans)	?	?	?
$RHC=C(R)-R$	+	+	?
$R-C(R)=C(R)-R$	+	+	+

The results imply that the polymerizations of the olefins, as accelerated by heat and pressure, occur more slowly in the tetrasubstituted ethylene, which is evidently due to the considerable steric hinderance.

Zelinsky Institute of Organic Chemistry and
Spectroscopy Commission of the USSR Academy
of Sciences (Physicomathematical Sciences Section)

Received September 27, 1956

LITERATURE CITED

[1] M. G. Gonikberg, V. P. Butuzov and V. M. Zhulin, Proc. Acad. Sci. USSR 97, 1023 (1954).

[2] R. D. Obolentsev, Physical Constants of the Hydrocarbons in Liquid Fuels and Oils (1953).

[3] F. C. Whitmore and P. L. Meunier, J. Am. Chem. Soc 63, 2197 (1941).

[4] V. T. Aleksanyan, Kh. E. Sterin et al, Bull. Acad. Sci. USSR, Phys. Ser. 19, No. 2, 225 (1955).

[5] J. Goubeau, Die Raman-Spektren von Olefinen, Beih. Zs. angew. Chem 1948, No. 56.

THE SURFACE TENSIONS OF TERNARY Hg–Cd–K METALLIC SOLUTIONS AT 22° C

P. P. Pugachevich and V. B. Lazarev

(Presented by Academician I. I. Chernyaev, October 31, 1956)

It is clear that many effects due to impurities which are found in the most varied properties of multi-component metallic alloys in both the liquid and solid states may be understood from studies of the surface tensions of the multicomponent alloys. But up to now, so far as we are aware, a systematic study of the surface tension (σ) has not yet been made even for ternary metallic systems, much less multicomponent ones, while ternary metallic solutions are of greater practical interest than binary ones, since the vast majority of alloys used industrially are multicomponent systems. In the few studies of the surface tension in multi-component systems that have been made it has usually been the practice to study the effect of additives [1] or of gases [2], on the hypothesis that the basic composition of the alloy remains unaltered.

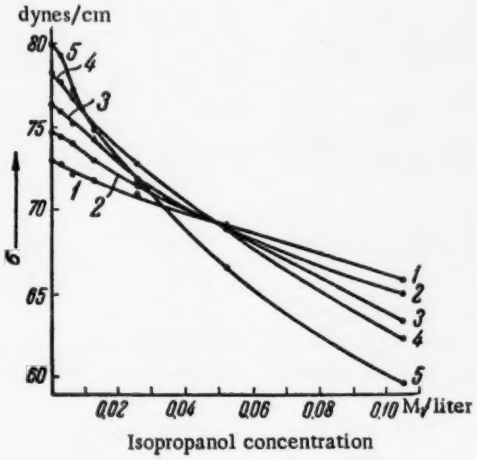

Fig. 1. Surface tension in the system water–isopropanol–sodium chloride at 18°C, after Semenchenko's data [8]. concentrations, in moles/liter, are: 1) 0.0; 2) 1.0; 3) 2.0; 4) 3.0; 5) 4.0

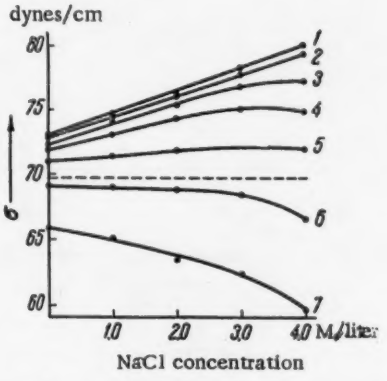

Fig. 2. Surface tension in the system water–isopropanol–sodium chloride at 18°C, after Semenchenko's data [8]. The isopropanol concentrations, in moles/liter, are: 1) 0.0000 2) 0.0033 3) 0,0066 4) 0.0131 5) 0.0263 6) 0.0525 7) 0.105

From the molecular theory of surface phenomena, developed by Semenchenko [3,2] for multicomponent solutions, we may expect that the adsorption effects in ternary metal solutions will not differ in type from like effects in other classes of ternary solutions. The main interest both from the theoretical and practical points of view lies in the case where, as regards a given solvent, one of the dissolved metals is surface-active, while the other is surface-inactive. This is due to the fact that, according to Semenchenko's theory, any multi-component system, as regards the effect of its components on the surface tension of the solution, can be

considered as a generalized ternary system.

We would, in particular, thus expect that at some concentration of the surface-active component, which Semenchenko [5] has called the buffer concentration, the surface tension of a ternary metal alloy will not depend on the content of the surface-inactive component, i.e. we may expect that in ternary metal systems we will find the same regularity in the surface tension changes as was observed by Seit [6], Palitzsch [7], Semenchenko [5,8,9,10] etc., when studying binary solutions of nonconductors in the presence of electrolytes. For example, Semenchenko found that the surface tension isotherms at 18° in the system water–isopropanol–sodium chloride intersect at a single point (Figure 1), which corresponds to an isopropanol concentration of 0.048 moles/liter. If we take the content of the surface-active material (isopropanol) as parameter, then the buffer point in such a system will correspond to an isotherm parallel to the axis of the surface-inactive material (electrolyte) which we have shown by the dashed line in Figure 2. It is clear from Figure 2 that the surface tension of the solution below the buffer concentration of isopropanol will be increased if the concentration of electrolyte in the solution is increased; at the buffer point, σ for the solution is not dependent on the electrolyte concentration; while above the buffer point the addition of the electrolyte to the solution will lead to a fall in the surface tension. This effect has been explained in Semenchenko's papers [5,8], and by others.

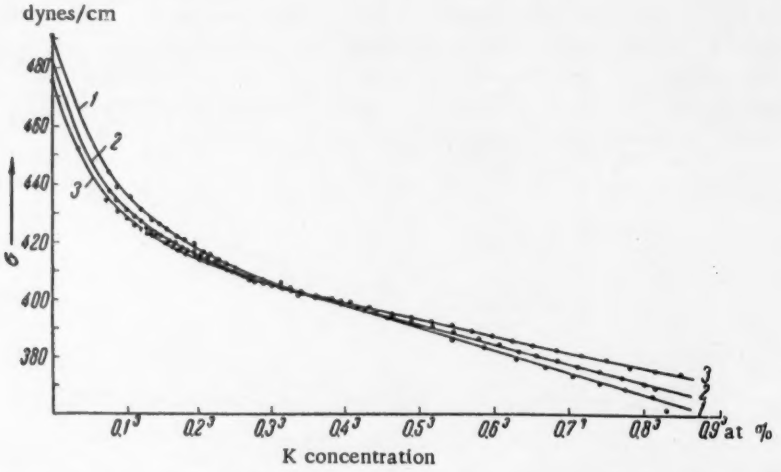

Fig. 3. Surface tension in the system mercury–cadmium–potassium at 22° C, from the data of Pugachevich and Lazarev. The cadmium concentrations, in at.%, are: 1) 1.6; 2) 5.6; 3) 7.1.

With the aim of checking the deductions from Semenchenko's theory as to the generality of the law of change in the surface tension of solutions which belong to different classes, we studied surface tension in the Hg–Cd–K system. The choice of the components for the system under study was determined by the fact that potassium, as many workers have shown, is surface-active with regard to mercury, while cadmium, according to Semenchenko's rule of generalized moments, should increase the surface tension of mercury, although it would appear [11] that this is not confirmed, and some workers [12] conclude on this basis that the generalized moments rule does not apply to Hg–Cd–K solutions.

If our choice of components is correct, then, from the above discussion, we should find a buffer concentration in the Hg–Cd–K system when we study the surface tension.

The measurements of σ Hg–Cd–K solutions were carried out in Pugachevich's combined apparatus [13] at 22°C; altogether 170 amalgams were studied, which contained from 0 to 0.620 at % K and from 0 to 7.15 % Cd. Figure 3 shows that at some potassium concentration, which was about 0.040 at. %, in our experiments, the surface tension of the ternary solution was not dependent on the concentration of the surface-inactive material (cadmium). This potassium content corresponds to the concentration buffer point. In solutions which contained potassium in amounts in excess of the buffer concentration, the effect of cadmium on σ for the solutions was the reverse of that below the buffer point, namely, increase in cadmium content to a fall in the surface tension of the solution.

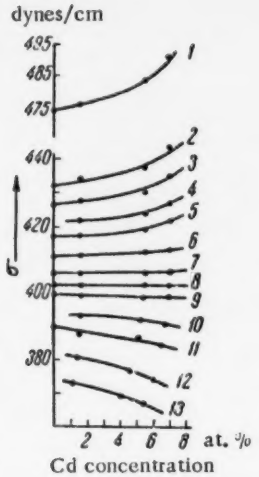

Fig. 4. Surface tension in the mercury-cadmium-potassium system at 22°C, from Pugachevich and Lazarev's data. K concentrations in at % are: 1) 0.0000; 2) 0.000502; 3) 0.00116; 4) 0.00250; 5) 0.00554; 6) 0.0126; 7) 0.0247; 8) 0.0400; 9) 0.0615; 10) 0.125; 11) 0.177; 12) 0.350; 13) 0.540

This is particularly clearly seen in Figure 4, which shows parts of the isotherms of surface tension for the amalgams we studied, when the content of the surface-active substance was taken as parameter: 8 on this figure relates to the potassium buffer concentration. It is also clear from this figure (isotherm 1) that the cadmium, as predicted by Semenchenko's rule of generalized moments, increases the surface tension of mercury, i.e., it is surface-inactive as regards mercury.

Comparison of Figures 1 and 2 with Figures 3 and 4 confirms the deductions from the molecular theory of surface effects developed by Semenchenko for the general adsorption processes in multicomponent solutions which fall in different classes.

LITERATURE CITED

[1] Yu. A. Klyachko, L. L. Kunin, N. S. Kreshchanovsky and E. S. Ginzburg. Proc. Acad. Sci. USSR 72, 927, 1950.

[2] B. V. Stark and S. I. Filippov. Bull. Acad. Sci. USSR, Div. Chem. Sci. No. 3, 413, 1949.

[3] V. K. Semenchenko. Coll. J., 11, 109, 1949.

[4] V. K. Semenchenko. Bull. sect. phys-chem. anal., 21, 14, 1952.

[5] W. K. Ssementschenko, E. A. Dawidowskaja, Koll. Zs., 73, 24 (1935).

[6] W. Seit, Zs. phys. Chem., 117, 257 (1925).

[7] S. Palitzsch, Zs. phys. Chem., 138, A, 379, 393, 411 (1928); 145, A, 97 (1929); 147, A, 51 (1930).

[8] V. K. Semenchenko. J. Appl. Chem., 7, No. 4, 75, 1930

[9] W. K. Ssementschenko,* A. F. Gratscheva, Koll. Zs., 73, 30 (1935).

[10] V. K. Semenchenko and Kh. Rustamov. J. Phys. Chem., 8, 383, 1936.

[11] V. K. Semenchenko, B. P. Bering and N. L. Pokrovsky, J. Phys. Chem., 8, 364, 1936.

[12] L. L. Kunin, Surface Phenomena in Metals, Moscow, 1955.

[13] P. P. Pugachevich and O. A. Timofeevicheva. J. Inorg. Chem. 1, 1387, 1956.

Kurnakov Institute of General and Inorganic Chemistry, USSR Academy of Sciencesx

Received October 27, 1956

* American translitération of V. K. Semenchenko – Publisher's note.

DIFFUSION OF ACTIVE CENTERS WITH SQUARE-LAW HOMOGENOUS CHAIN TERMINATION

Yu. S. Sayasov and N. S. Enikolyopyan

(Presented by Academician V. N. Kondratyev, October 23, 1956)

The present paper deals with the solution to the problem of the stationary spatial distribution of heterogeneously generated active centers on the assumption that they are removed at the surface, and also homogeneously upon collision, i.e. that we have a case of quadratic chain termination. (A problem of this type occurs, for instance, in pure hydrogen/chlorine mixtures in which there are no traces of oxygen, as these latter take up the active centers [1].) We shall assume that the rate of heterogeneous generation is much greater than that of homogeneous initiation, as is the case in reacting chlorine/hydrogen mixtures,* and that the reaction takes place in a plane-parallel vessel, the gap between the walls being $2\,\underline{l}$ (i.e. the problem is one-dimensional). Then the volume distribution of active centers is described by the differential equation:

$$D\frac{d^2n}{dx^2} - k_r(M)\,n^2 = 0, \tag{1}$$

where n ($1/cm^3$) is the concentration of active centers; k_r (cm^6/sec) is the recombination coefficient; (M) ($1/cm^3$) is the total concentration (mixture + products); x (cm) is a coordinate measured from the center of the vessel ($-\underline{l} \le x \le +\underline{l}$, $2l$ being the length of the vessel); D (cm^2/sec) is the diffusion coefficient of the active centers.

The boundary conditions take the forms

$$D\frac{dn}{dx} = -\tfrac{1}{4}\varepsilon v n + w_h \quad \text{when } x = l, \tag{2}$$

$$\frac{dn}{dx} = 0 \quad \text{when } x = 0, \tag{3}$$

where ϵ is the probability that the active centers will be removed at the vessel wall; v (cm/sec) is the average heat flow of the active centers; w_h ($1/cm^2 \cdot sec$) is the rate of hetergeneous generation.

Equation (3) is equivalent to the assumption that the conditions at both walls ($x = +\underline{l}$ and $x = -\underline{l}$) are the same, i.e. that the distribution $n(x)$ is symmetrical with regard to the center of the vessel, $x = 0$.

We now introduce the dimensionless variables

$$y = \frac{k_r(M)\,l^2}{D}\,n, \quad \xi = \frac{x}{l}.$$

* It can be shown that the rate of homogeneous generation, w_0, may be neglected as compared with the rate of heterogeneous generation, w_h, if $w_g/l \gg w_0$. For hydrogen/chlorine mixtures at 600°K and at a pressure of ~30 mm Hg, $l \sim 1$ cm, $w_h \sim 10^{11}$ cm^{-2} sec^{-1}, while the rate of thermal dissociation of Cl_2 is then $\sim 10^9$ cm^{-3} sec^{-1}, i.e., it is correct to neglect w_0.

The Equation (1) may be put in the form

$$\frac{d^2y}{dx^2} - y^2 = 0, \tag{1a}$$

and the boundary conditions (2) and (3) can be put as

$$\frac{\partial y}{d\xi} = -\alpha y + \beta \quad \text{when } \xi = 1; \quad \alpha = \frac{\varepsilon v l}{4D}, \quad \beta = \frac{w_h l^2 k_r(M)}{D^2}; \tag{2a}$$

$$\frac{dy}{d\xi} = 0 \qquad \text{when } \xi = 0. \tag{3a}$$

Equation (1) leads to a first-order equation, which, after condition (3a) has been used, is transformed to the form:

$$\left(\frac{dy}{d\xi}\right)^2 = {}^2/_3 (y^3 - y_0^3), \tag{4}$$

where $y_0 = y_\theta(0)$ corresponds to $\xi = 0$.

The solution to this equation may be found via Weierstrass's elliptic function $s = \wp(u)$, defined as $u = \int_s^\infty \frac{ds}{\sqrt{4s^3 - 1}}$ (equi-anharmonic case $g_3 = 0$, namely

$$y = e_2^{-1} y_0 \wp(u), \quad u = \omega_2 - e_2 ({}^2/_3)^{1/3} y_0^{1/3} \xi, \tag{5}$$

where $e_2 = \wp(\omega_2) = 4^{-1/3}$, $\omega_2 = 1.52995$.

Using the boundary condition of (2a) and formula (5), we get the equation which determines the constant of integration y_0:

$$({}^2/_3)^{1/3} (4\wp^3 - 1)^{1/3} y_0^{1/3} = -\alpha e_2^{-1} y_0 \wp + \beta, \tag{6}$$

where $\wp$ is taken at $\xi = 1$, i.e. when its argument $u = \omega_2 - e_2 ({}^2/_3)^{1/3} y_0^{1/3}$.

The distribution of active centers is given by the function of (5). The mean value of the concentration of active centers over the volume is clearly given by the expression

$$\bar{y} = \int_0^1 y \, d\xi = e_2^{-2} ({}^3/_2)^{1/3} y_0^{1/3} \int_{\omega_2}^{\omega_2 - e_2 ({}^2/_3)^{1/3} y_0^{1/3}} \wp(u) \, du =$$

$$= e_2^{-2} ({}^3/_2)^{1/3} y_0^{1/3} [\zeta(\omega_2 - e_2 ({}^2/_3)^{1/3} y_0^{1/3}) - \zeta(\omega_2)], \tag{7}$$

where $\zeta(u)$ is Weierstrass's zeta-function (the functions $\zeta(u)$ and $\wp(u)$ have been tabulated [2]).

In dimensional units the mean concentration of active centers, $\bar{n}$, is put in the form:

$$\bar{n}\,(1/\text{см}^3) = \frac{D}{k_r(M)\,l^2}\,\bar{y}\,(\alpha, \beta). \tag{8}$$

We shall study the function $\bar{y}\ (\alpha, \beta)$ for some limiting cases. We shall assume that the concentration of active centers changes slowly over the volume of the vessel, i.e. that $y_0^{1/2} \ll 1$. Then function (5) may be expanded in a power series with $y_0^{1/2}\xi$ as argument. Taking into account the fact that $d\wp/du = 0$ when $u = \omega_2$, and restricting ourselves to terms of order $y_0\xi^2$, we have in this case*

$$\wp = e_2(1 + {}^1/_2\, y_0\xi^2 + \ldots.), \quad \text{i. e.,} \quad y = y_0(1 + {}^1/_2\, y_0\xi^2 + \ldots), \tag{9}$$

$$\bar{y} = y_0(1 + {}^1/_6\, y_0 + \ldots). \tag{10}$$

The value of y_0 is found from equation (6) after we have substitued the expansion of (9) into it:

$$y_0^2 + \ldots = -\alpha y_0(1 + {}^1/_2\, y_0 + \ldots) + \beta. \tag{11}$$

We shall assume that $\alpha \ll 1$ and $\beta \ll 1$. Then it follows from (11) that

$$y_0 = -\frac{\alpha}{2} \sqrt{\frac{\alpha^2}{2} + \beta}. \tag{12}$$

When $\beta \ll \alpha^2/4$ $y_0 \cong \beta/\alpha$, and when $\beta \gg \alpha^2/4$ $y_0 \cong \sqrt{\beta}$. Thus we get the following final expressions for the mean concentrations:

$$\bar{n} = \frac{w_h}{{}^1/_4\, \varepsilon v} \qquad \text{when} \quad w_h \ll \frac{\varepsilon^2 v^2}{16\, l k_r(M)}; \tag{13}$$

$$\bar{n} = \sqrt{\frac{w_h}{k_r(M)\, l}} \quad \text{when} \quad w_h \gg \frac{\varepsilon^2 v^2}{16\, l k_r(M)}. \tag{14}$$

(13) and (14) have a simple physical meaning. At low rates of heterogeneous generation [Condition(13)] a small number of chains are generated at the walls, and so the probability of their interacting in the volume (which is proportional to $\bar{n}^2$) is small. This means that the mean concentration, $\bar{n}$, is determined by the

* The expansion of (9) may be found directly from (1) by substituting in it the series $y = \sum_{m=0}^{\infty} a_m \xi^{2/m}$ and determining the coefficients a_m from the recurrent relations.

dynamic equilibrium of the processes of generation and removal of active centers at the walls, $w_h = \frac{1}{4}\epsilon v\bar{n}$, hence we get formula (13).

On the other hand, when a large number of chains are generated per unit time at the walls, and thus the probability that they will interact in the volume is large compared with that of their removal at the walls, the mean concentration of active centers $\bar{n}$, is determined by the equality between the rate of generation of active centers per unit volume, w_h/l, and the rate of removal per unit volume $k_r(M)(\bar{n})^2$, hence we get the formula (14).

We shall now study the case where the concentration of active centers changes rapidly over the volume of the vessel. Since $\varphi(u)$ is large when $u \to 0$, namely $\varphi(u) = \frac{1}{u^3} + \frac{u^4}{28} + \ldots$ when $u \to 0$, then we must suppose that the rapid change in n implies that $u = \omega_2 - e_2 (2/3)^{1/3} y_0^{1/3} \ll 1$. The boundary condition of (6) gives in this case

$$(2/3)^{1/3} \frac{2}{u^3} y_0^{1/3} = -\alpha e_2^{-1} y_0 \frac{1}{u^3} + \beta. \tag{15}$$

Assuming $\beta \gg 1$ and $\alpha \ll \beta^{3/2}$. From (15) we get

$$y_0 \cong \frac{3\omega_2^2}{2l_2^2}, \quad \frac{1}{u} \cong 2^{-1/3} 3^{1/3} y_0^{-1/3} \beta^{1/3}.$$

Since when $u \to 0$ $\zeta(u) = \frac{1}{u} + \ldots$, then from (7) it follows that here

$$\bar{y} \cong 18^{1/3} \beta^{1/3}$$

or

$$\bar{n} = \left(\frac{18 w_h D}{l^3 k_r^2 (M^2)}\right)^{1/3} \quad \text{when} \quad w_h \gg \frac{\epsilon^2 v^2}{64 D k_r (M)}. \tag{16}$$

The values of $\bar{y}(\alpha, \beta)$, which do not satisfy the assumptions made above in duducing (13), (14) and (15), may be found numerically with the aid of the tables for $\varphi(u)$, $\zeta(u)$ [2]. The graphs of the function $\bar{y}(\alpha, \beta)$ given in Figure 1 for $\alpha = 0; 2; 4; 6; 8; 10$, were calculated in this way: with the aid of these it is easy to find the value of $\bar{n}$ for any proposed parameters which control the reaction.

By using the theoretical results given, and the experimental data on reaction rates in pure hydrogen/chlorine mixtures, we may draw some conlusions about the possible elementary processes involved in this reaction.

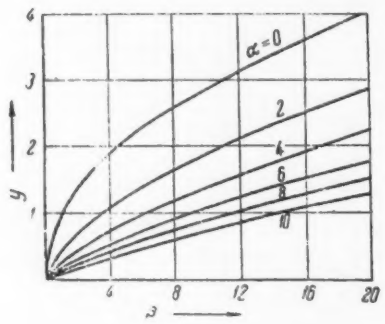

Fig. 1.

Under the conditions used by Markevich [3]: 310°, pressure on the chlorine/hydrogen mixture of 62 mm/Hg, $l = 2$ cm, $V_{Cl} \cong 6 \cdot 10^4$ cm/sec, $k_r = 10^{-32}$ and $\epsilon = 5 \cdot 10^{-4}$ we get

$$\frac{\epsilon^2 v^2}{16 l k_r (M)} \cong 1{,}5 \cdot 10^{17}.$$

Semenov and Voevodsky have found the value $w_h \sim 10^{11}$ cm^{-2} sec^{-1}. Thus it is clear that condition (13) is complied with.*

On increasing the pressure and diameter and re-

* And so $\bar{n}$ in this case is independent of k_r, and consequently k_r cannot be determined from the data of [3].

ducing ϵ we may ensure that condition (14) is fulfilled, and thus calculate k_1. When $\epsilon \sim 10^{-5}$ and $\frac{1}{\lambda} \sim 1$ cm, and assuming w_h proportional to pressure, we find that Condition (14) for the $H_2 + Cl_2$ reaction can be fulfilled for pressure $\gtrsim 5 \cdot 10^2$ mm Hg.

In conclusion we should note that by using the method described here – i.e. by using Weierstrass's functions – we may also study the diffusion of active centers under other conditions where square-law chain termination plays an important part (e.g. when chains are initiated at the walls and in the volume simultaneously, removal of active centers by impurities and by square-law recombination, etc.).

Institute of Chemical Physics,
Academy of Sciences, USSR

Received October 18, 1956

LITERATURE CITED

[1] N. N. Semenov, Some problems of chemical kinetics and reactivity, Acad. Sci. USSR, Press, 1954.

[2] E. Jahnke and F. Emde, Tables of functions, 1948.

[3] A. M. Markevich. J. Phys. Chem., 22, No. 7, 41, 1948.

CRYSTALLIZATION STRUCTURE FORMATION IN TRICALCIUM ALUMINATE SUSPENSIONS

E. E. Segalova, E. S. Solovyeva and Academician P. A. Rebinder

The special features of structure formation in aqueous suspensions of Portland cement during the first few hours after they have been made are determined in the main by the aluminate minerals, particularly by the tricalcium aluminate [1, 2].

It is of interest to study these processes, since the cement / water system can be influenced at this stage, and thus the structure of the cement controlled. In order to find out the general laws governing crystallite structure formation in the aluminate components we studied the structure formation in suspensions of one particular clinker mineral in detail, i.e. tricalcium aluminate, $3CaO \cdot Al_2O_3$ (C_3A).

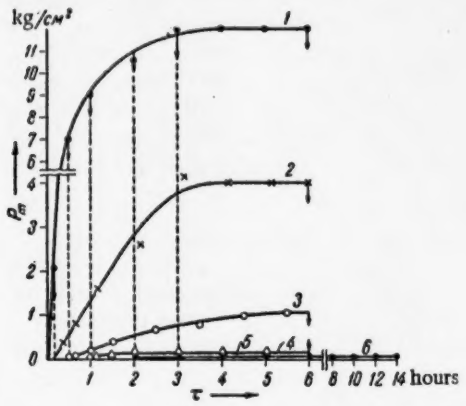

Fig. 1. Growth of the plastic strength P_m after destruction of the crystallite structure of the hydroaluminate at different stages in its formation in a suspension made up of 5% C_3A + 95% finely ground quartz sand + 33% H_2O in the dry mixture: 1) initial suspension (stirred for 45 sec when made); 2,3,4,5 suspensions which have been stirred a second time until the structure is completely destroyed, at 10 and 30 minutes, and 1 and 2-3 hours after preparation (the arrows denote the the times of remixing); 6) systems 1-5, restirred after 6 hours.

We studied mixtures of finely-ground powders 1-5% of tricalcium aluminate and 99-95% of quartz sand. The processes of structure formation in such a suspension are determined solely by the tricalcium aluminate, but a large amount of inert filler makes it easier to study these systems [3], and the conditions of hydration of the C_3A approximate those in cement slurries. The processes of structure formation have been delineated by us, as in our earlier papers [1,3], by the kinetics of the growth in plastic strength, as measured with a cone plastometer. The specimens of the suspension were placed in a special measuring vessel after preparation, and kept in a drier over water.

Figure 1 shows the kinetics of the rise in plastic strength for a suspension of 5% C_3A and 33% water (dry weight basis) which has been restirred at different stages in the formation of the crystallite structure in the hydroaluminate. As distinct from the suspensions of calcium sulfate hemihydrate we have studied [3], in the suspensions of tricalcium aluminate, even when the content of tricalcium aluminate is small and that of water large, the first stage, in which the formation of a crystallite structure in the system predominantly occurs, is of such short duration that it is difficult to detect it (Figure 1, 1). If the crystallite structure is disorganized while it is developing, a sharp fall in the strength occurs (Figure 1, 2-6), and stirring after 1-2 hours practically rules out further development of the crystallite structure.

Measurements of the kinetic rise in plastic strength and the chemical binding of the water in C_3A (Fig. 2)

show that both processes run parallel [3,4], and at 18-20° are mainly completed 5-6 hours after making the suspension. During the next 1-2 days only a very small increase in strength is found, which is accompanied by an equally small increase in the amount of chemically bound water.

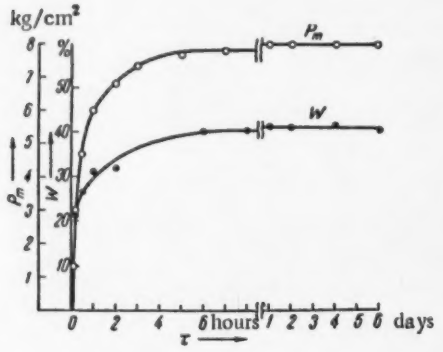

Fig. 2. Kinetics of crystallite structure formation and hydration of C_3A in a system made up of 5% C_3A + 95% ground quartz sand + 43% H_2O (dry weight basis). W is the amount of chemically bound water as a percentage of the weight of the C_3A.

A further increase in the strength of the crystallite structure formed by a factor of 2 may be had by drying the specimen: then subsequent moistening of the dried crystallite structure once again reduces the strength to the original value, which is explained as to the effect of adsorption fall in strength [5], which must be very markedly developed in these structures which have an internal surface. If the crystallite structure of the hydroaluminate is kept in moist conditions for a long time its strength begins to fall gradually, after passing through a maximum value. This is seen particularly clearly in structures which contain a large amount of water. For example in suspensions having 5% C_3A and 70-100% water (dry weight basis) the crystallite structure, which attains a plastic strength of 1-2 kg/cm², is completely destroyed at 20 days after preparation (the residual strength, at 0.1 kg/cm², corresponds to a coagulation structure composed of free crystals of hydroaluminate and sand). By analogy with the crystallite structure of calcium sulfate dihydrate [6], we explain these effects as a gradual dissolution of the thermodynamically non-equilibrium crystallization contacts which are formed between the hydroaluminate crystals when the crystallite structure forms and develops. In agreement with the lower solubility of the hydroaluminate as compared with calcium sulfate dihydrate the solution of the contacts and the recrystallization occur considerably more slowly in the crystallite structure of the hydroaluminate. These processes occur more rapidly on raising the temperature, and side by side with the usual recrystallization we get the hexagonal form of the hydroaluminate being transformed to the cubic.

During recent years a plasticizing additive has been widely used in building practice, this being a sulfite-alcohol liquor (sal). Its effect on cement slurries is mainly determined by its adsorptive interaction with the aluminate component of the cement clinker [1,2]. In this connection it was important to study the effect of adding sal on the structure formation of suspensions of tricalcium aluminate. These studies have shown that the addition of sal, which is adsorbed on the surfaces of the C_3A particles, on the one hand retards the processes of structure formation and hydration, and also the processes by which fresh crystals form, and on the other hand, by causing adsorptive peptization and dispersion of the parent C_3A particles, accelerates these processes. In addition, the added sal, like any other surface-active organic material, is adsorbed on the surfaces of fresh crystallites, thereby blocking possible contact sites and thus reducing the strength of the crystallite structure. The over-all effect of the additive on the strength of the crystallite structure depends on which of these factors predominates at any given concentration of the additive.

Table 1 gives the kinetic data on the rise in plastic strength and in the chemically bound water in suspensions containing 5% C_3A. The addition of sal is made with the water mix. It is clear from Table 1 that the addition of sal up to 1% retards the rise in strength and in the chemically bound water, and also reduces the final strength of the crystallite structure in the hydroaluminate.

Microscope studies on C_3A suspensions (Figure 3) have shown that when small amounts of sal are added we actually get a slowing-down of hydration, but that this leads, in the final reckoning, to coarser crystals of the hydroaluminate forming than occurs in the absence of the additive (Figure 3, d). The fall in the strength of the crystallite structure is evidently to be explained by the retardation of the hydration, reducing the probability that thermodynamically nonequilibrium contacts will form, and thus reduces the fraction of the strength due to these contacts. The fall in the strength is also enhanced by the adsorptive-blocking action of the additive.

TABLE 1

Increase in the Plastic Strength, P_m, and in the Chemically Bound Water, W, in Suspensions Containing 5% C_3A and 43% Water (dry weight basis) (preparative stirring – 45 seconds).

Time from start of experiment	Sal concentration in % of solid phase					
	0	0.5	1	3	5	8
	I. P_m in kg/cm²					
1 min	0.004	0.002	0.002	0.002	0.002	0.002
5 min	0.37	0.12	0.40	0.002	0.002	0.002
10 min	1.4	0.14	0.70	0.66	0.002	0.002
30 min	4.7	0.16	0.74	7.0	15.0	4.2
1 hour	6.0	0.19	0.85	10.0	27.5	41.0
3 hours	7.4	0.22	1.0	14.0	40.0	58.0
6 hours	7.8	0.27	1.2	16.0	48.0	72.0
1 day	8.0	0.40	2.0	20.0	55.0	82.0
3 days	8.0	0.65	2.4	20.0	56.0	82.0
5 days	8.0	2.1	3.6	20.0	55.0	81.0
10 days	8.0	4.0	4.2	20.0	56.0	80.0

Time from start of experiment	Sal concentration in % of solid phase			
	0	0.5	1.0	3.0
	II. W in % of C_3A*			
30 min	26.6	18.5	21.4	18.7
1 hour	31.0	21.5	23.6	21.4
2 hour	31.5	24.5	28.3	30.0
4 hour	36.0	26.7	32.4	35.6
8 hour	41.0	29.6	33.5	38.4
1 day	41.5	32.0	35.7	39.8
2 days	41.6	36.7	36.5	—
3 days	41.9	36.7	39.9	41.5
5 days	41.3	38.5	39.7	41.8
10 days	41.0	42.2	40.5	—

* According to the formula $C_3A \cdot 6$ aq, $W \approx 40\%$.

As the concentration of the surface-active additive rises, the retardation of hydration it causes also increases, as well as its dispersive effect on the parent C_3A particles (Figure 3,e). The retardation of the growth in the nuclei of the freshly formed phase caused by the adsorbed layers leads to the occurrence of a marked induction period in the structure formation, its length being greater the more sal added. Special experiments have shown that the amount of chemically bound water is practically zero during the induction period. Rapid hydration, together with the parallel increase in the plastic strength, begins at the end of the induction period, and leads to a hydroaluminate crystallite structure appearing in the system which has a very high strength. Stabilization of the nuclei by the adsorbed layers of additive retards the crystallization, and prevents screening layers due to the newly formed hydrates arising on the surfaces of the parent C_3A particles. All this facilitates a state of high supersaturation arising during the induction period, this being produced because the conditions are favorable to the formation of a large number of crystallization contacts and to the production of a crystallite structure of high strength. When large amounts of sal are added the strength of the hydroaluminate crystallite structure may be raised 8-10 times, as compared with the strength without the addition. An unusual marked fineness of the crystals of hydroaluminate formed is then observed (Figure 3,f); the separate crystals of the hydroaluminate cannot be resolved even in the electron

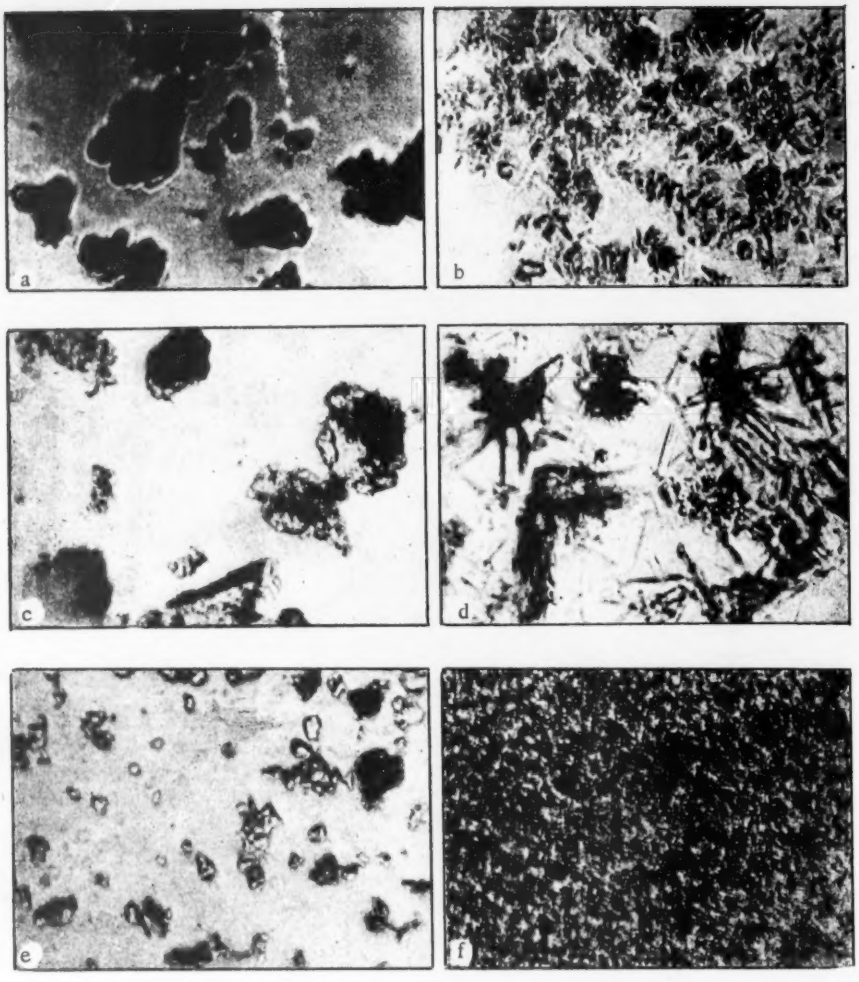

Fig. 3. "Photomicrographs of suspensions of C_3A (400 X): a, b are 0.7% suspensions in water; c and d are the same in a 0.01% solution of sal; e and f are a 5% suspension in a 10% solution of sal. Plates a, c and e refer to test specimens taken from the suspensions immediately after preparation (mixing time 30 secs); Plates b, d and f were taken after 3 hours. The hydration of C_3A was carried out in the microcuvette made up of the slide and cover-slip, where the test-specimen from the suspension was placed at 30 mins after preparation.

microscope at a magnification of 40,000. This is also shown by measurements of adsorption by dilute suspensions of C_3A. The largest adsorption of sal after terminal hydration reached 4.5 g sal per g C_3A.

When still greater amounts of additive are used the strength of the hydroaluminate crystallite structure falls, since the effect of stabilization and blocking of the possible contact sites predominates, due to the adsorption of sal.

Dept. of Colloid Chemistry
Lomonosov State University, Moscow

Received September 27, 1956

LITERATURE CITED

[1] E. E. Segalova, P. A. Rebinder and O. I. Lukyanova. Bull. Moscow State Univ. No. 2, 1954; P. A. Rebinder and E. E. Segalova, Nature, No. 12, 1952.

[2] S. V. Shestoperov, F. M. Ivanov, A. N. Zashchepin and T. Yu. Lyubimova, Cement concrete with plasticizing additives, Moscow, 1952.

[3] V. N. Izmailova, E. E. Segalova and P. A. Rebinder, Proc. Acad. Sci. USSR, 107, No. 3, 1956.

[4] O. V. Kuntsevich, P. E. Aleksandrov et al., Proc. Acad. Sci. USSR, 104, No. 4, 1955.

[5] P. A. Rebinder, L. A. Shreiner and K. F. Zhigach, Hardness reducers in boring, Moscow, 1944; P. A. Rebinder, Jubilee session in honor of the 30th anniversary of the Great October Socialist revolution, Acad. Sci. USSR Press, 1947; G. I. Logginov and M. P. Elinzon. Symp. on materials and structures in current architecture, Moscow, 1948, p 95.

[6] E. E. Segalova, V. N. Izmailova and P. A. Rebinder. Proc. Acad. Sci. USSR, 110, No. 5, 1956.

REGULARITIES IN THE INCLUSION OF COPPER, ANTIMONY, LEAD, COBALT, IRON AND ZINC IN CATHODE DEPOSITS OF TIN

V. L. Kheifets, E. S. Kozich and O. M. Danilovich

(Presented by Academician A. N. Frumkin, October 16, 1956)

The possibility of an impurity co-depositing with the main metal in a discharge is determined by a number of conditions: the position of the standard potential with respect to that of the main metal, the values of the currents drawn by the impurity and by the main metal, and the structure of the alloy formed between the impurity and the main metal near 100% main metal,etc. Depending on which of these conditions predominates in any given case, the laws governing the inclusion of the impurity in the cathode deposit may change.

The laws in some basic cases in the instances of cathode deposits of nickel and cobalt have already been dealt with by the present authors [1,2].

Tin, as distinct from nickel and cobalt, has a large transport number and is weakly polarized. For example in the electrolyte we have studied (which contained $SnSO_4$ 90 g/liter, H_2SO_4 20 g/liter,) phenolsulfonic acid 50 g/liter, and joiner's glue 4 g/liter the cathode potential of tin changed only 5-7 mv on going from current densities of 50 a/m^2 to 200 a/m^2. This enables us to assume that in the cases under consideration we should find some differences from the laws of impurity inclusion found with nickel and cobalt deposits.

In view of its position in the voltage scale and its high transport there is no doubt that copper must be found in tin cathode deposits at the limiting current. The copper content in the cathode deposit was determined by the dithizone method. As would be expected, the relation between the copper content in the deposit to its content in the solution was a linear one passing through the origin. As distinct from cases where the deposition of the main metal is strongly polarized, the line which defines the copper content in the cathode deposit of tin does not lie above the bisector of the angle between the coordinates, but coincides with it, which is explained by the slight polarizing action in tin discharge. At the same time the "constant" for the rate of inclusion of copper in cathode deposits often is practically the same as the constants for other metals which are found to deposit in the cathode deposits of nickel and cobalt at the limiting currents [1].

Copper is unique among the impurities we have studied in that its deposition is diffusion-limited. The depositions of all the other impurities, as found by investigation, are limited by the rate of the discharge stage. These impurities can be divided into two groups, though. Antimony and lead must be placed in the first group. The standard potential of antimony is more positive than that of tin, but the appreciable polarization of the discharge process in antimony leads to its deposition being limited by the discharge stage, in which connection we must take into account the polarization of the tin discharge, although this is slight. Lead is very close to tin in both standard potential and polarizability, and so it is also impossible to neglect the magnitude of the polarization in the discharge of the main metal with lead. Thus these two impurities should show laws relating to the case where the rate of deposition of the main metal and of the impurity is limited by the discharge stage. The antimony content in the metal was determined by radioisotope methods, the lead being determined spectrographically, and with dithizone.

Figure 1 shows the relation between the antimony content in the cathode deposit and its content in the

solution. It is clear from the figure that this relation is expressed by a curve of parabolic type, as is predicted from theory. Figure 2 shows the relation of the lead and antimony contents (curves 1 and 2, and curve 3, respectively) in the cathode deposit to the current density. It is clear from the figure that the lead content in the deposit increases rapidly up to a current density of ≃ 200 a/m², but thereafter changes slowly, as the diffusion resistance begins to operate.

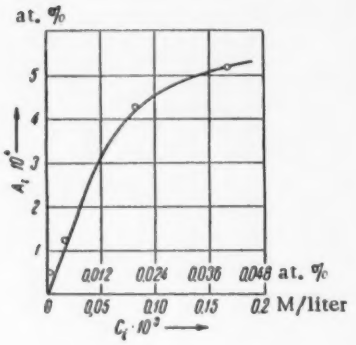

Fig. 1. Relation of the impurity content due to antimony in a tin cathode deposit to its content in the solution .

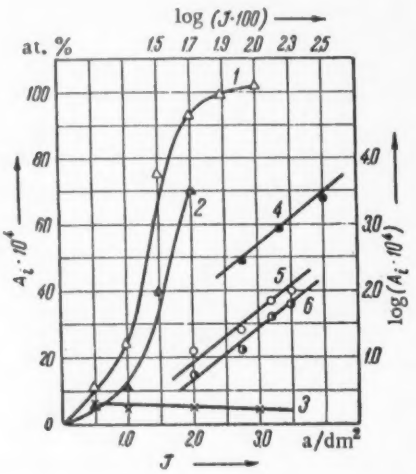

Fig. 2. Relation of the lead and antimony contents in tin cathode deposits to the current density: 1) lead, electrolyte contents 16 mg/liter; 2) lead, electrolyte content 11 mg/liter; 3) antimony, electrolyte content 1.6 mg/liter; 4) manganese in a cathode deposit of nickel (log-log coordinates), electrolyte content 6.5 mg/liter; 5) curve 1 in log coordinates; 6) curve 2 in log coordinates .

In the case of antimony its content in the cathode deposit is found to be almost independent of the current density. As follows from equation (10) of [1], for the case under consideration the following equation is correct:

$$\log A_i = N + \left(\frac{\alpha_1 Z_1}{\alpha_m Z_m} - 1\right)\log J, \qquad (1)$$

where A_i is the impurity content in the cathode deposit, N is a complex constant; α_1 is the division factor, from the kinetic equation for the discharge of the impurity; α_m is the same for the main metal; Z_1 is the valence of the impurity; J is the current density at which the metal is deposited.

It is clear from the equation that if $\alpha_1 Z_1 > \alpha_m Z_m$, the impurity content in the cathode deposit will increase. Instances of this are the inclusion of manganese in nickel and of lead in tin. If $\alpha_1 Z_1 = \alpha_m Z_m$, the impurity content should not depend on the current density, as is found in the case of inclusion of antimony in tin. Curves 1 (initial section) and 2 of Figure 2 transform to lines 5 and 6 in logarithmic coordinates, the gradients (≃1.7), being equal to those found in the case of inclusion of manganese in nickel (line 4).

Iron and cobalt are metals which are considerably more electronegative than tin, and, in addition, show little current transport. Zinc, although its current transport is large, is 0.62 v more negative than tin in the voltage series, and forms neither solid solutions nor chemical compounds with tin. It is therefore natural that, on the one hand, the rates of discharge of these metals should be determined by the rate of the discharge stage, and, on the other hand, the polarization of the discharge of the main metal, since it is small, cannot influence their inclusion in the deposit at all appreciably. If we suppose that the main metal deposits without polarization, and that the rate of deposition of the impurities is limited by the discharge stage, it is not difficult to get the equation [2]

$$A_i = \frac{100MC_i}{JC_m^{\alpha_1 Z_1 / Z_m}}, \qquad (2)$$

where C_i is the impurity content in the electrolyte; C_m is the concentration of the main metal in the electrolyte; M is a complex constant, which combines the value of the standard current transport of the impurity, the standard potentials etc; the balance of the symbols have been defined above. As an example, we tested the relation of A_i to the current density J for this group of impurities as regards the inclusion of cobalt in tin deposits. The results are given in Figure 3. It is clear from this Figure that Equation (2) is in complete agreement with this relation.

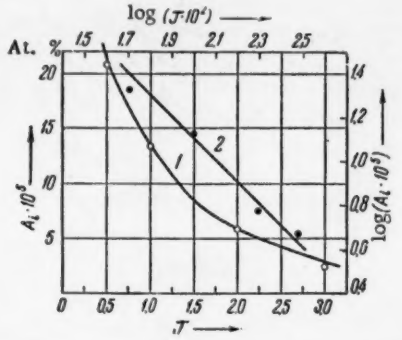

Fig. 3. 1) Relation of the cobalt content to the current density (cobalt content in the electrolyte 50 mg/liter); 2) the same in log coordinates.

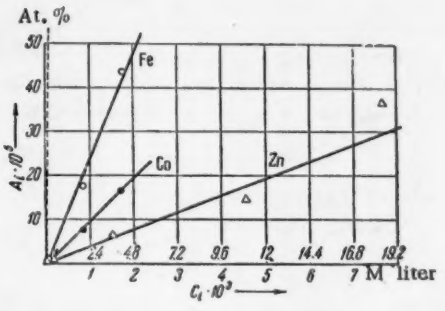

Fig. 4. Relation of the iron, cobalt and zinc impurity content in the cathode deposit to their contents in the electrolyte. The dotted line is the coordinate angle bisector.

As is to be expected from theory, a rise in the tin content of the electrolyte leads to an appreciable fall in the impurity content of the cathode deposit for those impurities of which the deposition is limited by the discharge stage. It follows from Equation (2) that C_i and A_i must be linearly related in this case, exactly as in deposition of the impurities at the limiting current. At the same time the different values of M for the various impurities must be referred to differences in the slopes of the lines, unlike impurities which deposit at the limiting current.

Figure 4 presents the data for iron, cobalt and zinc, which illustrate this situation. Radioisotope methods were used to determine the Fe, Co and Zn contents in the cathode deposit of tin.

TABLE 1

Main metal	Impurity	Stage which determines the deposition of the impurity	Stage which determines the deposition of the main metal	(Content in deposit)/(content in solution)
Ni	Cu, Zn, Pb, Cd, Co	Diffusion	Discharge	2.5
Co	Cu, Zn, Pb	Diffusion	Discharge	3.0
Sn	Cu	Diffusion	Polarization may be neglected	160
Ni	Mn	Discharge	Discharge	0.07
Sn	Pb	Discharge	Polarization must be allowed for	0.5
Sn	Sb	Discharge	Ditto	0.033
Sn	Fe	Discharge	Polarization may be neglected	0.0012
Sn	Co	Discharge	Ditto	0.0005
Sn	Zn	Discharge	Ditto	0.0002

It is of interest to compare the rate of inclusion of different impurities in the deposit. Table 1 gives just such a comparison. The ratios of deposition are characterized by the ratios between the impurity contents in the deposit to their contents in the solution, i.e. by the so-called distribution coefficient [3]. In the cases of Mn in Ni and of Sb and Pb in Sn we have used the initial sections of the curves, which are practically rectilinear.

It is clear from the table that when the rate of deposition of the main metal is determined by discharge, while the rate for the impurity is determined by diffusion, the individual properties of the impurity and of the main metal again begin to play a part, and the deposit is considerably richer in impurity than is the solution. When the depositions of the main metal and of the impurity show little polarization, the composition of the deposit at the limiting current will be the same as in the solution. And finally, when the deposition of the impurity is determined by the discharge stage, the deposit is considerably purer than the solution, and the rate of inclusion of the impurity depends on the individual properties of both the impurity and the main metal.

Sci.-Tech. and Development Institute
of the Nickel, Cobalt and Tin Industry,
Leningrad.

Received August 10, 1956

LITERATURE CITED

[1] V. L. Kheifets and A. L. Rotinyan, Proc. Acad. Sci. USSR, 82, No. 3, 423, 1952.

[2] A. L. Rotinyan and V. L. Kheifets, Light metals, No. 2, 24, 1954.

[3] G. A. Tsyganov and A. I. Chernilovskaya, Proc. Acad. Sci. Uzbek SSR, No. 9, 32, 1952; No. 6, 37, 1954.

AN INVESTIGATION OF THE HEAT CAPACITY, c_v, OF WATER AND WATER VAPOR IN THE CRITICAL REGION

Kh. I. Amirkhanov, Member Acad. Sci. Azerbaidzhan SSR and A. M. Karimov

The absence in the literature of data on the heat capacity c_v of water and water vapor and its dependence on temperature and on pressure can clearly be attributed to the existence of experimental difficulties [1]. For the determination of the heat capacity c_v, we have employed an adiabatic calorimeter, with a thermoelectric temperature regulator, such as has been earlier described [2].

It is known that the study of the behavior of the heat capacity not only demands adiabatic conditions in the calorimeter system but, also, equilibrium in the thermal field, a requirement whose attainment was facilitated in the present work by the fact that in the critical region, where the coefficient of thermal expansion, $\alpha = \frac{1}{v}\left(\frac{\partial v}{\partial T}\right)_p$, reaches very high values, the Groshof number also becomes quite large. For the initiation of turbulent movement in a liquid the condition $Gr \sim 5 \times 10^4$ must be fulfilled [5]. In our work with one-component system under a temperature difference of 0.01°, the magnitude of Gr was of the order of 10^7. Thus the natural development of turbulent movement in the critical region aided the rapid attainment of thermal equilibrium. The very construction of our calorimeter, with its metallic walls with a thickness reaching 7 cm, considerably speeded up the process of temperature equalization, as was indicated by identical readings on three thermocouples distributed vertically in the calorimeter according to the height of the liquid.

In the course of an experiment, temperature equilibrium between the phases ($T_1 = T_2$) was attained by waiting for the corresponding readings on the thermocouples and for the equalization of the pressures ($p_1 = p_2$), so that it could be claimed that full thermodynamic equilibrium was established in the system, i.e., that $\varphi_1(p, T) = \varphi_2(p, T)$ and that it was permissible, therefore, to carry out measurements without liquid agitation.

In a calorimeter of the type earlier described [2], the heat capacity c_v of water and water vapor was determined at various specific volumes, over a temperature interval which did not exceed 0.6°. At each specific volume the measurements were repeated several times. The maximum over-all error in the determination of the heat capacity c_v amounted to ~ 2.5%.

EXPERIMENTAL RESULTS

In Figure 1 there are shown those changes in the heat capacity of water which accompany the transition from a two-phase into a single-phase state. Far from the critical point the heat capacity c_v is subject to an abrupt alteration on passage through the boundary curve (Figure 1, 1) but as the critical point is approached, i.e., as the specific volume increases, the abruptness in the change in c_v tends to be lost although the absolute value of the jump in the heterogeneous region continued to increase [4,6].

In Figure 2 the boundary curve for water has been plotted in the coordinates (T, v). The boundary curve in the coordinates (p, v) can be constructed in a similar fashion, the critical region being clearly marked out.

The method of constructing this boundary curve on which the critical region is delineated is based on the following experimental fact which we have discovered (see Figure 1, 2): far from the critical region the heat capacity c_v for the two-phase state on crossing the boundary curve abruptly falls to the value of the heat capacity for the single phase, whereas in the critical region, beginning at a specific volume of 2.5 cm^3/g

and going up to 4.15 cm^3/g, the abruptness in the alteration of c_v is lost and the change stretches out over a considerable temperature interval, which interval for water can be as large as 4.5°. From the point at which the abrupt alteration in the heat capacity c_v ceases, this temperature interval increases in proportion to the approach to the critical point, attaining near the latter a maximum value of 4.5°. With a further increase in the specific volume, the temperature range diminishes and reaches a minimum of 0.6° at a specific volume $v = 4.15\ cm^3/g$. Still further increasing the specific volume leads again to an abrupt alteration in c_v. The critical region for water is thus limited in terms of volume to an interval ranging from $v = 2.5\ cm^3/g$ to $v = 4.15\ cm^3/g$ and in terms of temperatures to an interval of 4.5° [12].

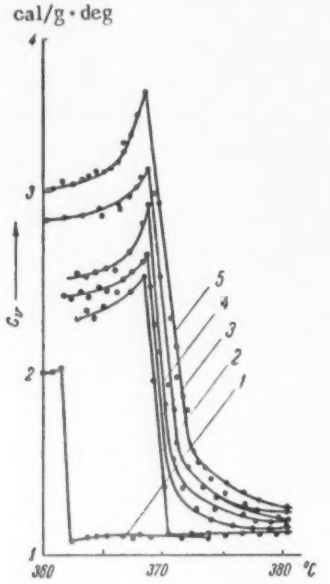

Fig. 1. The dependence of the heat capacity of water on temperature in the critical region, at various specific volumes: 1) 1.925, 2) 2.2415, 3) 4.160, 4) 2.870, 5) 3.235 cm^3/g.

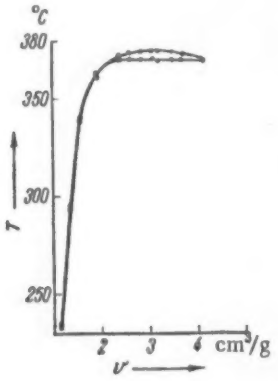

Fig. 2. The boundary curve for water, constructed from the change in the heat capacity, c_v, accompanying the transition from the heterogeneous into the homogeneous state.

The critical region which we have found for water in the coordinate (T, v), and which is limited to a temperature range of 4.5°, is in satisfactory agreement with the theoretical calculations of Band, who for this same region gives the temperature interval as 6.5°. The diagram in the (P, v) coordinates is similar to that in the (T, v) coordinates.

In Figure 3 for three isotherms in the hypercritical region there is shown the dependence of c_v of water on the specific volume. These experimental curves have the following characteristics. As the critical volume is approached along an isotherm, the heat capacity increases and ultimately reaches a maximum value, the heat capacity c_v having a maximum in the hypercritical region just as does the heat capacity c_p [7-10].

With a further increase in the specific volume, i.e. in proportion to the movement away from the critical point, the heat capacity rapidly diminishes. At the critical point there is reached the absolute value of the maxima of the heat capacity c_v. At temperatures higher than the critical, the relative maxima diminish. It is to be seen from Figure 3 that the heat capacity, in contradiction to the van der Waals' theory, is a function, not only of the temperature, but of the volume as well.

In Figure 4 there are shown the maximum values of the heat capacity c_v for intersection with the boundary curve. According to the theory of V. K. Semenchenko [5, 11], the heat capacity for intersection with the boundary curve reaches its maximum at the critical point. From this it follows that the critical volume should correspond to the maximum on this "curve of maxima." For water this maximum represents a value $v_c = 3.23\ cm^3/g$.

The result obtained by us for the critical volume of water is $v_c = 3.23\ cm^3/g$, a value which differs by 2.5% from the value of the critical specific volume ($v_c = 3.30\ cm^3/g$) shown in common by the VTI tables, the new table of M. P. Vukalovich [12] and the determination of V. A. Krillin and V. N. Zubarev [13].

DISCUSSION OF RESULTS

The results of our experiments indicate that far from the critical point the heat capacity of water changes abruptly during the passage from the two-phase

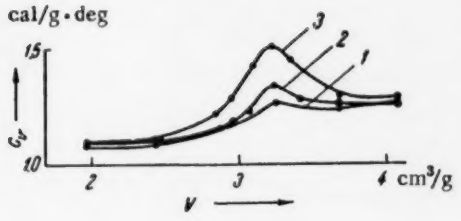

Fig. 3. The dependence of the heat capacity c_v of water on the specific volume, along the critical and hypercritical isotherms: 1) 381°, 2) 373°, 3) 374.2°.

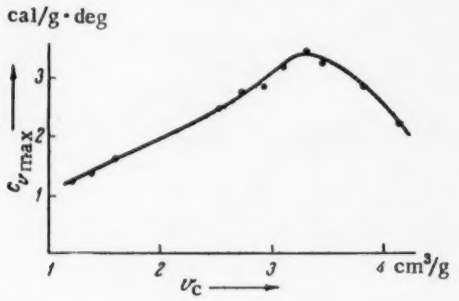

Fig. 4. The maximal values of the heat capacity c_v, of water in the heterogeneous region, at various specific volumes.

into the single-phase condition, the absolute value of these discontinuous jumps increasing in proportion to the approach to the critical region and reaching a maximum at the critical point. From the classical point of view, the increase with temperature of the heat capacity c_v of water in the two-phase state and the discontinuous decrease of c_v which accompanies the transition into a single phase, can be explained by the fact that in the transition region added heat goes not only to increase the temperature of the separate phases, but also to bring about that rupture of the molecular bonds in the polymolecular compounds which takes place during the process of molecular dissociation. The heat of vaporization cannot essentially influence the change in the heat capacity because as the critical point is approached its value tends toward zero [14], whereas the magnitude of the jump in c_v increases. On transition into a single phase, the process of dissociation and vaporization suddenly ceases, which leads to a discontinuous diminution in c_v. Naturally, the rupture of the molecular bonds, which results in a decreased degree of association, depends on temperature and on pressure. Thus at the critical point the number of rupturing bonds and the intensity of these bonds reach maxima, which in turn leads to a maximum increase in the value of c_v. For liquids, this region of dispersion, i.e., the region in which the dissociation process takes place, must depend on the degree of molecular association. For this reason, the region of the critical state must be different for different liquids. The molecular mechanism of the maxima of the heat capacity at hypercritical temperatures (see Figure 3) must be similar to that just described. It is not possible with the van der Waals' equation to explain, either qualitatively or quantitatively, the behavior, as considered above, of substances at temperatures which are different from the critical.

Actually, rewriting van der Waals' equation in the form $p = \frac{RT}{v-b} - \frac{a}{v^2}$, we find $\left(\frac{\partial^2 p}{\partial T^2}\right)_v = 0$. Accordingly, $\left(\frac{\partial c_v}{\partial v}\right)_T = T\left(\frac{\partial^2 P}{RT^2}\right)_v = 0$. i.e., the heat capacity, c_v, should not depend on the volume and must be a function of the temperature alone. Experiment shows (see Figure 3) that these conditions are fulfilled only for the maxima on the critical and the hypercritical isotherms. For other specific volumes, the relation $\left(\frac{\partial c_v}{\partial v}\right)_T = 0$ is not valid for either the critical or the hypercritical isotherms, i.e., the van der Waals equation is not applicable to them.

It is to be seen from Figure 3 that the maxima c_v (v) lie on a critical isochore which is nearly linear.

The presence in the hypercritical region (and at constant volume) of maxima in the heat capacity c_v in relation to the temperature, which maxima are similar to those met for c_p [8-11], confirms the existence of the anomalous course of the heat capacity in this region.

The Dagestan Branch of the Academy of Sciences of the USSR

Received May 9, 1956

LITERATURE CITED

[1] V. A. Krillin, A. E. Sheindlin, Osnova eksperimentalnoi termodinamiki (The Principles of Experimental Thermodynamics) 1950.

[2] Kh. I. Amirkhanov, A. M. Kerimov DAN (Proc. Acad. Sci USSR) 110, 578, 1956.

[3] L. D. Landau and E. M. Lifshits, Mekhanika sploshnykh sred (The Mechanics of Continous Media) 1953.

[4] V. K. Semenchenko ZhFKh (J. Phys. Chem.) 26, 1337, 1952.

[5] V. K. Semenchenko, V. P. Skripov ZhFKh (J. Phys Chem.) 25, 362, 1951.

[6] G. Meier, Statisticheskaya mekhanika (Statistical Mechanics) IL, 1952.

[7] D. L. Timrot, N. B. Vargaftnik, S. L. Rivkin, Izv. VTI (Bull. Thermotech. Inst.) No. 4, 1948.

[8] D. L. Timrot, S. L. Rivkin, M. I. Chastukhina, Izv. (Bull. Thermotech. Inst.) No. 8, 1949.

[9] A. E. Sheindlin, Teploenergetika (Heat Energetics) No. 3, 26, 1954.

[10] T. N. Andrianova ZhTF (J. Tech. Phys.) 23, 1108, 1953.

[11] V. K. Semenchenko ZhFKh (J. Phys. Chem.) 21, 1461, 1947.

[12] M. P. Vukulovich, Tablitsa, Termodinamicheskie svoistva vody i vodyanovo para (Tables, The Thermodynamic Properties of Water and Water Vapor) 1951.

[13] V. A. Krillin, V. N. Zubarev, Teploenergetika (Heat Energetics) No. 11, 19, 1955.

[14] I. P. Krichevsky, N. E. Khazanova, ZhFKh (J. Phys. Chem.) 29, 1087, 1955.

CONCERNING THE NATURE OF THE THERMAL TRANSFORMATIONS IN THE ALKALI BOROSILICATE GLASSES

D. P. Dobychin and N. N. Kiseleva

(Presented by Academician A. N. Terenin September 18, 1956)

As is known [1-4], the structures of those porous glasses which are obtained by treating the alkali borosilicate glasses with acid solutions depend not only on the original glass composition, but also on the thermal treatment and the conditions of leaching [5, 6]. With a view to solving the problem of controlling the structures of porous glasses, and for the study of the structures of borosilicate glasses, we have undertaken an investigation of the kinetics of those processes which occur during the thermal treatment of a sodium borosilicate glass.

This investigation was carried out through a sorption study of the structures of those porous glasses which were obtained from the thermally treated glass Na-7/23*, use being made of a quartz spiral balance. Water was employed as the sorbate. We have already reported [7] that the pore radius in the porous glasses resulting from leaching of samples of Na-7/23 glass which had been subjected to an extensive thermal treatment at 530°, increased in proportion to the time of treatment. On the other hand, the pore radius and the pore volume in the porous glasses resulting from the leaching of samples which had undergone thermal treatment, even for one half hour, at 650° showed constant values which were not changed by lengthening the time of thermal treatment of the glass.

The independence of the condition of acid leaching and the magnitude of the pore radius and the over-all pore volume in a porous glass which had been thermally treated at 780° indicates that the finely porous silica net which is washed out of the "high temperature" porous glass by alkalies is not a "secondary silicic acid" which had coagulated in the pores during an acid leaching of the glass [8,9].

In 1956 E. A. Porai-Koshits, D. I. Levin and N. S. Andreev [10] showed that the pore size in those porous glasses which resulted from a double leaching (in acid and then in alkali) increased with the length of time of the thermal treatment of the original glass, Na-7/23, thus confirming a fact which is fundamentally important for the understanding of those processes which occur during the thermal treatment of sodium borosilicate glasses.

The present communication is devoted to the presentation of the results which we have obtained from a study of the kinetics and the nature of these processes.

Thermal treatment was carried out on a single batch Na-7/23 glass in two different initial conditions: A) a glass which had been quenched from 850° and B) a glass which had been subjected to a crude annealing by gradual cooling from higher temperatures.

Leaching was carried out at 50° in a 3 N HCl solution, the latter being taken in the proportion 15 cm^3 per 1 g of leached glass (powdered, fraction 100 - 150 μ).

The experimental results are presented in Figures 1 and 2 in the form of curves showing, for the original glasses A and B respectively, the alteration in pore radius and volume as a function of the extent of thermal treatment at various temperatures.

The glass A, which was quenched from 850° had the finest pores ($\sim$ 8 A) and the smallest over-all pore volume (V_s = 0.160 cm^3/g). As the time of the thermal treatment of this glass was increased under temperatures

* Here and in what follows, 7 mole % Na_2O, 23 mole % B_2O_3, and 70 mole % SiO_2.

up to 580°, the magnitude of the pore radius in the resulting porous glasses continually increased, along with the over-all pore volume, up to a definite constant value (Figure 1).

The porous glass which was obtained from the original B glass had a somewhat greater pore radius (47 - 48 A) and over-all pore volume (0.197 cm^3/g) and also a somewhat wider distribution of volume over pore radii, than did the porous glass which was obtained from glass A. The type B glass had slowly solidified from higher temperatures: its structure reflected those processes of growth of chemically inhomogeneous regions which had taken place during the time of cooling.

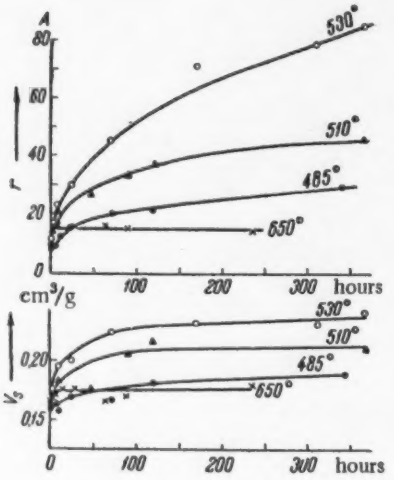

Fig. 1. The dependence of the pore radius and volume in the porous glass on the time and the temperature of the thermal treatment of the original A glass.

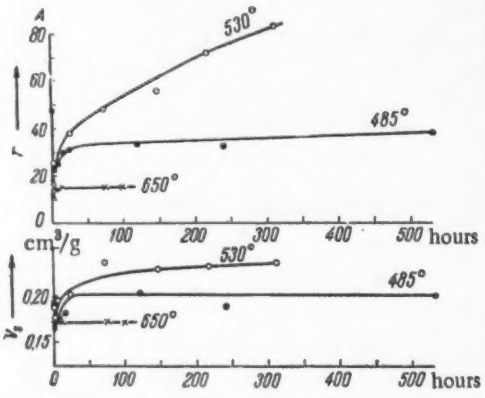

Fig. 2. The dependence of the pore radius and volume in the porous glass on the time and the temperature of the thermal treatment of the original B glass.

The kinetic curves which were obtained for samples of type B passed through an initial minimum (Figure 2). Depending on the time of thermal treatment of the initial B glass, the magnitude of the pore radius of the porous glass at first rapidly falls to a definite minimum value and then again increases. At the same time, the magnitude of the over-all pore volume initially falls and then rises, clearly approaching a value constant for a given temperature. Thus at least two structural processes take place during the thermal treatment of the glass Na-7/23: the first, and more rapid, manifests itself in a decrease in the magnitude of the pore radius and over-all pore volume; the second, and slower, gives rise to a continuous rise in the pore radius and over-all volume, up to a fixed value. The rates of both of these processes rapidly increase with the temperature. Insofar as a process of the first kind is not observed in samples of the type A, we presume that this first (rapid) process is connected with the breakdown of the existing regions of chemical inhomogeneity, the reconstruction of the space lattice of the glass and the reorientation of chemical bonds. On the other hand, that slow process which brings about a continuous growth in the pore size in the porous glass is related to diffusional transfer of matter in the glass.

Around 585° we have found a critical value (or a narrow critical region) of temperature above which a brief thermal treatment of the initial glass (at 650°, one half hour) suffices, in order that the pore radius of the porous glass obtained by acid leaching should take on a constant and, moreover, small value, which is independent of the extent of the thermal treatment (Table 1).

We believe that at this temperature there begins to form in sodium borate regions a continuous silica net, which is not destroyed by the acid [7].

Above 585° the magnitude of the pore radius in the porous glass decreases with an elevation of the temperature of the thermal treatment. Below 730° the opalescence of the glass continually increases in proportion to the length of thermal treatment, although no rapid change in the rate of its propagation can be detected in the 585° region.

An increase in the pore radious at a relatively constant pore volume indicates that there is a decrease, during the course of thermal treatment, in the over-all number of pores in the porous glass and, consequently, in the number of regions of chemical inhomogeneity in the original glass. A decrease in an over-all number of particles with an increase in their mean size points to a process of isothermal distillation and

TABLE 1

The Influence of the Extent of the Thermal Treatment of the Glass Na-7/23 Which Had Been Quenched from 850° (Sample A) on the Magnitude of the Pore Volume and Radius in the Porous Glass Obtained by its Leaching with 3 N HCl at 50°

	Temperature of thermal treatment										
	580°						590°		600°		620°
Time, hours	0	1	5	48	120	480	48	240	120	264	48
V_s, cm³/g	0.160	0.171	0.180	0.213	0.244	0.291	0.180	0.177	0.174	0.162	0.176
r, A	~8	15	34	39	170	200	19	20	24	18	15

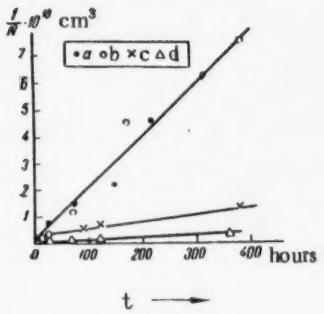

Fig. 3. The dependence of the magnitude of the unit volume, 1/N, on the time of thermal treatment $t\left(\frac{1}{N}=\frac{1}{N_0}+kt\right)$ a) Initial, 530° b) Quenched, 530° c) Quenched, 510° d) Quenched, 485°

condensation. Supposing that the processes which are taking place in the investigated glasses result from the attempt of these systems to attain thermodynamic equilibrium, we consider the following analogy to be in order. As O. M. Todes has shown [12], the kinetics of the condensation process are described by equation [1], which is formally analogous to the Smolukhovsky equation for the coagulation of colloidal particles, but differs from it in the value of the velocity constant.

$$\frac{1}{N}=\frac{1}{N_0}+k\cdot t. \qquad (1)$$

Here, N is the number of particles per unit volume of the system at the time t; N_0 is the number of particles per unit volume at the initial time; and k is the velocity constant for the process.

Equation (1) has a statistical character and is strictly valid only after a definite time interval, during which the system enters into a stationary type of distribution. This period is the shorter, the higher the temperature.

Supposing the pore form to be close to that of a sphere, the number of pores (and, accordingly, the number of leached regions of chemical inhomogeneity, as well) in 1 cm³ of porous glass can be calculated from the equation

$$N=\frac{V_s}{\frac{4}{3}\pi r^3}\cdot\frac{1}{\frac{1}{\Delta}+V_s}, \qquad (2)$$

where V_s is the over-all volume, r is the pore radius of the investigated porous glass and $\Delta = 2.18$ g/cm³ is the specific gravity of the "baked" porous glass (quartzite).

The calculated results are shown in Figure 3 in the coordinates 1/N, T; where 1/N is the magnitude of the unit volume.

It is clear from Figure 3 that the kinetics of the process of the growth of those regions of chemical inhomogeneity which are leached out by the acid is quite satisfactorily described by the equation (1) of O. M. Todes. In Table 2 there are presented values for the velocity constant of condensation at various

TABLE 2

Glass	t, °C	k, cm^3/hour · 10^{30}
A	485	0.0965
	510	0.27
	530	2.04
B	485	0.0667
	530	1.99

temperatures, these being determined from the slopes of the straight lines 1/N (t).

The mean value of the apparent energy of activation of the condensation process in glass Na-7/23 proves to be equal to 90 kcal/mole, which clearly indicates a connection with processes of viscous flow in the glass [13].

A deciphering of the nature and the kinetics of those processes which occur in sodium borosilicate glass during its thermal treatment would open up the possibility for the controlled production of porous glasses having a specified structure, including those which are bidispersing and which have wide pores (with radii of the order of hundreds or thousands of A).

Received September 10, 1956

LITERATURE CITED

[1] I. V. Grebenshchikov, T. A. Favorskaya Tr. GOI (Trans. State Optic. Inst.)7, No. 7, 1931.

[2] I. V. Grebenshchikov; Mat. soveshch. po stekloobraznomu sostoyaniyu (Material, Conference on the Glassy State) Leningrad, 1939.

[3] I. V. Grebenshchikov, O. S. Molchanova ZhOKh (J. Gen. . Chem.) 12, 588, 1942.

[4] O. S. Molchanova, Dissertation, Leningrad, 1943.

[5] L. A. Kachur, Dissertation, Leningrad, 1946.

[6] S. P. Zhdanov, Dissertation, Leningrad, 1949.

[7] D. P. Dobychin, Stroenie stekla, Tr. soveshch. po stroeniyu stekla (The Structure of Glass; Trans. Conference on the Structure of Glass) 1953; Izd. AN SSSR (Acad. Sci. USSR Press) 1955, Page 176.

[8] S. P. Zhdanov, Stroenie stekla, Tr. soveshch. po stroeniyu stekla (The Structure of Glass; Trans. Conference on the Structure of Glass) 1953; Izd. AN SSSR (Press Acad. Sci. USSR) 1955, Page 162.

[9] E. A. Porai-Koshits, S. P. Zhdanov, D. I. Levin, Izv. AN SSSR OKhN (Bull. Acad. Sci. USSR, Div. Chem. Sci.) 1955, No. 3, 395.

[10] E. A. Porai-Koshits, D. I. Levin, N. S. Andreev, Izv. AN SSSR OKhN (Bull. Acad. Sci. USSR, Div. Chem. Sci.) 1956, No. 3, 287.

[11] D. I. Levin, S. P. Zhdanov, E. A. Porai-Koshits, Izv. AN SSSR OKhN (Bull. Acad. Sci. USSR, Div. Chem. Sci.) 1955, No. 1, 31.

[12] O. M. Todes, Dissertation, Moscow, 1944; Problemy kinetiki i kataliza (Problems of Kinetics and Catalysis) 7, 137, 1949; Koll. Zhurn. (Colloid. J.) 15, 391, 1953.

[13] V. A. Florinskaya, Tr. GOI (Trans. State Optic. Ins.) 19, No. 131, 1950.

THE THERMODYNAMICS OF THE REACTION OF DEPHOSPHORIZATION OF IRON

I. Yu. Koshevnikov and L. A. Shvartsman

(Presented by Academician G. V. Kurdyumov November 5, 1956)

A great deal of work has been devoted to the investigation of the distribution of phosphorus in the metal–slag system [1-4]. Because of experimental difficulties, however, exact values have not been obtained for the thermodynamic functions for the reaction of dephosphorization of iron by slags of various compositions.

In the present work there has been applied a new method for investigating the equilibrium distribution of phosphorous [5] which, in principle, amounts to the successive saturation of the metal at constant temperature with radioactive phosphorus which had been initially introduced into the slag. From the temperature dependence of the distribution coefficient of the phosphorus L_P, it is possible with this method to calculate, not only the heat effect, but also the entropy change in the dephosphorization reaction with a slag of definite composition.

For any choice of molecular composition of the molten slag, the equilibrium constant for the reaction

$$P + {}^5/_2 Fe^{++} + 4O^{--} \rightleftarrows PO_4^{-3} + {}^5/_2 Fe \qquad (1)$$

can be written in the general form:

$$K_a = L_P \varphi (\sum C_i) f (\sum \gamma_i), \qquad (2)$$

where $\varphi (\Sigma C_i)$ is the ratio of the equilibrium concentrations of those substances, with the exception of phosphorus, which participate in the reaction and $f (\Sigma \gamma_i)$ is the ratio of the activity coefficients of all of the participants of the reaction. These functions are of unknown form. Under the experimental conditions, however, $\varphi(\Sigma C_i)$ does not depend on the temperature. Accordingly

$$\frac{d \ln K_a}{dT} = \frac{d \ln L_P}{dT} + \frac{d \ln (\Sigma \gamma_i)}{dT}, \qquad (3)$$

from which

$$\frac{d \ln L_P}{dT} = \frac{\Delta H^0 - \Sigma \Delta H_{mix}}{RT^2} = \frac{\Delta H}{RT^2}. \qquad (4)$$

The quantity ΔH, which is determined from the equation

$$\log L_P = -\frac{\Delta H}{4{,}573\, T} + B, \qquad (5)$$

proves to be equal to the heat change, ΔH^0, for the reaction between the pure substances plus the heats of mixing, $\Sigma \Delta H_{mix}$.

As standard states there have been taken 1% solutions of the phosphorous in the metal and in the slag. The quantity B is then equal to $\Delta S^0/4.573$ where ΔS^0 is the entropy change for the transfer of phosphorus from the 1% iron solution into the 1% slag solution. The quantities ΔH and ΔS^0 depend on the slag composition.

Experimental fusions were carried out in the induction furnace of the apparatus which is schematically represented in Figure 1. About 50 g of electrolytic iron was introduced into the magnesite crucible 1 which was fixed in the cup 3 by the magnesite filling 2. Through the quartz tube 4 in the water-cooled metallic cap 5 there was carried out the introduction of purified nitrogen and the measurement of the temperature of the molten iron, use being made of the prism 6 and an optical pyrometer of the MOPT - 48 type. Through the funnel 9 slag containing radioactive phosphorus (P^{32}), was delivered onto the surface of the molten iron 8 at constant temperature. This slag rapidly fused and passed through the walls of the cruicible 1 into the filling. A definite quantity of the P^{32} was thereby transferred from the slag into the iron. Decision as to the attainment of equilibrium in the phosphorus distribution was based on the constancy of the activity in 3-4 metallic samples which were removed by suction through the 2 mm quartz tube 10.

The quantity L_P was calculated as the ratio of the count rates for slag powders and for metallic samples from "thin layers." The magnitude of the errors of determination amounted to ± 1.8% for L_P and ± 2.7% for ΔH. Experiments were carried out over the temperature interval 1560-1810°.

As the simplest standard system there was chosen a ferrous slag into which those cations (Ca^{++}, Sr^{++} and Ba^{++}), which markedly differ from one another in regard to radii, had been introduced in the form of oxides.

The data on the distribution of phosphorus between the iron and the ferrous slag is described by the equation

$$\log L_P = \frac{10900}{T} - 6.41, \tag{6}$$

according to which the magnitude of ΔH is equal to -50,000 cal/ g-atom. In this case

$$K_a = AL_P \frac{\gamma_{PO_4^{-3}}}{\gamma_P}, \tag{7}$$

where A is a coefficient for passing from weight percentages to mole fractions.

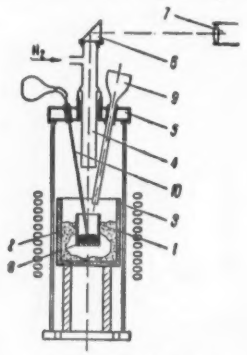

Fig. 1. Diagram of the apparatus.

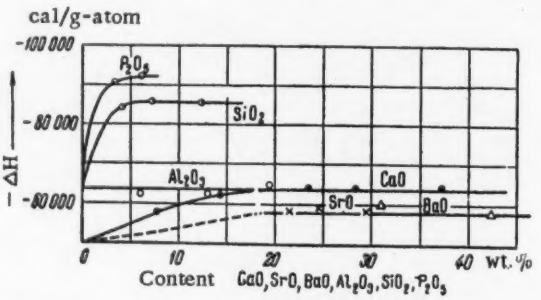

Fig. 2. The relation between ΔH for the dephosphorization reaction and additions of CaO, SrO and BaO to the ferrous slag and of SiO_2, P_2O_5 and Al_2O_3 to calcio-ferrous slag.

From the temperature dependence of K_a we find

$$\Delta H^0 = \Delta H + \Delta H_{mix}^{PO_4^{-3}} - \Delta H_{mix}^{P}. \tag{8}$$

ΔH_{mix}^{P} remains unchanged for slags of more complex composition since a solution of phosphorus in iron

is ideally dilute at small concentrations. Thus an alteration in the value of ΔH, as determined for slags of more involved structure, is a mere reflection of an alteration in the magnitude of the heat of mixing of P_2O_5 with the slag melt.

The cation Ca^{++}, as well as those of Sr^{++} and Ba^{++}, possessing larger radii than Fe^{++}, increase the heat of Reaction (1) by 14,000 and 9,000 cal/g-atom, respectively (Fig. 2). This does not lend support to an assumption of the formation of phosphates of Ca, Sr and Ba during dephosphorization, but rather indicates an increase in the stability of the PO_4^{-3} ion. Up to a certain definite limit there is possible a gradual replacement of the Fe^{++} positions in the PO_4^{-3} coordination sphere by Ca^{++}, Sr^{++}, or Ba^{++}; beyond this the composition remains constant. At the same time ΔH for Reaction (1), gradually increasing, reaches a definite value which is also invariant. The maximal value of the heat change accompanying Reaction (1) is observed for FeO—CaO melts. The failure of ΔH to increase on replacing CaO by SrO or BaO can be explained with the help of the following assumptions. In the sequence Fe^{++}, Ca^{++}, and as a result of the particular ratio of radii, "closed" quasi-crystalline structures are to be anticipated in those micro-regions of the slag melt which contain the phosphate ion [6].

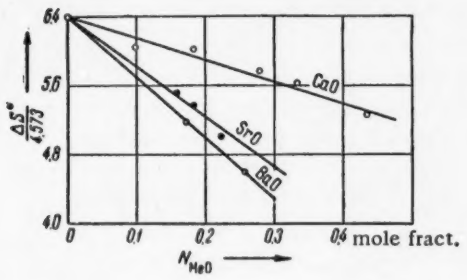

Fig. 3. The influence on the entropy change in the dephosphorization reaction of additions of CaO, SrO and BaO to the ferrous slag.

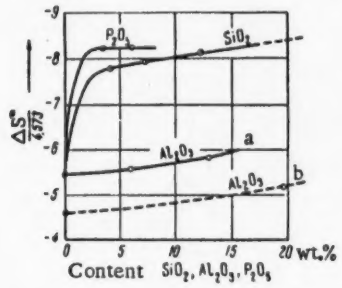

Fig. 4. The influence on the entropy change in the dephosphorization reaction of additions of SiO_2, P_2O_5 and Al_2O_3 to the calcio-ferrous slag.

$$a - \frac{\%\ CaO}{\%\ FeO + \%\ Fe_2O_3} = 0.4;$$

$$b - \frac{\%\ CaO}{\%\ FeO + \%\ Fe_2O_3} = 2.05$$

Similar structures are observed in cubic lattice crystals when the ratio R_{cation} / R_{anion} is less than 0.414 [6]. In the sequence under consideration this ratio is less than 0.39 and amounts, respectively, to $R_{Fe^{++}}/R_{PO_4^{-3}} = 0.303$ and $R_{Ca^{++}}/R_{PO_4^{-3}} = 0.387$. For a "closed" structure, weakening the electrostatic force of the cations leads to a strengthening of the covalent P-O bond in the phosphate ion and this appears to be the cause of the increase ΔH for Reaction (1).

The cations of Sr^{++} and Ba^{++} are larger than Ca^{++} and with the introduction of these into the ferrous slag the quasi-crystalline structures in the above-mentioned micro-regions of the melt clearly open up, since the ratio R_{cation}/R_{anion} in this case exceeds 0.414 and amounts to 0.465 and 0.523. As a result there arise in the melt cation – cation and anion – anion repulsive forces which increase the energy of fusion and, at the same time, compensate for the energy gain arising from the interaction of the anions with the relatively weak cations Sr^{++} and Ba^{++}.

It has been found that an increase in the concentration of CaO or of SrO or BaO in the ferrous slag leads to a continuous increase in the entropy change for Reaction (1). Thus there is an increase in the entropy change of Reaction (1) with an increase of cation radius in the order Fe^{++}, Ca^{++}, Sr^{++}, Ba^{++}, this corresponding to a loosening of the "structures" of the slag melt, i.e., to an increase in the "free volume" in which the relatively large PO_4^{-3} ions can be distributed. Analysis of the experimental data also shows that at a fixed molar concentration of CaO, SrO or BaO in the ferrous slag, the dephosphorizing ability of the oxides increases with the cation radius.

The quantitative influence of CaO on L_P can be expressed by the following equation, valid for $N_{Ca^{++}}$ greater than 0.18:

$$\log L_P = \frac{14\,000}{T} - 6.41 + 2.5\,N_{Ca^{++}}, \qquad (9)$$

where N_{Ca}^{++} is the ion fraction of calcium (according to M. I. Temkin [7]) and 6.41 is the entropy term of Equation (6).

Thus the cations Ca^{++}, Sr^{++} and Ba^{++} aid dephosphorization by increasing both ΔH and ΔS^0. For the relatively weak cations Sr^{++} and Ba^{++}, however, the influence of the entropy factor is, in comparison with that of the energy factor, more pronounced than is the case with the stronger Ca^{++} cation.

The acid oxides SiO_2 and P_2O_5 exert a substantial influence both on the thermal effect and on the entropy change of Reaction (1). Addition of SiO_2 or P_2O_5 into the slag of the FeO-CaO system at $N_{Ca}^{++} > 0.18$ leads to an increase of ΔH for the dephosphorization reaction (see Figure 2). This can be interpreted by supposing that the PO_4^{-3} ions which are formed through Reaction (1) unite in the slag either with the SiO_4^{-4} and the PO_4^{-3} groups or with the more involved silicon -phosphorus- oxygen complexes. It is clear that the process of polymerization is accompanied by the liberation of heat, this also being a cause for the increase ΔH for reaction (1). Confirmation of this is the sharp decrease in the entropy of reaction (1) which goes along with an increase of the concentation of SiO_2 or P_2O_5 in the FeO-CaO slag (Figure 4).

It is important to note that for the dephosphorization reaction the relationship between the energy and the entropy factors is such that with additions of SiO_2 or P_2O_5 to the FeO-CaO slag, increasing concentration in the first case decreases the magnitude of L_P and in the second increases it.

Data on the influence of alumina shows that ΔH for the reaction of dephosphorization is not changed by the addition of Al_2O_3 to the slag of the FeO-CaO system (see Figure 2). With the rise in the concentration of Al_2O_3 there is observed, however, a steady decrease in the entropy, without any sort of abrupt concentration change (see Figure 4). This corresponds to the fact that the acid properties of Al_2O_3 are weaker than those of SiO_2 or P_2O_5 and, at the same time, points to the presence in the investigated melts of aluminum in the anionic form.

The results of this investigation show that an important influence on the equilibrium in the anionic [8] dephosphorization reaction is exerted by the entropy factor in the free energy expression, this factor depending on the magnitude of the charges and on the mutual positions of the ions in the slag melt.

The Institute of Metallography and Metal Physics
of the Central Scientific-Research Institute
of Ferrous Metallurgy

Received October 25, 1956

LITERATURE CITED

[1] T. B. Winkler, I. Chipman, Met. Technol., April (1946).

[2] K. Balajva, A. Quarell, P. Vajragupta, J. Iron Steel. Inst. 153, 115 (1946).

[3] V. A. Kamensky, E. V. Abrosimov, Sborn. tr. Mosk. inst. stali (Collected Trans. Moscow Steel Inst.), 12, 1939.

[4] W. Fischer, H. Ende, Stahl u. Eisen, 72 (23), 1398 (1952).

[5] V. F. Surov, O. V. Travin, L. A. Shvartsman, Problemy metallovedeniya i fiziki metallov (Problems of Metallography and the Physics of Metals) Collection (1955), 4.

[6] L. Pauling, Priroda khimicheskoi svyazi (The Nature of the Chemical Bond) 1947.

[7] M. I. Temkin ZhFKh (J. Phys. Chem.) 20, 105, 1946.

[8] H. Flood, K. Grjotheim, J. Iron Steel Inst., 171(1), 64 (1952).

CONCERNING THE DENDRITIC CRACKS WHICH DEVELOP IN PLEXIGLAS UNDER THE ACTION OF ELECTRONIC IRRADIATION*

B. L. Tsetlin, N. G. Zaitseva and Academician V. A. Kargin

During an investigation of the transformations which take place in specimens of polymethyl acrylate (the samples studied were of Plexiglas, a technical organic glass, based on polymethyl acrylate) under the action of high energy radiation, we discovered that in a number of cases cracks of unique dendritic form originated and developed in these specimens.

This phenomenon attracted our attention since an elucidation of the cause and the mechanism of the disintegration of structural materials resulting from the action of radiation of this type would be of great significance in solving the problem of the application of such substances under working conditions which involve radioactive radiational activity. In the course of further investigation, there were established a number of features of the development of these dendritic cracks, all of which point to the fact that a truly new phenomenon is here under observation, one which is not similar to any of the known processes of crack formation in plastic masses.

This phenomenon is characterized by the following:

1. The dendritic cracks originate and grow only in the event that a defect is present in the specimen--either one which has been artifically "induced" or one which, existing independently, is related to the technological history of the sample (to its mechanical treatment, for example).

2. The development of the dendritic cracks in specimens of organic glass proceeds with a definite velocity which is proportional to the dose strength. Originating at the mechanical defect, the dendritic cracks gradually and uniformly embrace the whole irradiated area of the specimen. The external form of the cracks and the process of their development in samples of Plexiglas are shown in Figures 1 a, b and c (the mechanical defect was originally induced into the specimen with a punch).

3. When several defects are present in a specimen there is a simultaneous development of several dendrites, the branches of which do not mutually intersect or intertwine. A clear-cut boundary forms between those branches of different dendrites which are growing outward toward one another (Figure 1 d).

4. Cracks develop only in the irradiated portion of a specimen. This is shown in Figure 1, e (the ring-shaped section of this specimen which is not penetrated by the cracks was covered, during exposure, by a metallic ring; in the course of their development the cracks bypass this sector as if it were a kind of impediment).

5. The formation and the development of dendritic cracks in Plexiglas is observed only under the action of high speed electrons. Cracks do not appear as a result of x-ray irradiation.

6. The dendritic cracks arise only in those specimens for which the thickness is in excess of that depth of material which is penetrated by the electron beam. The accelerator, which served as the source of high speed electrons in our experiment, so functioned (700 Kv potential) that the minimal thickness which was adequate for crack development amounted to 1.7-2 mm.

---

* This work was carried out in 1950-51; the results were presented in a report of the Institute of Physical Chemistry of the Academy of Sciences of the USSR, No. 676 (April, 1953).

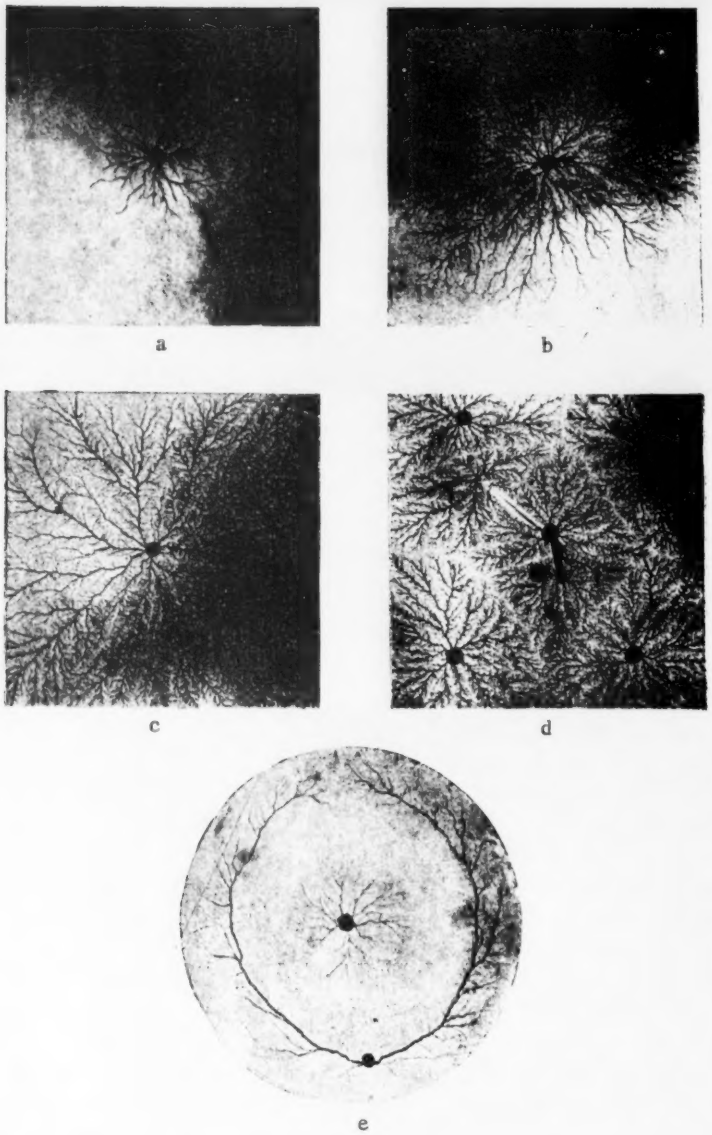

Fig. 1. The character of the development of the dendritic cracks in Plexiglas (dose strength, 1.9×10^{18} ev/cm^3·sec; specimens photographed in transmitted light: a, b, c) Crack distribution in a specimen with a single "defect" (irradiation of 10 sec, 1 min and 15 min, respectively); d) Crack system in a specimen with several "defects" (15 min irradiation); e) Cracks in a specimen, a ring-shaped section of which was covered with a screen during exposure (5 min irradiation).

7. The nature and the rate of the process of development of the dendritic cracks are uniquely determined by the distribution of the defects and the dose strength; they do not depend on those internal strains which can exist in the glass-like polymer. Thus on irradiating a specimen of Plexiglas which had been previously annealed by heating for many hours at a temperature of 130° C, the net of dendritic cracks which developed (naturally, after the induction of a mechanical defect) was the same as that which resulted from the irradiation of

unannealed specimens. This same net of cracks also developed in a specimen which had been previously strongly strained at 130° and then rapidly cooled; there was a complete absence of any tendency toward "orientation" of the cracks in the direction of the internal strain (the presence of such strain was established by viewing the sample through crossed polaroid plates).

8. The dendritic cracks are internal cracks and do not appear on the surface of the specimen. This fact was established by direct microscopic investigation of the samples.

9. These cracks are "empty"; they are not "canals" through which gases formed during irradiation of the Plexiglas can escape into the surrounding atmosphere. This follows from the observation that the cracks are readily colored during their growth, i.e., they fill up with dye solution if the latter, during irradiation of the specimen, is in contact with the defect from which the cracks originate. This phenomenon was studied in experiments which were carried out with the irradiated specimens placed in a flat cell (of a depth somewhat less than their thickness) which was filled with an aqueous methyl violet solution (in this case the defect was induced on the side surface of the specimen).

10. The rate of crack growth decreases with an increase in the temperature under which the specimen is irradiated, as is shown in Figure 2. This indicates that relaxation phenomena play a definite role in the process of the development of the dendritic cracks.

It has been further established that this process of development of dendritic cracks under the action of high speed electrons is common to all organic glasses • which underscores the interest attaching to the phenomena here described.

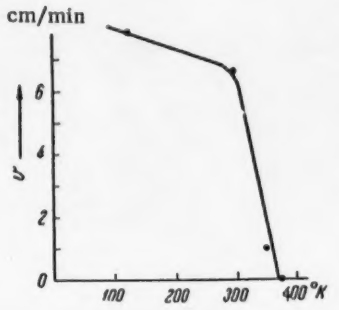

Fig. 2. The relation between the temperature and the rate of propagation of dendritic cracks in Plexiglas. Dose strength 1.9×10^{18} ev / $cm^3 \cdot sec$.

The experimental data which as been obtained is clearly insufficient to warrant drawing definite conclusions regarding the mechanism of the process which is under discussion. However, the observations which have been made permit certain preliminary conclusions as to the probable causes of this phenomenon.

It is obvious that the cracks arise as a result of the appearance of internal strains in the irradiated material, these causing the destruction of the specimen at its points of greatest weakness, which are the openings of those micro-cracks which are formed during the induction of the mechanical defect. The dendritic character of the developing cracks is related to the fact that the strains which arise from the action of irradiation are uniformly distributed across that entire section of the specimen which is perpendicular to the direction of the electron beam. For the complete development of the crack net, this leads to equality of the sums of the crack areas in each element of specimen surface, regardless of the distance of this element from the defect. At any one time, irregularity in crack growth at various points in a specimen is caused by the fact that crack growth can begin only at a defect position. Spreading in this way, beginning with a defect, the crack gradually distributes itself throughout the entire specimen and in the course of its development, being itself nonhomogeneous ("defective"), it undergoes branching. Thus the cracks are larger in those elementary sections where their absolute number is small and, where there are many of them (as a result of branching), their mean size is smaller, which, in turn, fixes the dendritic form.

For the elucidation of the possible causes of the phenomenon under consideration it is important to note that the crack development is closely connected with the existence of a clear-cut boundary between the irradiated and the nonirradiated layers of the specimen; this follows directly from the previously adduced characteristics of the crack development. It is obvious that on this boundary there arise mechanical strains; in part, because of volume contraction of the Plexiglas resulting from its radiochemical destruction (it is known that this is

• Data on crack development in various organic glasses will be separately reported.

accompanied by the liberation of a large quantity of gaseous products; see, for example [1, 2]) and, in part, because of an accumulation of electronic charge. In the formation of these strains, it is likely that a large role is played by the low molecular products from the radiochemical disintegration of the polymer, these products forming supersaturated solutions throughout the entire specimen volume. These low molecular products can be adsorbed in the openings of those micro-cracks which are present in the "defective" specimen. The molecules of such products, adsorbed near the boundary of the layer of material which is traversed by high speed electrons, can have an excess of like charges (because of the capture of electrons which have been decelerated in the specimen). The electrostatic interaction of these charges also brings about, in all likelihood, a further growth in the micro-cracks, from which there are again formed "fresh" surfaces for adsorption, and so forth. The branched crack system of dendritic form appears as the result of this process which is continually taking place during the action of irradiation.

The Institute of Physical Chemistry
of the Academy of Science of the USSR

Received November 16, 1956

LITERATURE CITED

[1] V. A. Karpov, Session of the Academy of Sciences of the USSR on the Peaceful Uses of Atomic Energy, July 1-5, 1955; Meeting of the Section on Chemical Science. Acad. Sci. USSR Press, 1955, page 3.

[2] P. Alexander, A. Charlesby, M. Ross, Proc. Roy. Soc., 223, 392 (1954).

THE ROLE OF THE GASEOUS MEDIUM IN PROCESSES OF DISINTEGRATION OF COAL

I. L. Ettinger, E. G. Lamba and V. G. Adamov

(Presented by Academician A. A. Skochinsky June 6, 1956.)

Much practical interest attaches to the question of the influence on the mechanical properties of coal of the gaseous medium in which the coal exists in most beds. This consideration was responsible for the initiation of work toward the explanation of the role of the gaseous medium in the processes of disintegration of coal. The technique applied in this work has been described in an earlier communication [1]. In the present investigation there has been studied the relation between the effect of the gaseous medium on the strength of pit coals and the natural dislocations in their structure, or the extent of their metamorphism, as well as the effects of different gases.

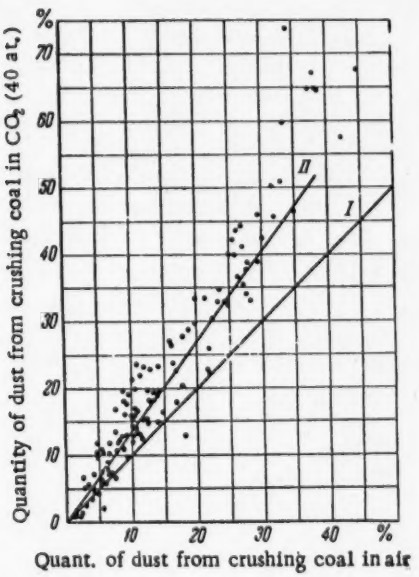

Fig. 1. The relation between the crushing of coal in the coal-air and the coal-CO_2 systems.

Those manifold defects which are concentrated at the weak points of solid bodies exert a pronounced influence on their mechanical properties. These defects can be of very different magnitudes, ranging from imperfections in the crystal lattice up to visible fissures or cracks. Surface defects are particularly important for such a highly porous body as coal, since the latter, in the bed, exists in a gaseous medium which it is capable of adsorbing readily on its surface.

The work of P. A. Rebinder and his collaborators [2, 3] has shown that adsorbed molecules penetrate into the depth of a solid by two-dimensional migration through positions of weakened bonds and along thin, incompletely developed fissures. As a result of the decrease in surface tension, these adsorbed molecules aid in the development of new surface defects, or micro-fissures, and prevent these latter from again fusing together. These ideas, which have been developed for the solid-liquid system, can be extended to the coal-gas system. During deformation new interfaces are formed which penetrate into the coal as wedge-shaped cracks. In the presence of an easily adsorbed gas, these newly originated surfaces become covered with adsorbed layers. The penetration of such layers is hindered by steric factors, in the event that the width of the cracks is less than the dimensions of the adsorbed molecules.

The natural micro-cracks are defects which, as a result of gas adsorption, bring about a decrease in the strength of pit coals in the bed. The initial conditions of formation of coal beds and the subsequent tectonic processes lead to the appearance in these beds of separate sections of high degree of structural dislocations [1, 4]. As the degree of dislocation in the coal rises, the depth of the micro-cracks increases and the mean distance between them diminishes.

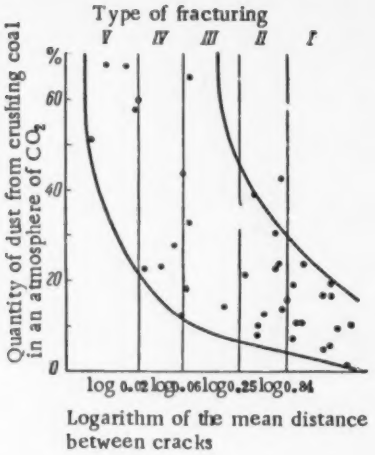

Fig. 2. The relation between the natural fracturing of coal and its crushing in the coal-CO_2 system.

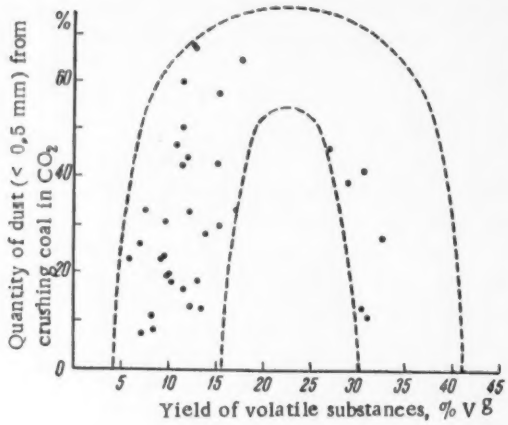

Fig. 3. The influence of the extent of metamorphism on the crushing of fractured coals (fracture types IV and V) in CO_2.

We have carried out investigations of the strength of the coals in a group involving five types of structural dislocations (more than 100 specimens). The coal hardness was determined in air, CO_2 and CH_4 at a pressure of 40 atmospheres. Carbon dioxide, as well as methane, is characterized by physical adsorption. The coal samples were tested in air after they had been degassed of methane following their removal from the bed.

In Fig. 1 there has been plotted on the axis of abscissas the amount of dust which is formed during crushing of the coal in air (in percent of sample weight) and on the axis of ordinates the quantity of dust formed during crushing in CO_2.

In the absence of action of the carbon dioxide gas on the coal, the quantity of the dust in two experiments would be the same, i.e., the points corresponding to the various specimens should be distributed with a definite spread around the straight line I. However, the points fall above this line and in such a way that they depart from it more and more as the yield of dust in air increases. The physical meaning of this phenomenon is the following: the hard coals with low degree of fracturing do not possess those concealed defects (micro-cracks) on which the gases might act in the direction of decreasing hardness. Coals with a higher degree of fracturing, ones which are easily crushed, even without the action of a gaseous medium, are characterized by a large number of micro-cracks along which gas can penetrate from the external medium. As a result of such penetration, the hardness of weak coals is still further diminished, sometimes by a factor of two, in comparison with the hardness of the coal in air.

The experimental points which cover the relation between the yields of dust in air (Q_{air}) and in carbon dioxide (Q_{CO_2}) are distributed around the straight line II. By the method of least squares it is possible to find the magnitude of the coefficient k in the equation of this line

$$Q_{CO_2} = kQ_{air} \qquad (1)$$

The result thus obtained is k = 1.34.

In Figure 2, in semi-logarithmic coordinates, there has been plotted the mean distance between cracks (as a measure of the fracturing in the coal) and the yield of dust in an atmosphere of CO_2. The relationship between the fracturing of the coal and the dust yield is here quite obvious.

Because of the diminution of the free surface energy through gas adsorption, there is a penetration of gas into the original micro-fissures of tectonic and endogenic origin and additional deformation arises there from the splitting effect of these adsorbed layers. Thus it is not only on the large surfaces, but in the micro-fissures as well, that disintegration of the coal takes place as the result of the mechanical interaction which occurs in the gaseous medium. If such initial disintegration is lacking in the coal, the gas itself is unable to bring about the appearance of new gas-coal interfaces to facilitate the disintegration of the coal along new surfaces.

In analogous experiments which were carried out in the coal-methane system, the observed effect was

the same as in the coal-CO_2 system, but not so pronounced. The mean increase in the dust yield in methane, as compared with air, was equal to 1.25.

In the coal bed, where the coal is saturated with gas under natural conditions, the influence of the gaseous medium on the coal strength is manifest in the following way: the reported instances of the softening of coal by gassing of the cut amount, , not to a softening, but rather to a failure of the coal to harden. On the edge of the coal seam there is formed a very thin layer which is almost 100% methane. Under active ventilation this layer is, as it were, continually stripped away. The yield of gas from those coal layers which are close to the front of the face is thereby considerably increased while the rate of diffusion of gas out of the depth of the coal in the seam toward the edge of the face lags behind the rate of gas evolution in the working. The gas pressure in the pre-face zone of the seam accordingly falls somewhat, the loosening action of the adsorbed gas in the micro-cracks diminishes and the miner is subjectively aware of an effect of coal hardening. When, however, the ventilation is cut off, its stripping action ceases and the coal no longer hardens.

It is an interesting question as to whether it is possible in a laboratory experiment to bring about the fusion of the micro-cracks by uniform compression of the coal. A diminution of these micro-cracks should diminish the effect of the action of the gaseous medium. Experiments were carried out in a high-pressure apparatus, the coal being placed in oil. To prevent this oil from penetrating into the coal, the specimens were wrapped in thin sheets of rubber. Uniform compression of the samples was carried out at pressures of 1000, 2000, 3000 and 4000 kg/cm^2. No difference was noted, however, in the action of the gaseous medium on the compressed and on the uncompressed specimens. The differences in the results of their crushing fell within the limits of this usual distribution of data. It is obvious that the adsorbed gas layers which remain in the micro-fissures do not permit these to close up under uniform compression.

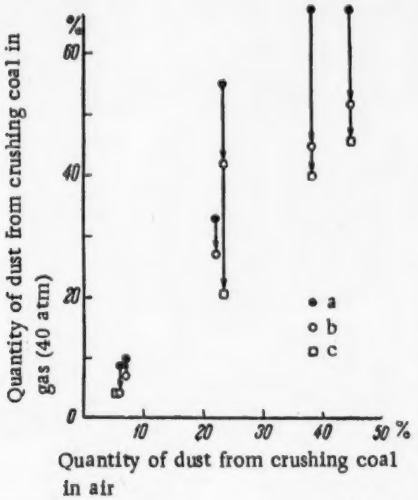

Fig. 4. The decrease in the strength of coals resulting from their saturation with various gases. Experiments: a) Carbon Dioxide, b) Methane, c) Hydrogen

Within the limits of a single petrographic type the less stable coals are those of an intermediate degree of metamorphism (K or PS). The younger and the older coals possess higher stability under mechanical action [5].

In order to follow the connection between the effect of gas action on the strength of coals and the extent of their metamorphism, coals have been compared which had the same degree of fracturing but different yields of volatile substances.

In Figure 3 (coals of types IV and V fractures) the greatest yield of dust is observed for coals of intermediate degrees of metamorphism; this is in agreement with the results of other authors. The natural fracturing of pit coals is a basic factor in the softening action of gas on the coal. The extent of metamorphism under a single type of fracturing is similarly reflected in the mechanical properties of the coal in the system air-coal and in the system (easily adsorbed) gas-coal.

Adsorbed layers distribute themselves over the surface of a solid body by two-dimensional migration of surface-active molecules. When the gas approaches the openings of the micro-fissures, those molecules which are most firmly adsorbed on the surface of the coal will leave behind all of the other molecules and will insure the greatest effect of the action of the gaseous medium. In such a case the highest activity must be shown by the gas which is best adsorbed. If this adsorption effect were lacking, the greatest activity would be associated with the gas of smallest molecular dimensions.

In Figure 4 there are shown the results of the diminution of the mechanical strength of pit coals under the action of various gases. The highest activity is found with carbon dioxide, followed by methane, whereas hydrogen is practically without influence, although the effective diameters of the molecules are: H_2 2.74 A, CH_4 4.14 A, and CO_2 4.59 A. The sorptive capacity of coals with regard to these gases also decreases in the

order CO_2, CH_4, H_2. This confirms the correctness of the picture which has been obtained of the sorptional action of gases on the mechanical properties of coals.

In conclusion, we consider it a pleasant duty to express our thanks to L. E. Shterenberg for his aid in the selection of coal samples and in their classification and to V. S. Voblikov for help in carrying out the experiments on the uniform compression of the coals.

Received June 5, 1956

LITERATURE CITED

[1] I. L. Ettinger, E. G. Lamba, V. G. Adamov, DAN (Proc. Acad. Sci., USSR) 49, No. 6, 1057, 1954.

[2] P. A. Rebinder, L. A. Shreiner, K. F. Zhigach, Poniziteli tverdosti v bureny (Reducers of Hardness in Drilling) Izd. AN SSSR (Acad. Sci. USSR Press, 1944).

[3] L. A. Shreiner, Tverdost khrupkikh tel (The Hardness of Brittle Bodies) Izd. AN SSSR (Acad. Sci. USSR Press, 1949).

[4] I. L. Ettinger, E. S. Zhupakhina, L. E. Shterenberg, V. S. Yablokov, Tr. Soveshch. po razrabotke ugolnykh mestorozhdeny na bolshikh glubinakh (Proceed. Conference on the Working of Coal Veins at Great Depths) 1955.

[5] E. M. Taits, V. E. Koifman, Z. S. Tyabina Tr. Geol.-issled. byuro Ministerstva ugoln. prom. (Proceed. Geological-research Bureau of the Department of Coal Mining) Vol. 4, 1948.

THE MECHANISM OF POLARIZATION DURING POLAROGRAPHY OF THE SIMPLE IONS OF NICKEL AND COBALT

Ya I. Turyan

(Presented by Academician A. N. Frumkin September 15, 1956)

Insufficient study has been given to the problem of the mechanism of polarization during polarography of those ions of Ni^{2+} and Co^{2+} which give rise to the so-called irreversible waves. There is even very little data to be found in the literature on the polarographic characteristics of the simple ions of Ni^{2+} and Co^{2+} in the presence of various "indifferent" electrolytes. This has led to a number of contradictory results. Thus, $\varphi_{1/2}$ Co^{2+} in some works [1, 2] is equal to −1.23 v, whereas in others [3] it is equal to −1.44 v (normal calomel electrode).

In reference [4] there was investigated the polarization during the polarography of the simple ions of Ni^{2+} and Co^{2+} with a background of 0.1 M KNO_3. Certain data [4], in particular the slope of the straight line $\varphi, \log\frac{i}{i_d - i}$, speak for the applicability of the theory of delayed discharge as an explanation of the mechanism of polarization. For further testing of the theory of delayed discharge it was very important to investigate the influence of the nature and the concentration of the background and to this problem the present work is devoted.

This investigation* was carried out in an apparatus of the manual type with the normal calomel electrode for reference. The reference electrode and the measuring devices were standardized from the polarogram of Tl^{+} in 1 M KNO_3. The temperature of the measurements was 25 ± 0.3°. For the study of Ni^{2+} the capillary characteristic was $m^{2/3}t^{1/6} = 1.60\ mg^{2/3}\ sec^{-1/2}$; for the study of Co^{2+} it was $m^{2/3}t^{1/6} = 1.02\ mg^{2/3}\ sec^{-1/2}$. The resistance of the cell was determined from the polarogram of Cd^{2+}, which was introduced into solution after taking the polarogram of Ni^{2+} or Co^{2+}. Polarography was carried out in the absence of suppressors of maxima. With a view to excluding the possibility of complex formation, nitrates, perchlorates and sulfates were chosen as backgrounds.

Nickel. The data obtained (Tables 1, 2; Figures 1, 2) make it possible to explain the irreversibility of the polarographic wave of Ni^{2+} by the delay of ionic discharge. According to the theory of A. N. Frumkin concerning the delayed discharge [5, 6], the equation of the irreversible polarographic wave has the form:

$$\varphi = \text{const} - \frac{RT}{\alpha nF} \ln i_D - \frac{1-\alpha}{\alpha}\psi_1 - \frac{RT}{\alpha nF} \ln \frac{i}{i_d - i}, \qquad (1)$$

from which the half-wave potential is:

$$\varphi_{1/2} = \text{const} - \frac{RT}{\alpha nF} \ln i_D - \frac{1-\alpha}{\alpha}\psi_1. \qquad (2)$$

* G. S. Koshkina and B. Sh. Peltina participated in the experimental part of this work.

TABLE 1

The Constants of the Diffusion Current and the Half-Wave Potentials of the Simple Ions of Nickel and Cobalt on a Background of Various "Indifferent" Electrolytes

Background	Ni^{2+}		Co^{2+}		Background	Ni^{2+}		Co^{2+}	
	i_D μa / m moles · mg$^{2/3}$ · sec$^{-1/2}$	$-\varphi_{1/2}$, V	i_D μa / m moles · mg$^{2/3}$ · sec$^{-1/2}$	$\varphi_{1/2}$, V		i_D μa / m moles · mg$^{2/3}$ · sec$^{-1/2}$	$-\varphi_{1/2}$, V	i_D μa / m moles · mg$^{2/3}$ · sec$^{-1/2}$	$\varphi_{1/2}$, V
$NaNO_3$					Na_2SO_4				
0.01 *M*	4.32	0.96			0.2 *M*	3.19	1.12	3.09	1.31
0.03 "	4.10	0.99			0.4 "	1.58	1.12	2.89	1.42
0.1 "	4.11	1.03			1 "	0.54	1.12	2.60	1.50
0.3 "	4.60	1.07			$Ca(ClO_4)_2$				
1 "	2.71	1.09			0.01 *M*	3.27	1.04		
$NaClO_4$					0.034 "	2.95	1.06	2.87	1.27
0.01 *M*	4.45	0.96			0.1 "	2.89	1.08	2.78	1.32
0.034 "	4.43	1.00	3.01	1.17	0.34 "	2.32	1.09	2.89	1.36
0.1 "	4.30	1.03	3.12	1.23	1 "	1.06	1.08		
0.34 "	4.52	1.06	3.27	1.26	$Ca(NO_3)_2$				
1 "	2.74	1.07	3.22	1.31	0.01 *M*	4.21	1.05		
Na_2SO_4					0.034 "	3.73	1.07		
0.034 *M*	4.02	1.04	3.25	1.21	0.1 "	3.08	1.09		
0.1 "	3.52	1.08	3.13	1.25	0.34 "	1.87	1.10		

Here i_D is the constant of the diffusional current. The dependence of the negative ψ_1-potential on the concentration of a uni-univalent electrolyte is expressed by the equation [6]:

$$\psi_1 = \text{const}' + \frac{RT}{F} \ln c. \qquad (3)$$

All of these equations are well confirmed by the experimental data:

1. The relation φ, $\log \frac{i}{i_d - i}$ is linear [Figure 1, Equation (1)] with a slope of 0.060 - 0.080. Taking 0.070 as a mean slope, we obtain the result $\alpha = 0.42$. This conclusion, which has been earlier developed [4] for 0.1 M KNO_3, can be extended to solutions of perchlorates, sulfates and nitrates of varying concentrations.

2. The half-wave potential does not depend on the concentration of Ni^{2+} [Table 2, Equation (2)].

TABLE 2

Half-Wave Potentials of the Simple Ions of Nickel and Cobalt at Various Concentrations Of These Metals

Background 1 M $NaNO_3$		Background 1 M $NaClO_4$	
$C_{Ni^{2+}}$ mM/l	$-\varphi_{1/2}$, V	$C_{Co^{2+}}$ mM/l	$-\varphi_{1/2}$, V
0.11	1.08	0.20	1.31
0.18	1.09	0.39	1.30
0.32	1.09	0.57	1.30
1.03	1.09	1.50	1.32

3. A linear relation is observed between $\varphi_{1/2}$ and the logarithm of the concentration of the uni-univalent background [Figure 2, Equations (2, 3)]. A ten-fold increase in the background concentration displaces $\varphi_{1/2}$ in the negative direction by 0.074 v, which from Equations (2) and (3) gives $\alpha = 0.44$, a value which agrees well with that obtained from the slope of the straight line φ, $\log \frac{i}{i_d - i}$. The somewhat lower value for $\varphi_{1/2}$ at c = 1 M (Figure 2) and the passage $\varphi_{1/2}$, log c curve through a maximum in the case of the solutions Na_2SO_4, $Ca(ClO_4)_2$, and $Ca(NO_3)_2$, (Figure 2) is to be explained by a decrease in the constant of the diffusional current with increasing background concentration (see Table 1). Actually, the

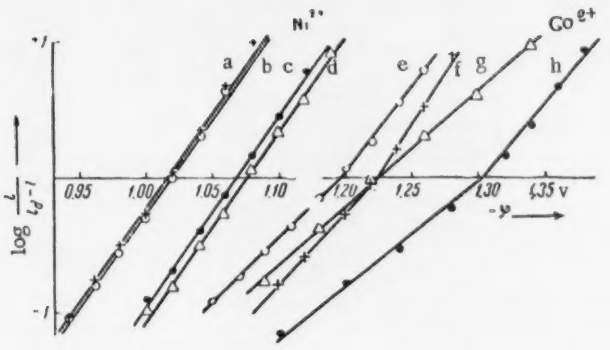

Fig. 1. The relation φ, $\log \frac{i}{i_d - i}$: $\underline{Ni^{2+}}$: a) 0.1 M $NaClO_4$ (tan α = 0.063); b) 0.1 M $NaNO_3$ (tan α = 0.064); c) 0.1 M $Ca(ClO_4)_2$ (tan α = 0.070); d) 0.1 M Na_2SO_4 (tan α = 0.072); $\underline{Co^{2+}}$: e) 0.1 M $NaNO_3$ (tan α = 0.106-0.080); f) 0.1 M $NaClO_4$ (tan α = 0.096-0.068); g) 0.1 M Na_2SO_4 (tan α = 0.116); h) 0.1 M $Ca(ClO_4)_2$ (tan α = 0.128-0.086). Concentration of metals, 0.1-0.2. m moles/liter.

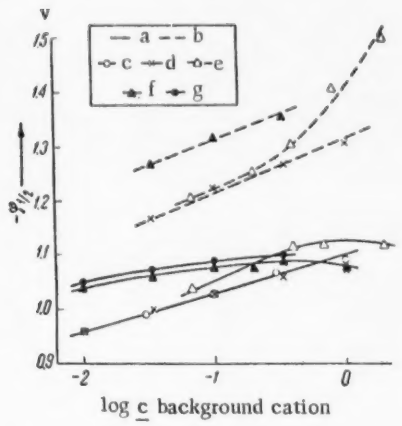

Fig. 2. The dependence of $\varphi_{1/2}$ of Ni^{2+} and Co^{2+} on the logarithm of the concentration of the background cation: a) Ni^{2+}, b) Co^{2+}, c) $NaNO_3$, d) $NaClO_4$, e) Na_2SO_4, f) $Ca(ClO_4)_2$, g) $Ca(NO_3)_2$.

introduction of a correction for the change of i_0 [according to Equation (2)] leads to an increase in the value of $\varphi_{1/2}$ with increasing background concentration.

4. The nature of the anion (NO_3^-, ClO_4^-) is practically without influence on the value of $\varphi_{1/2}$ Ni^{2+}. In the presence of SO_4^{2-}, $\varphi_{1/2}$ is displaced in the negative direction (Figure 2), which may be the result of association of the Ni^{2+} and SO_4^{2-} ions. Other authors [7, 8] have already observed a similar effect of sulfates on the potential of deposition of Ni^{2+} on a solid cathode. It is interesting to note the considerable decrease in the constant of the diffusional current with increasing concentration of sulfate (see Table 1). The replacement of a univalent cation background (Na^+) by a divalent one (Ca^{2+}) leads to a displacement of $\varphi_{1/2}$ in the negative direction (Figure 2), a fact which is connected with the movement of the ψ_1-potential in the positive direction [Equations (2, 3)].

We note in conclusion that in investigating the electrolysis of Ni on a solid cathode [8], it was also possible to explain the mechanism of polarization by delayed ionic discharge.

Cobalt. A series of facts indicate the theory of delayed discharge to be also applicable for the explanation of the irreversibility of the polarographic wave of the simple cobalt ions.

1. The half-wave potential does not depend on the concentration of Co^{2+} (Table 2).

2. Between $\varphi_{1/2}$ and the logarithm of the concentration of the uni-univalent background there is observed a linear relationship with a slope of 0.105 (Figure 2), from which there follows α = 0.36, a result somewhat lower than for Ni^{2+}.

3. As in the case of Ni^{2+}, use of a background with a polyvalent cation Ca^{2+} leads to a significant of $\varphi_{1/2}$ in the negative direction (Figure 2) at the expense of a movement of the ψ_1-potential toward the positive side. A background with SO_4^{2-} -anions shows a more negative $\varphi_{1/2}$, especially under large sulfate concentrations, than does a background with ClO_4^- -anions (Figure 2). Obviously, this is connected with the phenomenon of association, just as in the case of Ni^{2+}.

There are, as well, divergences in the polarographic behavior of Co^{2+} in comparison with that of Ni^{2+}; namely the Co^{2+} wave on a background of nitrates or of perchlorates is not symmetrical, and the relation φ, $\log \frac{i}{i_d - i}$ has a break at the point $\varphi_{1/2}$ (see Figure 1). This straight line break is, in many experiments, not large, especially on a nitrate background, and for this reason it was not noted in earlier work [4]. The cause of the lack of symmetry in the Co^{2+} wave is not yet clear. On the whole, the Co^{2+} wave is more inclined than that of Ni^{2+}, which qualitatively agrees with the above noted smaller value of the coefficient α.

The Kishinev State University

Received October 7, 1956

LITERATURE CITED

[1] I. M. Kolthoff, J. J. Lingaine, Polyarografiya (Polarography) 1947.

[2] Ya. Geirovsky, Tekhnika polyarograficheskogo issledovaniya (The Technique of Polarographic Analysis) 1951.

[3] I. M. Kolthoff, J. J. Lingane, Polarography, 2, N. Y., 1952.

[4] Ya. I. Turyan, M. M. Smyk, Uch. zapiski Kishinevsk. gos. univ. (Annals of the Kishinev State University) 14, 11, 1954.

[5] A. Frumkin, Zs. phys. Chem., (A) 164, 121 (1933)

[6] A. N. Frumkin, V. S. Bagotsky, Z. A. Iofa, B. N. Kabanov, Kinetika elektrodnykh protsessov (The Kinetics of Elec trode Processes) 1952.

[7] N. Isgarischew, H. Rawikowitsch, Zs. phys. Chem., 140, 235 (1929).

[8] A. L. Potinyan, V. Ya. Zeldes, E. Sh. Ioffe, E. S. Kozich, ZhFKh (J. Phys. Chem.) 28, 73, 1954.

CONCERNING THE FLOW OF LIQUIDS IN NARROW GAPS BETWEEN APPROACHING PLANE SOLID BODIES

G. I. Fuks

(Presented by Academician P. A. Rebinder August 4, 1956)

The relation between the width of the gap separating plane parallel circular disks in a liquid of viscosity η and the time, t, required for pressing these disks together or for pulling them apart is given by the Stephan-Reynolds Equation in the form

$$t = \frac{3\pi r^4 \eta}{4F}\left(\frac{1}{h_1^2} - \frac{1}{h_2^2}\right), \tag{1}$$

where r is the radius of the disks; H_1 and H_2 are the initial and the final widths of the gap between them and F is the normal force which is pressing the disks together or separating them. For the case of large gap widths Equation (1) has been theoretically justified [1] and experimentally confirmed in the works of a number of authors [2, 3], including our own [4].

In the separation of adhering disks, h_2 is as a rule $\gg h_1$, and Equation (1) can be written in the following form:

$$t = \frac{3\pi r^4 \eta}{4Fh_1^2}, \tag{2}$$

That is, the time for separation is inversely proportional to the square of the magnitude of the initial gap width.

Carrying F and η into the left-hand side of the equation, thus leaving in the right-hand member only the geometrical dimensions of the disks and the gap, and dividing both sides of the equation by S, the disk area, there is obtained

$$\frac{t\sigma}{\eta} = \frac{3\pi r^4}{4h_1^2 S} = \psi, \tag{3}$$

where $\sigma = F/S$ is the specific force which is pulling the disks apart. The product $t\sigma$ has the dimensions of dynamic viscosity, whereas the ratio $t\sigma/\eta$ is a dimensionless coefficient, characterizing the mobility of the liquid in the gap between the disks. Introduced in [4] in another connection, this quantity was designated as the coefficient of boundary condensation and was represented by the symbol ψ.

In earlier communications [5, 12] there has been described a method which permits the measurement, with an accuracy of 0.01 seconds, of the time for pressing together and for pulling apart plane parallel disks;

simultaneously the width of the gap between these disks can be determined over the interval from 20 to 0.02μ. Application of this method indicated that Equation (1) is not valid for disks which are separated by sufficiently thin layers of mineral, or other lubricating oils, by solutions of stearic acid in organic solvents and by aqueous electolytic solutions. This is shown, in particular, by the fact that $\underline{t}$ and ψ strongly depend on the composition of the liquid and the material of the disks and on the time of their preliminary contact. New experimental data (Table 1 and Figure 1), obtained by this same method, show that during the flow of the indicated liquids in the narrow gap between approaching disks the following deviations are to be observed from the law which is expressed by Equation (1): 1) there is a delayed flow of the liquid out of (and into) the space between the disks; 2) a residual layer is formed which, over the time of measurements (up to 36 hours), is not exuded by loads as high as 8 kg/cm^2; 3) $\underline{t}$ increases with increasing duration of contact and 4) the relationship between $\underline{t}$ and $1/F$ and $1/h_1^2$ is nonlinear.

TABLE 1

The Gap Between Horizontal Plane Parallel Disks Immersed in Liquid and its Dependence on the Time of Contact and on the Force which is Pressing the Disks Together (Temperature 20± 2°, Disk Area 1.13 cm^2)

Disk material	Liquid	Force pressing disks together, kg/cm^2	Duration of contact, min	Gap in μ
Quartz	0.005 N aq. NaCl soln.	0.08	60	0,27
"	0.1 N aq. NaCl soln.	0.08	60	0.41
"	Ditto	4.0	10	1.16
"	Ditto	4.0	20	0.095
"	Ditto	4.0	30	0.045
"	Ditto	4.0	60	0.045
Steel	0.5% stearic acid in butyl alc.	2.0	10	0.15
"	Ditto	2.0	30	0.045
Quartz	Ditto	2.0	30	0.025
Brass	Ditto	2.0	30	0.06
Steel	Turbine oil "L"	0.08	10	2.18
"	Ditto	0.08	60	1.13
"	Ditto	0.08	120	0.36
"	Ditto	1.0	10	0.375
"	Ditto	1.0	60	0.195
"	Ditto	1.0	120	0.08

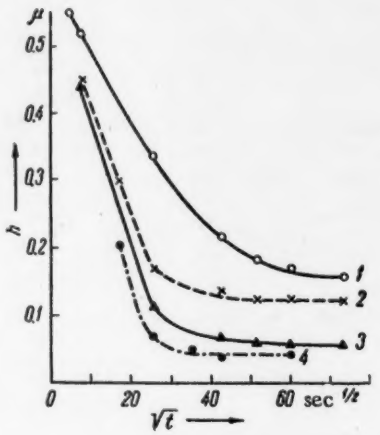

Fig. 1. The change in the gap, $\underline{h}$, between disks with the time, t, under the action of loads of 0.2 kg/cm^2 (1 and 2) and 4 kg/cm^2 (3 and 4) in transformer oil (1 and 3) and in 0.01 N aqueous NaCl solution (2 and 4).

Our technique is not sufficiently sensitive for conclusions to be reached as to the change of the depth of the residual layer with time. Indirect data [6, 7] permit the supposition that this depth does not remain constant, but within the limits of the sensitivity of the method this layer is completely stable (see, for example, in Table 1 the gap in NaCl solution after 30 and 60 minutes of contact).

The delayed flow of liquid into or out of the narrow gap between disks is interpreted as the result of an increase of its viscosity and is characterized by a change in the coefficient of boundary condensation. For times of disk contact from 1 up to 60-120 minutes under pressures of 1 kg/cm^2 and greater, ψ for the investigated liquids increases by a factor of 1.5-2.0. ψ solutions of the fatty acids in oils under pressures of 0.08-0.4 kg/cm^2 rises in the course of the indicated time of contact by 20-fold and more. The magnitude of the coefficient of boundary condensation depends essentially on the material of the disks and on the composition of the liquid. For specimens of purified turbine oil "L" it is equal to $98 \cdot 10^5$ when between steel disks and to $4.8 \cdot 10^5$ with quartz disks (in both cases: the disk radius 0.6 cm, the specific load 0.6 kg/cm^2, the duration of contact 10 minutes and the temperature 20°). Under these same conditions ψ for benzene between steel disks is 9000; between quartz disks it is 80.

TABLE 2

The Increase of the Ratio of the Viscosity of the Boundry Layer to the Volume Viscosity, measured by the Method of Disk Separation (Temperature 20°

Disk material	Liquid	Initial gap in μ	Ratio of boundary to vol. viscosity
Quartz	Benzene	0.02	1.0
Steel	Fraction of vacuum distillate of turbine oil η_{20} = 35.5 cp	0.10	2.9
"	Ditto	0.12	1.7
Quartz	Ditto	0.05	1.4
Brass	Ditto	0.10	3.2
"	Bone oil	0.10	4.6
Quartz	0.01 N NaCl solution	0.07	2.0
"	0.1 N NaCl solution	0.07	2.7
"	Ditto	0.12	1.5

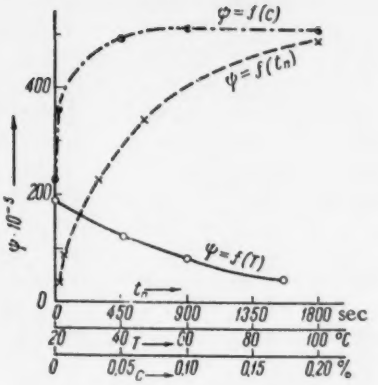

Fig. 2. The dependence of ψ for turbine oil "L" between steel disks on the time of disk contact, t_n (pressure 1 kg/cm²), the temperature, t (t_n = 600 sec; pressure 2 kg/cm²) and the concentration of oleic acid, C (t_n = 600 sec; pressure 1 kg/cm²).

An increase in the concentration of the surface-active substances and electrolytes lead to a rise in the coefficient of boundary condensation. The typical form of the dependence of ψ on these factors is presented in Figure 2. With increasing temperature, the loosening time decreases but ψ can rise, fall, or even remain unaltered, depending on the interrelationship between the temperature coefficients, the loosening time, and the volume viscosity.

Having calibrated the disks with a liquid which, for practical purposes, does not form a boundary layer (for example, benzene on quartz) and having determined by an independent method the loosening time of the disks and the gap between them, it is possible, with the aid of Equation (2), to calculate the viscosity of the investigated liquid in the boundary layer. Certain results from such measurements are shown in Table 2. The data obtained indicate that the viscosity rises with a diminution of the thickness of the boundary layer and, up to a certain limit, with an increase of the concentration of the surface-active substances and electrolytes; on the whole, however, the viscosity of the boundary layer exceeds the volume viscosity by no more than a factor of 5. The resulting ratio of boundary to volume viscosity agrees, in order of magnitude, with the latest results from the measurements of boundary viscosity by the blowing method [8, 9].

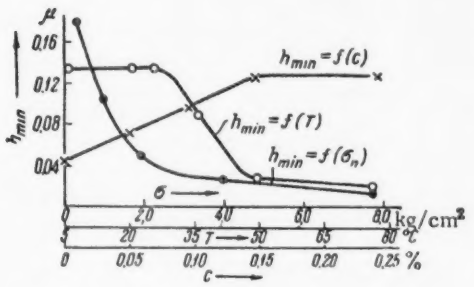

Fig. 3. The residual gap, h_{min}, between steel disks in a fraction of turbine oil "L"; σ_n is the compressing force in kg/cm² and C is the concentration of stearic acid in %.

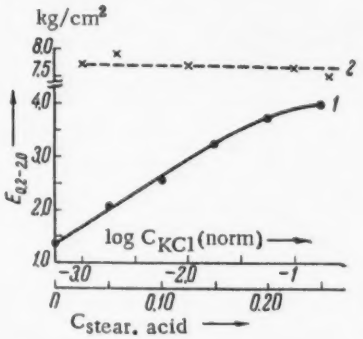

Fig. 4. The influence of the concentration of stearic acid on the compressibility of the residual layer between steel disks of a solution of this acid in a fraction of the the vacuum distillate of turbine oil (1) and of the concentration of KCl on the compressibility of the residual layer of an aqueous solution between quartz disks (2). Temperature 20°.

The magnitude of the residual layer, as well as the boundary viscosity, is determined by the nature of the solid bodies and the liquid. On quartz, well purified benzene does not, in general, leave a residual layer which can be measured by our method. The residual layer thickness of a fraction of the vacuum distillate of turbine oil "L" on steel is equal to 0.09μ; on quartz it is equal to 0.04μ (compressing force 2 kg/cm^2). The influence of the remaining essential factors is shown in Figure 3. It is important to note the difference in the temperature dependence of the loosening time and the thickness of the residual layer. The first invariably diminishes with rising temperature (if side chemical reactions do not occur) and the curve $\psi = f(t)$ has a monotonic course. With mineral oils and solutions of fatty acids, the thickness of the residual layer at low temperature does not depend on the value of the latter; with increasing temperature there appears a region of sharp diminution of the magnitude of the residual layer, which region can be considered as that of partial disorientation of the structure of the boundary layer ("fusion"). This temperature is different for various liquids but it is always lower than the temperature of fusion of the boundary layer as this is measured under high contact pressures, for example, in the four-ball friction machine [10].

Since the thickness of the residual layer depends on the normal pressure, it is possible, for a definite pressure interval, to evaluate the compressibility of this layer with the aid of a conventional coefficient of uniaxial compression, estimated just as is the modulus of compression. The change in this characteristic, $E_{0.2-2.0}$, in the pressure interval from 0.2 to 2.0 kg/cm^2 is given in Figure 4. The ease of compression of the residual layer, at least in its peripheral part, and the dependence of the deformation of this layer on the concentration of surface-active substances are striking.

In the described effect there are manifest the specific molecular-surface properties at the solid-liquid interface. This is indicated by the dependence of the indicated effect on surface-active substances and electrolytes. It points to the formation, at a depth of the order of 0.1μ, of a special structure in the surface layers of the investigated liquids (for further details as to the thickness of boundary layers, see [4, 5]). The nature of the described effect is not uniform; in particular, it is determined by reversible and by irreversible phenomena. If the residual layer of an electrolytic solution is compressed and the load then removed, the layer is partially, but not completely, reestablished. In the first effect we see the manifestation of an equilibrium loosening pressure [11], whereas the decrease in the viscosity and the irreversible residual layer are connected with kinetic phenomena. We note that the delayed separation and approach of disks is also the consequence of a decrease in the effective gap which results from the formation of a quasi-solid residual layer.

The Scientific-Research Institute
of the Watchmaking Industry

Received July 18, 1956

LITERATURE CITED

[1] W. Stephan, Zs. Berl. Akad. Wissensch., 69, 713 (1874); O. Reynolds, Phil. Trans. Roy. Soc., 177, 157 (1886); J. Bikerman, Colloid Sci., 2, 163 (1947).

[2] E. Ormandy, The Engineer, 143, 362, 393 (1927).

[3] Yu. L. Margolina, S. S. Voyutsky Zav. lab. Fact. Lab.) 14, 321, 1948.

[4] G. I. Fuks, Sborn. Chasovye mekhanizmy Coll., Clock Mechanisms) 1955, page 186.

[5] G. I. Fuks, Zav lab. Fact. Lab.) 21, 12, 1455, 1955.

[6] G. I. Fuks, V. M. Klychnikov, E. V. Tsyganova, DAN (Proc. Acad. Sci., USSR) 65, 307, 1949; G. I. Fuks, V. M. Klychnikov, Tr. Vsesoyuzn. inst. udobr., agrotekhn. i agropochvoved (The All-union Institute for Fertilizers, Agr. Eng. and Soil Sci., Vol. 28, 215, 1948.

[7] A. D. Malkina, B. V. Deryagin, Koll. zhurn. (Colloid, J.) 12, 431, 1950.

[8] V. V. Karasev, B. V. Deryagin, Koll. zhurn. (Colloid. J.) 15, 365, 1953; B. V. Deryagin, V. V. Karasev DAN (Proc. Acad. Sci., USSR) 101, 281, 1955.

[9] B. V. Deryagin, E. F. Pichugin, Tr. 2-i konfer. po treniyu i iznosu v mashinakh (Proc. Second Conf. on Friction and Wear in Machines) 3, 1949, page 101.

[10] M. M. Khrushchev, R. M. Matveevsky, Vestn. mashinostr. (Machine Industry Bull.) No. 1, 12, 1954; I. W. Menter, J. Tabor, Proc., Roy. Soc., A 204, 514, 1951.

[11] B. V. Deryagin, Koll. zhurn. (Colloid. J.) 17, 207, 1955.

[12] G. I. Fuks, Tr. 3-i konfer. po kolloidnoi khimii (Proc. Third Conf. on Colloid. Chem.) Izd. AN SSSR (Acad. Sci. USSR Press) 1956, page 387

THE CORRECT FORM OF THE EQUATION OF CAPILLARY CONDENSATION IN POROUS BODIES AND ITS APPLICATION TO THE DETERMINATION OF THEIR STRUCTURE FROM ADSORPTION AND SORPTION ISOTHERMS, AND TO THE SOLUTION OF THE REVERSE PROBLEM

B. V. Deryagin

(Corresponding Member of the Academy of Sciences, USSR)

When adsorption processes are absent, calculation of the vapor sorption isotherm for a porous body of known structure, as well as the solution of the reverse problem, can be effected using Kelvin's formula. The presence of adsorption layers complicates this calculation as it becomes necessary to take into account the total mass of such layers and the difference between half the pore width at the level of the menisci and the radius of curvature of the latter. To resolve the latter difficulty, this difference, when working with Kelvin's formula, is usually taken to be equal to the thickness of the corresponding adsorption layers.

However, the author has shown [1] that this method of accounting for the effect of adsorption on capillary condensation is incorrect* because the curvature of the surface of the meniscus does not remain constant (dotted line in Fig. 1) right up to the line where it meets the surface of the adsorbed layers AA, where it should diminish abruptly, but rather varies gradually (continuous curve) under the influence of the same forces which give rise to polymolecular absorption. We shall now deduce the equation of capillary condensation in porous bodies which applies exactly when the effect of the curvature of pore walls on adsorption equilibrium is negligible.**

Consider the equilibrium between the adsorbent and the vapor at a pressure p, and let S denote the total surface of the adsorbed layer AA; V is the volume occupied by the capillary-condensed phase (shaded area in Fig. 1) having a molar volume v; W = amount sorbed, in moles; Γ = amount adsorbed, in moles/cm^2. Consider (Fig. 2) a virtual "desorption" process (at p = const., Γ = const.) of (-dW) moles (shaded area***) by isothermal reversible distillation into the liquid phase having a vapor pressure p_0. During the process S will increase by dS, and V will change by

$$dV = v(dW - \Gamma dS), \tag{1}$$

where v is is the molar volume of the capillary-condensed phase.

From the definition of the chemical potential we get for the corresponding increase in free energy dU:

$$dU = -(\mu_0 - \mu)dW, \tag{2}$$

where μ is the chemical potential of the vapor at pressure p, and μ_0 is that at pressure p_0. If U_0 is free energy

---

* A similar error was made by Langmuir in attempting to take into account the effect of the thickness of wetting films on capillary rise [3].

** The same method of approach can be followed without this restriction, but the resulting formulas are then more complicated [1].

*** The reasoning outlined here is quite general and does not depend on any particular pore shape; a single slit-shaped pore is shown in the diagram for the sake of simplicity.

of the system at $p = p_0$ when all the pores are filled, then

$$U - U_0 = S(\omega - \omega_0) + (s - s_0)\sigma + F - F_0, \tag{3}$$

where ω_0 and ω are the free energies per unit area respectively, of the adsorbent-liquid phase interface and of the interface between the adsorbent (including an adsorbed film of thickness $\underline{h}$) and the vapor at a pressure p; σ is the surface tension of the liquid in the liquid-vapor interface; $\underline{s}$ is the total surface area of the menisci under the conditions discussed; s_0 is the same surface area at $p = p_0$; F is excess bulk free energy (excluding the contribution due to the term containing ω_0) of the capillary-condensed liquid as compared with that of the bulk phase, F_0 is the corresponding quantity at $p = p_0$. Differentiating (3) at ω = const., and taking into account (2), we obtain

$$(\mu_0 - \mu)\, dW = -(\omega - \omega_0)\, dS - \sigma\, ds - dF. \tag{4}$$

In the case of complete wetting and for a layer of sufficient thickness $\underline{h}$, $\omega = \omega_0 + \sigma$.

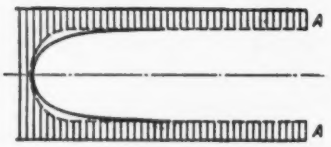

Fig. 1

For smaller values of h [1],

$$\omega = \omega_0 + \sigma\cos\theta + f(h), \tag{5}$$

where θ is the contact angle; $f(h) = \int_h^{h_0} P(h)dh$; $P(h)$ is the 'disjoining' pressure [2] of the layer; and h_0 the thickness of the film inequilibrium with the saturated vapor [7] ($h_0 \neq \infty$ at $\theta \neq 0$).

In the more simple case, when the effect of the curvature of the surface of the adsorbed layers on the elasticity of the vapor, i.e. on the adsorption equilibrium, may be neglected, we obtain, introducing the specific volume $\underline{v}$:

$$v\,P(h) = \mu_0 - \mu; \quad f(h) = \int_{\Gamma}^{\Gamma_0} (\mu_0 - \mu)\, d\Gamma, \tag{6}$$

whence, taking into account 5 , we get:

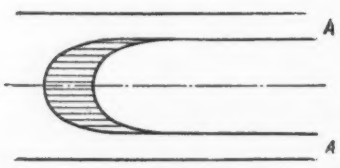

Fig. 2

$$\omega - \omega_0 = \sigma\cos\theta + \int_{\Gamma}^{\Gamma_0} (\mu_0 - \mu)\, d\Gamma$$

$$= \sigma\cos\theta + RT\int_{\Gamma}^{\Gamma_0} \ln\left(\frac{p_0}{p}\right) d\Gamma. \tag{7}$$

Clearly, the second term on the right-hand side of equation (4) may be neglected when $ds/dS \ll 1$, i. e., when the cross sections of the pores vary slantwise.

The third term on the right-hand side of equation (4) may be neglected subject to the following conditions: (1) the difference between the densities of the capillary-condensed and the free liquids may be neglected; (2) the width of the pore gap is so large that the ranges of influence of diametrically opposite sections of the wall surface on the capillary-condensed liquid layers do not overlap; the molecular structure (of the capillary-condensed liquid) is identical with that of the bulk phase with the exception of boundary layers of the former which satisfy condition (2).

If these conditions are fulfilled, we can obtain from (1), (4) and (7) the relation

$$-\frac{dV}{dS} = v\Gamma + \frac{v}{\mu_0 - \mu}\left[\sigma\cos\theta + \int_{\Gamma}^{\Gamma_*} (\mu_0 - \mu)\, d\Gamma\right], \tag{8}$$

or, integrating by parts and transforming:

$$-\frac{dV}{dS} = \frac{v}{\mu_0 - \mu}\left[\sigma\cos\theta + \int_{\mu}^{\mu_*} \Gamma\, d\mu\right] = \frac{v}{RT\ln\frac{p_s}{p}}\left[\sigma\cos\theta + RT\int_{p}^{p_s} \frac{\Gamma}{p}\, dp\right]. \tag{9}$$

In the simplest case of a slit with parallel walls (for example near the point of contact of two spheres, or of a sphere and a plane) the derivative $(-dV/dS)$, having dimensions of length, is equal to D/2 (Fig. 1), where D is the width of the slit. In the case of pores of nearly cylindrical shape, $(-dV/dD)$ is equal to half the hydraulic radius. In general, $(-dV/dS) \equiv H$ may be regarded as a measure of the width of the pores in the plane of the cross sections at the level of the menisci. Equation (9) is a generalization of Kelvin's formula taking into account the effect of adsorption layers on capillary condensation.

Let us now apply this equation to the solution of the following problems:

1. To find the vapor sorption isotherm for a porous body of known structural characteristics, for example, when the function $V = V(H)$ is known,* being given the adsorption isotherm of the same vapors on a plane surface of the same nature as the pore walls.

2. To find the structural characteristics of a porous body being given the sorption and adsorption isotherms of the vapor on a plane surface of the same nature as the pore walls.

3. Being given the sorption isotherm for a porous body of known structure, to find the pore width at the sites of the menisci, as a function of the vapor pressure.

4. To find the adsorption isotherm $\Gamma = \Gamma(p)$ from sorption observations on a porous body of known structure in the presence of capillary condensation.

Problem 1. Having found from (9) $H = -dV/dS$, we may, using the structural characteristics, find V – the volume of the filled pores, and adding $S\Gamma(p)$ we can determine the amount of vapor sorbed, W, at a given pressure p. In this way we can plot the sorption isotherm point by point.

Problem 2. The change in free energy during an actual (not virtual) equilibrium desorption process can be found directly from a determination of the chemical potential:

$$U - U_s = \int_{W}^{W_*} (\mu_0 - \mu)\, dW, \tag{10}$$

* E.g., as found from measurements by the method of forcing mercury.

where μ is a function of the variable of integration W.

Equating (10) to (3), the second and third terms on the right-hand side of the latter being neglected as very small, we get:

$$S = \frac{\int_{W}^{W_0} (\mu_0 - \mu)\, dW}{\sigma \cos\theta + \int_{\Gamma}^{\Gamma_0} (\mu_0 - \mu)\, d\Gamma} \simeq \frac{RT \int_{W}^{W_0} \left(\ln \frac{p_0}{p}\right) dW}{\sigma \cos\theta + RT \int_{\Gamma}^{\Gamma_0} \left(\ln \frac{p_0}{p}\right) d\Gamma}. \tag{11}$$

In particular, for the total surface of the sorbent we obtain

$$S_0 \simeq \frac{RT \int_{W_c}^{W_0} \left(\ln \frac{p_0}{p}\right) dW}{\sigma \cos\theta + RT \int_{\Gamma_c}^{\Gamma_0} \left(\ln \frac{p_0}{p}\right) d\Gamma}, \tag{12}$$

where W_c and Γ_c correspond to any vapor pressure at which capillary condensation no longer occurs. If, of course, the process of desorption takes place under conditions which do not quite correspond to equilibrium conditions (as, for example, in the case of bottle-shaped pores), then the actual values of S and S_0 will be less than those calculated by means of Formulas (11) and (12).

It will be seen from (9) and (11) that if the functions $W = W(p)$ and $\Gamma = \Gamma(p)$ are known from the experimental data, a series of pairs of corresponding values of S and $H = -dV/dS$ can be obtained by simple graphical integration assigning to the pressure arbitrary values $p < p_s$. This enables us to plot the graph of $-dV/dS$ versus S. Hence, by graphical integration, we can find $V = V(S)$, and thus construct the graph of $V = \Phi(-dV/dS)$.

Problem 3. From equations (8) and (11) we get

$$-Sd\left(\frac{dV}{dS}\right) = \frac{v d\mu''}{(\mu_0 - \mu')^2} \int_{W''}^{W_0} (\mu_0 - \mu')\, dW', \tag{13}$$

where W' is a function of μ', and W" is the function of μ''.

Integrating both sides, the left-hand side by parts, and reversing the order of integration on the right-hand side, we obtain

$$Z \equiv (V_0 - V) - SH = v \int_{W}^{W_0} \frac{(\mu' - \mu)}{(\mu_0 - \mu)}\, dW' = \\ = v(\mu_0 - \mu)^{-1} \int_{W}^{W_0} (\mu' - \mu)\, dW'. \tag{14}$$

Finally, integrating by parts, we get

$$Z = v(\mu_0 - \mu)^{-1} \int_{\mu}^{\mu_0} (W_0 - W')\, d\mu'. \tag{15}$$

If the structural characteristics of the body are known and, therefore, V and S are known as functions of H, then Z may be regarded as a known function of H; $Z = \psi(H)$. Using Equation (16), H may then be found by means of the formula:

$$H = \Psi^{-1}\left[\frac{v}{\mu_0 - \mu} \int_{\mu}^{\mu_0} (W_0 - W')\, d\mu'\right], \tag{16}$$

i.e. by graphical integration and the subsequent use of the graph of H plotted against Z.

Problem 4. If H is known as a function of p either from the solution of Problem 3 by the above method, or from optical observations, as in Chmutov's experiments [5],* the adsorption Γ can be found, as is evident from (9), by means of the formula:

$$\Gamma = -\frac{1}{v}\frac{d[(\mu_0 - \mu)H]}{d\mu} = \frac{H}{v} + \frac{(\mu_0 - \mu)}{v}\frac{dH}{d\mu} = -\frac{1}{u}\frac{d(H \ln(p_0/p))}{d \ln (p_0/p)}. \tag{17}$$

If H has been obtained from sorption isotherms, it is simpler and more accurate to use the equation $\Gamma = \frac{W - Vv}{S}$, where V and S are, by proposition, known functions of H.

Institute of Physical Chemistry, Academy of Sciences, USSR Received November 21, 1956

LITERATURE CITED

[1] B. V. Derjaguin, Acta Physicochim. URSS, 12, 181 (1940); J. Phys. Chem., 14, 137 (1940).

[2] B. V. Derjaguin, Disc. Farad. Soc. No. 18 (1954); Trans. Farad. Soc., 36, 406 (1940); Acta Physicochim. URSS, 5, 1 (1936); Colloid J., 18, 207 (1955).**

[3] J. Langmuir, Science, 88, 430 (1938).

[4] A. N. Frumkin, Acta Physicochim. URSS, 9, 313 (1938).

[5] K. V. Chmutov, J. Phys. Chem., 9, 345 (1937).

[6] J. L. Shereshefsky, J. Phys. Chem., 59, 607 (1955).

[7] B. V. Deryagin and Z. M. Zorin, J. Phys. Chem., 29, 1010, 1755 (1955), Proc. Acad. Sci. USSR, 98,93 (1954)

* The experiments of Shereshefsky, [6], though closely similar, require for their interpretation that the effect of the wall curvature of the conical capillary used by him be taken into account.

** Original Russian pagination. Sec. C. B. translation.

ON THE PROBLEM OF A KINETIC THEORY OF GELATION PROCESSES

I. F. Efremov and S. V. Nerpin

(Presented by Academician A. N. Frumkin, November 21, 1956)

The problem of the formation of gels, pastes and various tactoidal structures has been attracting the attention of investigators for a comparatively long time, and opinions as to the nature of these systems diverge considerably. The study of gelation processes in dilute sols and suspensions shows that gel formation in a series of similar systems may be explained by a process of fixation of the colloidal particles separated by comparatively long distances under the action of long-distance forces of molecular and ionic-electrostatic origin [1].

When we examine the behavior of colloidal particles under conditions which determine the formation of gels of like structure it appears possible to draw an analogy between the transition of bodies of molecular structure from the liquid into the solid state on the one hand and gelation of dilute sols on the other. In the latter case, instead of forces of attraction and repulsion between the individual molecules, we have forces arising from molecular attraction and ionic-electrostatic repulsion between the colloidal particles. The analogy becomes obvious when we compare the potential energy curve for the interaction of two molecules (Fig. 1a) with the portion of a similar curve for the interaction between colloidal particles separated by distances greater than that corresponding to point A in Fig. 1b. The fact that in the latter case there exists a potential energy barrier and a still lower energy level outside the limits of the former, indicates that the fixation of the colloidal particles may have the character of relaxation processes.

On the basis of these considerations it is possible to establish the nature of shear rigidity which is the main feature of a gelled system, and also to examine the behavior of colloidal particles within the body of the gel. To do this it is necessary to consider the interaction not of a single pair of particles but of the entire collection of the particles constituting the quasi-crystalline lattice of the gel.

The mutual fixation of the particles at distances corresponding to the position of the potential energy minima should simultaneously bring about a state of minimum potential energy in the system as a whole, satisfying the condition $dU_{syst}/dh = 0$.*

If the system is subjected to a reversible infinitesimal shear this condition will be disturbed and the energy level of the system will increase. In accordance with the well-known relation $dF = dR$ where R is the work of external forces and F the free energy, such an increase can only be brought about by the application of external shear forces. At small angles of shear φ $dR = \tau d\varphi$, where τ is the shear strain. Hence we have

$$\tau = \frac{dE}{d\varphi} \qquad (1)$$

* Such a state does not, of course, signify that the system is in true thermodynamic equilibrium corresponding the lowest possible energy level. In our case, however, this minimum level is temporarily unattainable because of the existence of the potential energy barrier. This effect is responsible for the relaxation character of subsequent processes which determine the course of aging of the gelled system.

and the shear rigidity:

$$G = \frac{d\tau}{d\varphi} = \frac{d^2F}{d\varphi^2}. \qquad (2)$$

Under these conditions the system will behave as a gel if the period of relaxation of the colloidal particles, either in the course of a slip, or during their transition to a vacant site within the quasicrystalline lattice, will substantially exceed the period of action of the given external forces. If one of these conditions is not fulfilled, the system will either undergo a rapid aging process, or its elastic properties will be masked by fluidity.

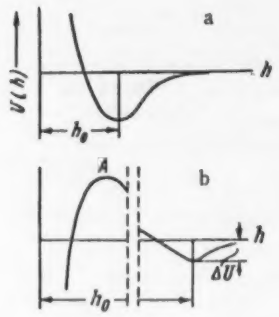

Fig. 1. Potential energy curves a) for the interaction of two molecules, b) for two colloidal particles in the presence of a potential energy trough situated some distance away.

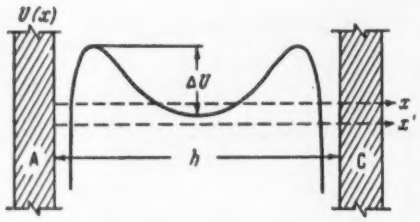

Fig. 2. Total potential energy curve for the interaction of a "test" particle with particles A and C.

As a first approximation in the examination of the collective interaction of the colloidal particles constituting the gel lattice, let us consider the type of the potential energy curve for a "test" particle B situated symmetrically with respect to two rigidly fixed neighboring particles A and C (Fig. 2). In this case the depth of the potential energy trough, ∇U which determines the extent of fixation of the particles in the nodes of the lattice, is considerably greater than in the case of two individual interacting particles (Fig. 1b). In the latter case, in order that the potential energy trough which merely determines the relative distance between the particles, might appear, it was necessary that some distance away forces of attraction should be greater than forces of repulsion. However, in the case of collective interaction such troughs will exist at the sites taken up by intermediate particles even if at some points forces of repulsion will exceed forces of attraction. It is obvious that such potential energy troughs can bring about the mutual fixation of the particles of the colloidal system at determined distances only if the volume of the medium, which determines the maximum displacement of the disperse phase particles at the boundary, is finite.* In addition, a certain minimum concentration of the disperse phase is necessary, otherwise the potential energy troughs will be small as compared with the energy of Brownian motion, and fixation of the particles will not take place. If the volume of the medium be infinite, or if the concentration in a finite volume is less than the minimum concentration, gelation will be possible only when there will exist potential energy troughs with a negative energy difference (see Fig. 1); under such conditions gelatin will have a local character (flocculation and formation of tactoidal structures).

Two factors which have an essential influence on the conditions of fixation of the particles are their shape and dimensions. It is well-known that the resultant of molecular attraction forces depends on the shape of the approaching surfaces. It can be easily shown that this resultant also depends on the thickness of the interacting particles, while the resultant of ionic-electrostatic repulsion forces is practically independent of it.

* To this type of quasi-crystalline lattices evidently belong the hexagonal lattices of particles of the synthetic latex investigated by Hamilton and Hamm.

Making use of the macroscopic theory of molecular interaction of condensed bodies [3], but assuming that the interaction of individual micro-volumes, having the properties of the condensed phase, is, approximately, additive, we can, by summing the energy of the individual micro-volumes, obtain a general expression for the energy of interaction of two laminae per unit area:

$$U = -\frac{A}{2h}\left[1 - \frac{2}{(1 + b/h)^2} + \frac{1}{(1+2b/h)^2}\right], \tag{3}$$

where A is a constant, and b the thickness of the lamina.

For b = ∞ we shall obtain, instead of Equation (3), an expression which is familiar from the exact macroscopic theory [3] and which corresponds to the case of the interaction of two semi-spaces separated by a gap of width h:

$$U_\infty = -\frac{A}{2h^2}.$$

Hence,

$$\frac{U}{U_\infty} = 1 - \frac{2}{(1 + b/h)^2} + \frac{1}{(1+2b/h)^2}.$$

This relation is represented in Fig. 3 by the curve $\frac{U}{U_\infty} - \left(\frac{b}{h}\right)$, which shows that the influence of the thickness of the particles on their energy of interaction is insignificant only when they are separated by very small distances (of the order of 10^{-1} of their thickness). For distances of the same order as the dimensions of particles, the molecular component of their energy of interaction is approximately equal to half its limiting value.

On the basis of the results presented in [4] and [5] and taking into account Equation (3) above, it is possible to obtain an expression for the interaction of two laminae. For example, in the case when the distance between the particles is considerably less than the thickness of the ionic atmosphere, the expression will have the form

$$U = \frac{\pi}{2} D \left(\frac{kT}{Ze}\right)^2 \frac{1}{h} - \frac{\zeta\delta\sigma}{h^2}\left[1 - \frac{2}{(1 + b/h)^2} + \frac{1}{(1+2b/h)^2}\right], \tag{4}$$

where D is the dielectric permeability of the medium; Z is the electrovalence of the counter-ion; e is the electron charge; ζ is a constant, approximately of the order of unity; b is the thickness of the particle (lamina); δ is size of the molecules making up the particle; σ is the interfacial tension at the particle-solution interface; h is the distance between the particles and kT has the usual meaning.

The different curves U (h) in Fig. 4 correspond to different thicknesses of three interacting particles. From a comparison of these curves it will be seen that for a decrease of particle thickness from 20 to 5 mμ the potential energy trough deepens more than four times. The existence of higher energy barriers and of deeper potential energy troughs in the case of particles of laminar shape should, of course, bring about greater rigidity of fixation of such particles as well as increase their resistance to slip as compared with spherical particles. In order to describe real quasicrystalline lattice structures it is necessary to take into account the

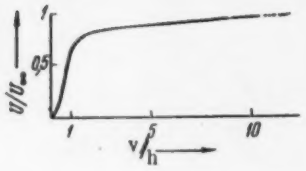

Fig. 3 Curve for the energy of interaction of two colloidal particles as a function of the ratio of their thickness b to the width h of the gap between them.

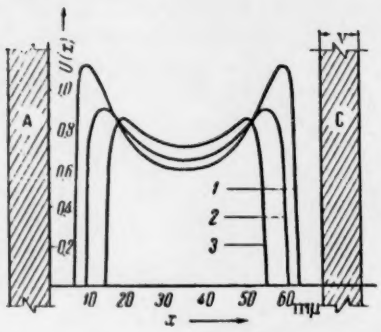

Fig. 4. Potential energy curves for the interaction of colloidal particles of different thickness: 1) b = 5 mμ; 2) 10 mμ; 3) 20 mμ.

polydisperse character of the colloidal particles. Fundamentally, however, the behavior of the particles within the gel lattice should be similar to that described in the cases just discussed. An analogy of such behavior is to be found in the appearance of elastic properties both in crystalline as well as in amorphous bodies.

The considerations outlined at the beginning of this communication concerning the nature of gelation processes may be extended to include such systems as highly concentrated emulsions and foams. In the latter case the equilibrium state of the film separating the gas bubbles is determined by the algebraic sum of the molecular component of the "disjoining" pressure, having a positive sign (corresponding to the tendency of the bubbles to come closer to one another), and the ionic-electrostatic component of this pressure, having a positive sign.

A distinct feature of foam-like systems is the fact that when they are sheared the process is accompanied not only by deformation of the layers separating the particles, but also by a change of the specific surface [6]. Let us take the simplest case when the system has been sheared and the potential energy of interaction of molecules within the layers separating the droplets has remained the same and has not affected the differential of that portion of the free energy which depends on surface tension; in this case we can write down the expression $dF = d(\sigma\omega)$, where σ is the surface tension and varies with the concentration of the molecules of the stabilizer on the interface separating the phases, and ω is the specific surface of the system.

Using the latter expression we can obtain from (1) and (2), after corresponding transformations,

$$\tau = \frac{2\varphi}{d}\left(\sigma + \omega\frac{d\sigma}{d\omega}\right), \tag{5}$$

$$G = \frac{d\tau}{d\varphi} = \frac{2}{d}\left(\sigma + \omega\frac{d\sigma}{d\omega}\right), \tag{6}$$

where d is the dimension of the droplet.

The Lensoviet Institute of Technology,
Leningrad

Received November 16, 1956

LITERATURE CITED

[1] I. F. Efremov, Colloid J., 15, No. 6 (1953); 16, No. 4 (1954); 18, No. 3 (1956).

[2] J. F. Hamilton, F. A. Hamm, J. Appl. Phys., 27, No. 2, 190 (1956).

[3] E. M. Lifshits, Proc. Acad. Sci. USSR, 97, 643 (1954); 100, 879 (1955); J. Expt.-Theor. Phys., 29, 94 (1955).

[4] B. Deryagin and L. Landau, Ibid., 11, 802 (1941); Ibid. (Reprinted), 15, 662 (1945); Acta Physicochim. URSS, 14, 633 (1941).

[5] S. V. Nerpin, Dissertation, Inst. of Water Transport Engineering, Leningrad, 1956.

[6] B. V. Deryagin, J. Phys. Chem., 2, 745 (1931); Kolloid Zeitschr., 64, 1933; B. V. Deryagin and E. V. Obukhov, J. Phys. Chem., 7, 297 (1936).

THE ROLE OF HYDROGENATION IN CORROSION FATIGUE OF STEEL

G. V. Karpenko

(Presented by Academician P. A. Rebinder, October 20, 1956)

In foregoing papers [1] we have developed certain ideas concerning adsorption-electrochemical processes in the mechanism of corrosion fatigue of steel and we have drawn attention to the fact that it is not possible to correlate the intensity of general corrosion with the development of corrosion fatigue. In the present communication we introduce some ideas supplementing our views on corrosion fatigue of steel at high stress amplitudes.

When a metal is subjected to the simultaneous action of a corrosive medium and of repeated alternating stresses, there occur phenomena of adsorption, diffusion and corrosion (electrochemial phenomena). The attacking corrosive medium affects all the accessible anodic sites on the surface of the metal; however, before the actual corrosion process sets in adsorption of the surface-active components of the medium (specific adsorption of ions or molecules) will take place. This adsorption will bring about a lowering of the strength of the metal [2], a process which is inevitable from thermodynamic considerations; under conditions of cyclic loading this phenomenon manifests itself in a lowering of the durability of the steel in adsorption fatigue [3].

On the cathodic sites on the metal surface there will be adsorbed hydrogen ions. As these ions are reduced to atomic hydrogen the latter will diffuse into the metal lattice and bring about its hydrogenation (possibly giving rise to the formation of hydrides) and will thus lead to "hydrogen" embrittlement. "Hydrogen" embrittlement of cathodic sites on the metal may have an effect on the resistance of the steel to corrosion fatigue, if the hydrogen has affected deeper-lying regions within the metal. This appears possible during deformation of the metal when the hydrogen penetrates into the bulk of the metal across planes along which the latter has been sheared.

Experiments carried out in this laboratory by M. I. Chaevsky have shown that hydrogenation of steel during its deformation by static forces proceeds at very great rates across planes of shear.

The experiments consisted of placing cylindrical samples of soft steel No. 3, 10 mm in diameter, in a bath containing an acid electrolyte, the steel rods being employed as cathodes or anodes,* and submitting them to a stretching force on a tensile-testing machine, at a constant rate ($v = 16$ mm/min), to breaking point within 1-2 minutes. Under these conditions breakdown through embrittlement occurred with the plastic steel cathodes along the shear planes, as will be clearly seen in Fig. 1a. In the course of the process the tensile strength of the steel decreased by about 10%, while the actual stresses dropped by half. The samples which were employed as anodes did not lose any of their plasticity or elasticity and their breakdown under tension followed the same pattern as that observed in samples tested in air (see Figs. 1b and 1c). In the case when the anode was of copper and the cathode of steel, when no hydrogen was evolved at the cathode, none of these effects were observed.

In the experiment described hydrogen ions were being reduced on the surface of the steel sample subjected to deformation, and the atomic hydrogen formed penetrated into the depth of the metal across shear planes formed during the deformation process; subsequently it diffused into the lattice of the metal causing it to become brittle. The tensional forces then caused failure of the samples through breakdown at the sites affected by

* Current, 20 amp; current density, 55 amp/dm^2.

hydrogen, which sites lie in the sheared planes.

A striking feature of these experiments is the enormous rate with which the process of hydrogenation of the metal takes place. This can only be explained if one assumes that not only does distortion of the metal lattice take place in the planes of shear, but that there is also formed a large number of micro-fissures. As these are formed the hydrogen is being sucked into them, thus penetrating into the body of the metal at high speeds which are considerably greater than the rates of bulk or even of boundary diffusion.

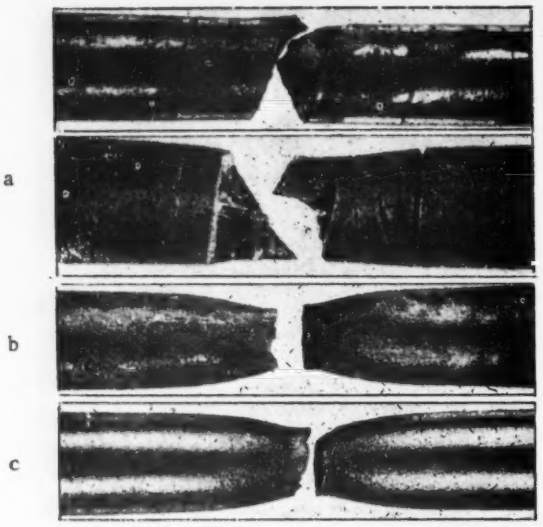

Fig. 1. Ruptured Rods of Steel No. 3; a) the sample was used as cathode; b) the sample was used as anode; c) the sample was ruptured in air.

The sections of the metal situated between planes at which the defects occurred and which under the usual conditions account for the increased elasticity of the sheared zone, possess a distorted lattice which has increased permeability to diffusion as a result of activation. It is well known that the rate of diffusion into a distorted lattice is several orders higher than that for a regular lattice. S. T. Konobeevsky showed [4] that the rate of diffusion of nickel into deformed copper is more than 1,000 times faster than its rate of diffusion into undeformed copper.

Our experiments lead us to suppose that in the case of polycrystalline metals such as steel, which exhibit a large number of sites at the metal-medium boundary, which behave as micro-cathodes and micro-anodes, very fast hydrogenation of the cathodic sites takes place during the cyclic load application in the corrosive medium. It is obvious that such sites constitute weak points at which breakdown through brittleness takes place at great stress amplitudes soon after the load is applied. Under these conditions the length of time during which the sample is exposed to the action of the medium, is insufficient for the anodic sites to be affected by corrosion, i.e. for weak sites to be formed as a result of loss of strength due to corrosion effects.

This confirmed by the fact that at high stress amplitudes the surfaces of the planes at which breakdown of the steel samples occurs in corrosive media, do not exhibit any oxidized sites and no products of corrosion can be found in the fissures formed as a result of fatigue. At the same time fatigue breakdown in corrosive media occurs at considerably lower stresses, for all values of stress amplitude, than in air.

At lower stress amplitudes, when the time required to bring about breakdown of the metal under cyclic load is considerably longer, there will be sufficient time for all the factors which decrease the strength of the metal, such as adsorption, diffusion and corrosion effects, to come into play. Under these conditions the fissures formed as a result of fatigue contain products of corrosion, and the surface of the ruptured ends of the sample is usually strongly oxidized.

The author wishes to express his gratitude to Academician P. A. Rebinder and to Dr. V. I. Lichtmann for their useful criticisms.

Institute of Mechanical Engineering and Automation
Academy of Sciences of the Ukrainian SSR, Lvov

Received October 18, 1956

LITERATURE CITED

[1] G. V. Karpenko, Proc. Acad. Sci. USSR, 77, No. 5 (1951); Coll. Vol. Problems of Mechanical Engineering and Strength of Materials in Machine Construction, Edit. 3, 29 (1954); Coll. Vol. Corrosion of Metals and Methods Used in Combating It. Moscow, 1955.

[2] P. A. Rebinder, Jubilee Volume publ. on the occasion of the 30th Anniversary of the Great Socialist October Revolution, Acad. Sci. USSR Press, Vol. 1, 1947, p. 533.

[3] V. I. Lichtmann, P. A. Rebinder and G. V. Karpenko, "The Effect of Surface-Active Agents on Deformation Processes in Metals", Acad. Sci. USSR Press, 1954.

[4] S. T. Konobeevsky, Bull. Acad. Sci. USSR, Chem. Series, No. 5, 1209 (1937).

PHOTOOXIDATION OF WATER BY DYES ON THE SURFACE OF SEMICONDUCTORS

G. A. Korsunovsky

(Presented by Academician A. N. Terenin November 19, 1956)

In a recent paper by T. S. Glikman and M. E. Podlinyaeva [1] the authors have, on the basis of kinetic investigations of the photoreduction of thiazine dyes on zinc oxide, expressed the view that water takes part in this photoreaction directly as the substrate of oxidation. Starting from the same premises, though slightly different from those expressed by the above authors, we have investigated the photoreduction of methylene blue on zinc oxide, titanium dioxide and cadmium sulfide, using the hydroxylation of benzene as a method of detecting hydroxyl radicals.

The mechanism of photooxidation of water on zinc oxide, in the presence of oxygen, which is currently accepted is as follows [2]:

$$\begin{aligned} &ZnO \xrightarrow{h\nu} e + ZnO^{+}, \\ &e + O_2 \rightarrow O_2^{-}, \\ &O_2^{-} + H_2O \rightarrow HO_2 + OH^{-}, \\ &OH^{-} + ZnO \rightarrow ZnO + OH^{\cdot} \\ &HO_2 \rightarrow {}^1/_2H_2O_2 + {}^1/_2O_2. \end{aligned} \qquad (1)$$

The discharge of the hydroxyl ion on the positive center of a microcrystal of the semiconductor (ZnO^{+}), formed as a result of electron capture by a molecule of oxygen, leads to the formation of the hydroxyl radical. Having a high oxidizing power, the latter either reacts with the HO_2 radicals present and with hydrogen peroxide, thus reducing the yield of the peroxide, or brings about the oxidation of organic reducing agents, if such are present [3]. Even the benzene molecule which is highly resistant to oxidation, is, by interacting with hydroxyl radicals, transformed into phenol, diphenyl and higher hydroxy derivatives, as has been observed in different photo- and radiochemical reactions accompanied by the appearance of the free hydroxyl [4].

Even though a direct electron transfer from ZnO to H_2O that is without the participation of an intermediate electron carrier such as oxygen is fundamentally possible, because the affinity of H_2O for the electron is of the same order as that of oxygen [5], nevertheless we have never observed any subsequent decomposition of water to OH and H followed by evolution of the latter in the molecular state, as has been suggested by V. I. Veselovsky [2], apparently because the reverse reactions are much more probable. However, apart from oxygen it is possible to use other electron carriers with a sufficiently high oxidation potential, as for example dyes. Many dies of different classes are capable of capturing the electron and subsequently undergoing photoreduction to the lueco compound.

In our experiments we used Kalbaum brand Analytical grade Zinc Oxide having a particle size of 1 μ. 100 mg of the powder was placed into the lower end of two Tunberg tubes, followed by 10 ml of a solution of

methylene blue, having a concentration of $1.5 \cdot 10^{-4}$ M, in saturated aqueous solution of benzene ($\sim 10^{-2}$ M) (see Fig. 1). The tubes were connected to a vacuum pump and evacuated to a pressure of $1-5 \cdot 10^{-5}$ mm Hg, the contents being frozen and thawed four times. Subsequently the tubes were disconnected and one of them was irradiated for one hour under the mercury lamp PRK-2 through a filter transmitting the mercury line 366 mμ. This treatment caused complete discoloration of the dye. After irradiation, the water in the solution of methylene blue was distilled under vacuum into the upper end of the tube by immersing the latter in liquid air and carefully heating the lower end. Finally the tubes were opened and the distillate was transferred through the outlet A into the cell of the SF-4 spectrophotometer. The distillate from the tube which was not irradiated, was transferred into the comparison cell. The absorption spectrum of the distillate, shown in Fig. 2, coincides with the absorption spectrum of phenol plotted in the same diagram.*

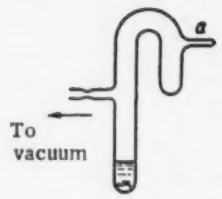

Fig. 1. Vacuum tube for irradiation of suspensions.

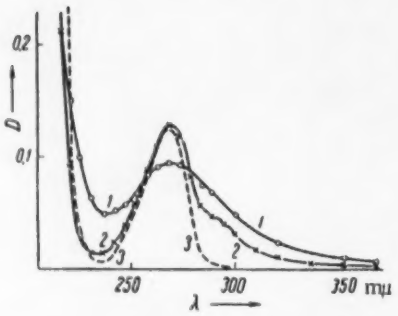

Fig. 2. Absorption spectra of the distillate obtained from suspensions of zinc oxide and titanium dioxide in aqueous benzene solution of methylene blue after irradiation in vacuo: 1) suspension of ZnO, 2) suspension of TiO_2, 3) phenol, $8 \cdot 10^{-5}$ M.

Formation of phenol can only take place through the combination of benzene and with the OH groups which are supplied either directly by the water, or as a result of the formation of zinc hydroxide [1]. However, as will be shown below, phenol is also formed on semiconductors which in aqueous solutions exhibit acid properties – a reason why, in our opinion, the direct participation of water is more probable in the case of neutral solutions.

The concentration of the phenol formed is approximately half the concentration of the dye dissolved, which corresponds to the following photoreaction:

$$\begin{gathered} e + K_p \rightarrow K_p^-, \\ K_p^- + H_2O \rightarrow K_pH + OH^-, \\ 2K_pH \rightarrow K_pH_2 + K_p, \\ OH^- + ZnO^+ \rightarrow ZnO[OH]_{ads}, \\ 2OH + C_6H_6 \rightarrow C_6H_5OH + H_2O \end{gathered} \qquad (2)$$

where K_p denotes the molecule of the dye.

The experiments with titanium dioxide (home produced, specification unknown, particle size 2–3 μ) were carried out in a similar manner. As is well known, titanium dioxide sensitizes the photoreduction of methylene blue in aqueous solutions [6]. In these experiments we have again detected phenol (Fig. 2), which indicates a photoreaction mechanism similar to that given for the reaction with zinc oxide. In fact, after irradiation in air of the titanium dioxide suspension in an aqueous solution of benzene, separation of the powder by centrifuging and recording of the absorption spectrum, we have detected phenol in approximately the same amount as that found in the case of zinc oxide.

On the other hand, when an aqueous suspension of titanium dioxide was similarly irradiated, not once was any hydrogen peroxide detected. This result led A. A. Krasnovsky to believe that the dioxide is inactive in aqueous systems [6]. As the formation of hydrogen peroxide is closely related to the formation of the

* Similar results were obtained by distilling the solutions in air after previous centrifuging. In both cases the phenol distills over with the water vapor.

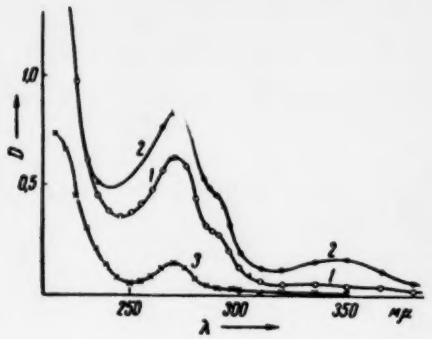

Fig. 3. Absorption spectra of the filtrate from suspensions of zinc oxide (1), titanium dioxide (2), and cadmium sulfide (3), in aqueous benzene solution after irradiation in the presence of air.

hydroxyl we have assumed that the absence of the hydroxide in the irradiated suspension of TiO_2 is due to its decomposition in the dark on the surface of the semiconductor. Experiments have shown that when a suspension of 100 ml of titanium dioxide is shaken up with 10 ml of $1.5 \cdot 10^{-4}$ M hydrogen peroxide in the dark for 30 minutes, the peroxide is completely decomposed, while in similar experiments with the same amount of zinc oxide the concentration of the peroxide did not change.

The third semiconductor investigated by us was cadmium sulfide manufactured by the Kalbaum firm, of "pure" grade and having a particle size of $0.5 - 1\mu$. It is known that irradiation of an aqueous suspension of cadmium sulfide with ultraviolet or blue light in the presence of oxygen gives rise to the formation of hydrogen peroxide in fairly high yield [7]; this has likewise been confirmed by our experiments. Nevertheless, the yield of phenol was found to be several times lower than in the case of ZnO and TiO_2 (Fig. 3). We explain this result as being due to the interaction of hydroxyl radicals with hydrogen sulfide formed as a result of partial hydrolysis of CdS. In this case we may expect oxidation of hydrogen sulfide to sulfuric acid. This was confirmed by qualitative test for the $SO_4^{"}$ ion by addition of barium chloride. In control experiments it was established that the filtrate obtained from a suspension of cadmium sulfide, when shaken with hydrogen peroxide of similar concentration as that formed during irradiation, does not give a precipitate of $BaSO_4$, and therefore, hydrogen peroxide cannot be regarded as bein responsible for the oxidation of hydrogen sulfide.

Irradiation of a suspension of cadmium sulfide in aqueous or aqueous—benzene solution of methylene blue in vacuo for long periods (up to 5 hours) brings about only a very slight discoloration of the dye. The discoloration proceeds particularly slowly in the case of the dye adsorbed on the surface of the semiconductor (about 60-70% adsorbed). Tests for phenol and sulfuric acid gave negative results, which apparently indicates a different mechanism of discoloration. It is possible that in this case the substrate of oxidation is provided by the hydrogen sulfide, the reducing power of which, by comparison with that of the dye, is higher than that of water.

In conclusion I wish to express my indebtedness to Academician A. N. Terenin for his constant interest in this investigation.

Received November 12, 1956

LITERATURE CITED

[1] T. S. Glikman and M. E. Podlinyaeva, Ukr. Khim. Zhur., 22, 479 (1956).

[2] V. I. Veselovsky and D. M. Shub, J. Phys. Chem., 26, 509 (1952); I. G. Calvert, K. Theuer, G. T. Rankin, W. M. McNevin, J. Am. Chem. Soc., 76, 2575 (1954).

[3] M. C. Markham, K. J. Zaider, J. Phys. Chem., 57, 363 (1953); H. G. Bates, N. Uri, J. Am. Chem. Soc., 75, 2754 (1953).

[4] F. T. Framer, G. Stein, J. Weiss, J. Chem. Soc., 1949, 3241; J. H. Baxendale, J. Magee, Trans. Farad. Soc., 51, 205 (1955).

[5] A. Farkas, L. Farkas, Trans. Farad. Soc., 34, 1113 (1938).

[6] C. Neuweiler, Zs. wiss. Phot., 25, 211 (1927); A. A. Krasnovsky, Dissertation, Chem.-Techn. Inst., Moscow, 1940.

[7] R. E. Stephens, B. Ke, D. Trivich, J. Phys. Chem., 59, 966 (1955).

FORMATION OF HYDROCYANIC ACID IN GAS MIXTURES COMPRESSED ADIABATICALLY TO HIGH PRESSURES

A. M. Markevich, I. I. Tamm and Yu. N. Ryabinin

(Presented by Academician V. N. Kondratyev, November 23, 1956)

In previous papers [1-4] we investigated the formation of nitric oxide by the method of adiabatic compression of gas mixtures at high compression ratios. By completing the entire process within periods of the duration of ten-thousandths of a second we succeeded, even in the case of pure air [1] and at compression ratios of 700 and pressures of 8000-9000 kg/cm^2, in obtaining yields of nitric oxide of up to 1%. This figure was raised to over 3% either by diluting the gas mixture with argon which, being a monatomic gas, permits realizing higher temperatures on compression, or by adding to the mixture a fuel gas such as methane, hydrogen and carbon monoxide, and thus raising the temperature of the mixture on compression due to the heat of combustion. This relatively high yield of nitric oxide synthesized from its elements was possible because the adiabatic apparatus with the propelling piston [3] permitted the realization not only of high pressures and temperatures, but also of relatively high rates of cooling.

The present paper describes the investigation of the synthesis of hydrocyanic acid by adiabatic compression. Thermodynamic considerations show that with rise in temperature the equilibrium of the reaction is shifted so as to favor the formation of hydrocyanic acid. In this respect the reaction of the formation of HCN resembles the synthesis of nitric oxide, where a rise in temperature likewise shifts the equilibrium in the direction favoring formation of NO.

Earlier it was shown [4] that when mixtures consisting of varying proportions of hydrogen, nitrogen, argon and carbon black (activated charcoal, soot) are compressed adiabatically, traces of hydrocyanic acid can be detected in the products resulting from the compression.

In this work we have investigated the formation of hydrocyanic acid in mixtures of nitrogen and hydrocarbons – methane and acetylene. Experiments with mixtures containing methane showed that in mixtures containing both gases in the poroportion of 1:1 no reaction occurred at pressures of up to 10,000 kg/cm^2. Reaction takes place only on addition of considerable amounts of argon, i.e. through an increase in the temperature developed during compression. The results of experiments with a mixture of 10% CH_4, 13% N_2 and 77% A are shown in Fig. 1, 1. The maximum yield of hydrocyanic acid amounted to about 1% of the initial volume of the mixture.

Considerably larger proportions of hydrocyanic acid were obtained with mixtures containing acetylene. With equimolar mixtures of acetylene and nitrogen, formation of hydrocyanic acid begins even at pressures of about 1,000 kg/cm^2. The maximum yield obtained at pressures of 5,000-9,000 kg/cm^2 was about 3%. The results of these experiments are represented by curve 2 in Fig. 1. As in the foregoing experiments, addition of argon to the mixture makes it possible to realize an increase in temperature on compression which, in turn, gives rise to higher yields of hydrocyanic acid. Curve 3 in Fig. 1 represents the results of experiments with a mixture consisting of 25% C_2H_2, 32% N_2 and 43% A.

The yield of HCN realized in these experiments was 4%.

In all the experiments described determination of the hydrocyanic acid content was carried out as follows. After being compressed adiabatically for 1-2 seconds, the gases were pumped off from the tube of

the adiabatic compression apparatus into an evacuated flask containing 10 ml of 0.1 N alkali. When absorption of the hydrocyanic acid was complete the contents of the flask were titrated with 0.01 N silver nitrate in the presence of potassium iodide [5]. The presence of hydrocyanic acid was also established by qualitative reactions. The experimental data are presented in Table 1.

TABLE 1

Compression ratio	Max. pressure developed during compression, kg/cm²	Yield of HCN, % v/v	Compression ratio	Max. pressure developed during compression, kg/cm²	Yield of HCN, % v/v	Compression ratio	Max. pressure developed during compression, kg/cm²	Yield of HCN, % v/v
Starting mixture: CH_4 10%, N_2 13% A 77%. Wt. of piston 375 g			Starting mixture: C_2H_2 50% N_2 50%, Wt. of piston 187 g			Starting mixture: C_2H_2 25%, N_2 32% A 43%. Wt. of piston 187 g		
420	3300	0.09	100	300	0.00	70	800	0.00
520	3600	0.17	146	900	0.03	85	1200	0.19
600	3800	0.25	173	1650	0.50	135	1600	1.02
610	4300	0.30	230	2400	1.18	152	1900	1.33
790	4800	0.53	270	2900	1.39	174	2250	2.03
910	4800	0.65	280	3550	1.87	215	2650	2.59
810	5200	0.58	330	4800	2.46	280	3250	3.14
1170	6000	0.87	330	4800	2.70	300	4200	3.60
1440	7480	0.95	385	4950	2.85	410	5300	4.00
1480	8300	0.98	330	5000	2.78	485	6500	4.00
1480	8500	1.01	365	5300	2.82	550	7400	4.08
			400	5300	3.09			
			430	6100	2.72			
			445	6700	2.67			
			475	7350	3.12			
			620	9200	3.04			

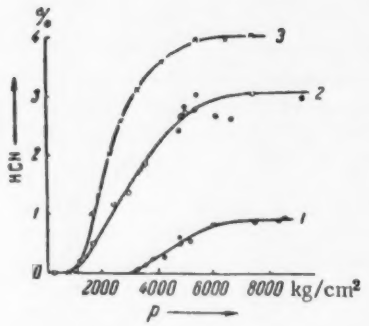

Fig. 1. Formation of hydrocyanic acid during adiabatic compression of gas mixtures: 1) CH_4 10%, N_2 13%, A 77%; 2) C_2H_2 50%, N_2 50%, 3) C_2H_2 25%, N_2 32%, A 43%.

In our opinion the results obtained are of interest not only as a demonstration of the synthesis of hydrocyanic acid by adiabatic compression of mixtures of nitrogen with hydrocarbons. Also worthy of special attention is the shape of the experimental curves (Fig. 1) which, as will be noted particularly in the case of mixtures with acetylene, are characterized by a transition towards saturation, An increase in pressure above 4,000-5,000 kg/cm² does not result in a corresponding increase of the content of HCN in the products of reaction. This shape of the curves cannot, for example, be explained as being due to the fact that at high compression ratios the temperature increases comparatively slowly with pressure and, therefore, there is little increase in the rate of reaction. It is also necessary to take into account the fact that in the pressure range of 4,000-8,000 kg/cm² the concentration of the reagents is doubled. All these considerations tend to show that the rate of reaction in the pressure interval in question should vary.

On the other hand, the thermodynamic calculations carried out by Krase and Mackey [6] cannot be used to explain this attainment of the saturation concentration as being due simply to the attainment of the thermodynamic equilibrium concentrations of hydrocyanic acid, because in this case the yield should have been considerably higher than 4% (Fig. 1, 3). The reason for the constancy of the yield of hydrocyanic acid at pressures above 4,000-4,500 kg/cm² must, apparently, be sought in the conditions of cooling which, in our case, are determined by the experimental conditions obtaining in the adiabatic system used. It is well known that under certain experimental conditions, or more accurately conditions of

cooling the results obtained show quite substantial divergence. Indeed, it is with the cooling process of reacting systems that the so-called notion of "fixation" is linked. In our opinion it is this phenomenon of fixation which must be taken into account in order to explain the constancy of the yield of HCN obtained in these experiments.

Let us suppose that at high compression ratios and correspondingly high temperatures the rate of reaction is such that during the compression interval there is sufficient time for the system to attain thermodynamic equilibrium. Under these conditions the rate of formation of hydrocyanic acid, W_1, will be equal to the rate of the reverse reaction, W_2. The concentration of hydrocyanic acid will correspond to its equilibrium value, $[HCN]^0$. As the temperature drops, $[HCN]^0$ will decrease in the proportion given by the equilibrium constant. However, as the temperature drops from T_1 to T_2 the actual concentration of hydrocyanic acid [HCN] will depend not only on the equilibrium value of $[HCN]^0_{T_2}$, but also on the rate of decomposition of the acid, W_2.

If during the cooling process W_2 is always considerably greater than $d[HCN]^0/dt$ (where t is the time), i.e. if

$$W_2 \gg \frac{d[HCN]^0}{dt}, \tag{1}$$

then the actual concentration of the acid [HCN] will always be approximately equal to its equilibrium concentration, and $[HCN]_T - [HCN]^0_T \approx 0$.

If, on the other hand, the reverse inequality

$$W_2 \ll \frac{d[HCN]^0}{dt}, \tag{2}$$

will be fulfilled during cooling, the actual concentration [HCN] will always exceed the equilibrium concentration, and $[HCN]_T - [HCN]^0_T > 0$.

Let us introduce a new variable $\varphi = dT/dt$ and transcribe Inequality (1) in the form:

$$W_2 \gg \varphi \frac{d[HCN]^0}{dT}, \tag{3}$$

where the rate of cooling φ is, in practice, always determined by the experimental conditions, and W_2 and $d[HCN]^0/dt$ are determined by kinetic and thermodynamic factors. With falling temperature W_2 decreases exponentially, while the variation of $d[HCN]^0/dT$ is determined by the expression for the equilibrium-constant.

If, with decreasing temperature, the left-hand side of Inequality (3) diminishes faster than the right-hand side, then, starting at some temperature T_k, the Inequality (3) will change sign and Inequality (2) will be fulfilled. Consequently, from a certain critical temperature T_k on, the difference $[HCN]^0_{T_k}$ will not be equal to zero.

Other conditions being equal, the value of T_k is determined only by the rate of cooling φ. The greater φ, the greater T_k is. For $T > T_k$ the reaction is, according to determinations carried out by Ya. B. Zeldovich [7], characterized by a high mobility, and $[HCN]_T - [HCN]^0_T \approx 0$. For $T < T_k$, when the reaction is slow, the actual concentration [HCN] remains approximately equal to $[HCN]^0_{T_k}$, i.e.

$$[HCN]^0_T < [HCN]_T \approx [HCN]^0_{T_K}. \quad (4)$$

In this, strictly speaking, lies the essence of the notion of fixation.

Consequently, the amount of hydrocyanic acid actually determined in the products of reaction may not at all correspond to the amount of HCN formed at the maximum temperature of the experiment, but may be considerably less.

To return to the experiments described above we may note that the cooling of the reaction products is an integral part of the adiabatic cycle. Calculation shows that in our experiments with the adiabatic apparatus available the rate of cooling in the region of a compression ratio of ~350 was of the order of 10^7 °C/sec and varied little with further increase in the compression ratio. This provides an explanation for the existence of the horizontal region of the curves in Fig. 1 in the pressure region beginning at 4,000-4,500 kg/cm^2.

Institute of Chemical Physics of the Academy of Sciences of the USSR

Received November 20, 1956

LITERATURE CITED

[1] Yu. N. Ryabinin, A. M. Markevich and I. I. Tamm, Proc. Acad. Sci. USSR, 95, 111 (1954).

[2] Yu. N. Ryabinin, A. M. Markevich and I. I. Tamm, Ibid., 112, 283 (1957).

[3] Yu. N. Ryabinin, J. Exp. Theor. Phys., 23, 461 (1952).

[4] Yu. N. Ryabinin, A. M. Markevich and I. I. Tamm, Proc. Acad. Sci. USSR, 94, 1121 (1954).

[5] L. Z. Soborovsky and G. Yu. Epshtein, Chemistry and Technology of Chemical Warfare Materials, 1938.

[6] N. W. Krase, B. Mackey, J. Phys. Chem., 32, 1488 (1928).

[7] Ya. B. Zeldovich, P. Ya. Sadovnikov and D. A. Frank-Kamenetsky, Oxidation of Nitrogen during Combustion, Acad. Sci. USSR Press, 1947.

THE DEPENDENCE OF THE AMOUNT OF HYDROGEN ADSORBED ON RANEY NICKEL AND PLATINUM CATALYSTS ON THE MEDIUM

Academician D. V. Sokolsky and K. K. Dzhardamalieva

One of the indispensible steps in catalytic hydrogenation processes is the preliminary activation of the reactants on the surface of the catalyst. The activation of hydrogen and of the unsaturated compound on the catalyst surface depends on the specific properties of the compound to be hydrogenated, on the nature of the catalyst and on the conditions under which the reaction is carried out; namely, the temperature, the pressure of the hydrogen in the gaseous phase, the speed of mixing and the nature of the medium in which the reaction is carried out. A change of the medium has a large effect on the strength with which the hydrogen is bound on the surface. By using different solvents it is possible to strengthen the bond between the hydrogen and the surface and thus vary the amount of hydrogen adsorbed on the surface of the catalyst [1, 2].

This paper describes an investigation of the effect of different concentrations of alkali and acid on the adsorption of hydrogen by Raney nickel and platinum catalysts in the course of hydrogenation of some organic compounds. The compounds chosen were sodium maleate and o-nitrophenol. The nickel catalyst was prepared by extracting a nickel-aluminum alloy with alkali. The platinum catalyst was prepared in the form of the oxide [3]. In the case of the nickel catalyst the experiments were carried out in aqueous solutions of sodium hydroxide at concentrations varying from 0.01 N to 15 N; the platinum catalyst was used in aqueous solutions of NaOH and H_2SO_4. The temperature was varied from 20 to 60°. A weighed amount of the catalyst (1 g of nickel or, respectively, 0.2 g of platinous oxide) was placed in the bulb and saturated with hydrogen in the given medium over a period of 1 hour. Excess hydrogen was then removed by a current of nitrogen and the substance to be hydrogenated was added to the contents of the bulb. Hydrogenation of the substance by the adsorbed hydrogen was brought about by vigorously shaking the bulb.

As the reaction progressed the potential of the catalyst was measured with respect to the reversible hydrogen electrode [4]. At definite intervals of time the shaking was interrupted and samples of the substance were taken in a current of nitrogen for subsequent determination of the amount of hydrogen extracted from the catalyst up to the given time. The analysis was carried out by dehydrogenating the samples on the platinum catalyst.

TABLE 1

Amount of Hydrogen (in ml) Extracted by Sodium Maleate from 1 g of Raney Nickel Catalyst over a Period of 2 Hours

Temperature, °C	Concentration of Alkali, N					
	0.01	0.05	0.1	0.5	1.0	5.0
20	67.4	68.4	60.3	—	36.5	25.8
40	73.1	68.3	62.5	57.9	55.5	45.4
60	77.9	69.1	65.7	60.2	58.0	52.3

The results of experiments on the hydrogenation of sodium maleate by hydrogen adsorbed on the Raney nickel catalyst are shown in Table 1.

It will be seen that as the concentration of alkali increases the amount of hydrogen extracted over 2 hours decreases; the maximum amount extracted is about 70-80 ml. It is known that 1 g of Raney nickel catalyst can adsorb up to 110-120 ml of hydrogen [2]. From this it follows that sodium maleate does not extract all the adsorbed hydrogen; it appears to be a substance

• Acad. Sci. Kazakh SSR.

having a comparatively low adsorption potential and capable of desorbing only those hydrogen atoms which are bound relatively loosely on the surface of the catalyst. Here the nature of the compound being hydrogenated becomes evident. [2, 5]. The maximum drop of potential of the catalyst in the course of the hydrogenation of sodium maleate amounts to 130-150 millivolts. This indicates that considerable quantities of hydrogen remain adsorbed on the surface of the catalyst. Accordingly, the amount of hydrogen extracted increases with rising temperature, while an increase in the concentration of alkali strengthens the bond between the hydrogen and the surface, making extraction of the former more difficult.

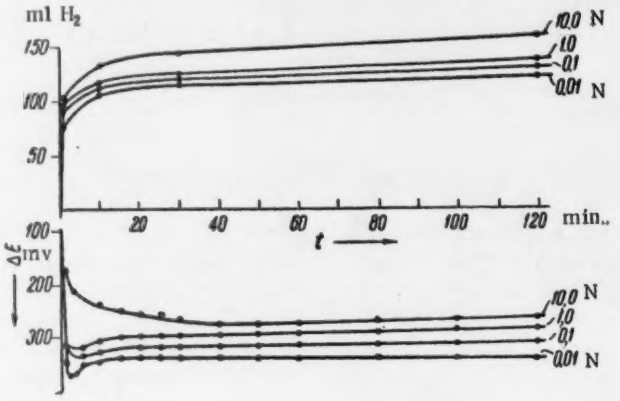

Fig. 1. Kinetic and potential curves for the hydrogenation of o-nitrophenol by hydrogen adsorbed on Raney nickel catalyst, at different concentrations of alkali. Temperature of experiment 60°.

In order to elucidate the relationship between the amount of hydrogen adsorbed and the concentration of alkali it was necessary to choose a substance which would be capable of extracting all the hydrogen adsorbed by the catalyst. The substance chosen was o-nitrophenol. The results of the experiments carried out under conditions similar to the foregoing are shown in Table 2.

TABLE 2

Amount of Hydrogen (in ml) Extracted by o-Nitrophenol from 1 g of Raney Nickel Catalyst over a period of 2 hours

Temperature, °C	Concentration of Alkali, N							
	0.01	0.05	0.1	0.5	1.0	5.0	10.0	15.0
20	105.7	107.0	113.2	113.6	113.7	125.2	—	—
40	115.2	118.9	123.6	125.3	125.6	135.0	—	—
60	127.4	132.8	136.6	137.3	137.7	148.5	160.6	—
80	—	—	—	—	—	—	164.4	—
	Potential referred to the reversible hydrogen electrode (E, mv)							
—	998	1050	1070	1110	1123	1150	1176	1198

It will be seen that the amount of hydrogen extracted increases with rise in concentration of alkali. At 60° the amount of hydrogen extracted increases from 127 ml for the 0.01 N solution to 160 ml for the 10.0 N solution of alkali.

In Fig. 1 are plotted kinetic and potential curves for the hydrogenation of o-nitrophenol by adsorbed hydrogen at different concentrations of alkali, at 60°. The time of extraction of the hydrogen is taken as the abscissa; the amount of hydrogen extracted and the potential drop of the catalyst with respect to the hydrogen electrode, ΔE, are plotted as ordinates. As will be seen from the diagram, the potential of the catalyst drops sharply in the first minute after the introduction of o-nitrophenol. The higher the concentration of alkali, the lower the drop in the potential of the catalyst. In 10.0 N alkali the potential drop

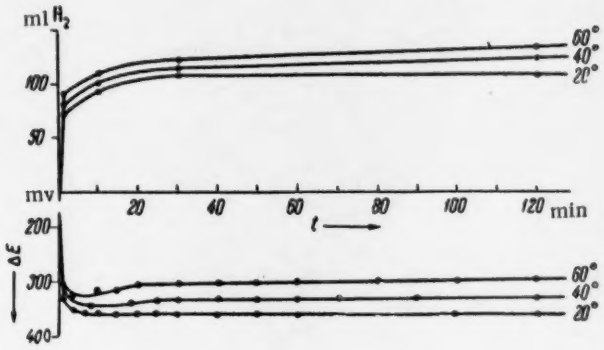

Fig. 2. Kinetic and potential curves for the hydrogenation of o-nitrophenol by hydrogen adsorbed on Raney nickel catalyst, in 0.5 N NaOH at 20, 40 and 60°.

amounts to 160 mv, while in 0.01 N it is greater than 350 mv. In the first minute the rate of extraction of the hydrogen is greatest. For example, in 0.01 N alkali 77 ml of hydrogen are extracted in the first minute, while after 2 hours of hydrogenation the amount extracted is 127 ml. Thus, more than half of the total hydrogen extracted is extracted in the first minute.

TABLE 3

Concentration of alkali, N	Amt. H_2 extr'd., ml	E, mv	Concentration of acid, N	Amt. H_2 extr'd., ml	E, mv
0.1	10.2	260	0.1	8.0	298
0.5	8.2	265	1.0	8.2	280
1.0	9.9	250	5.0	10.2	306
5.0	4.7	342	—	—	—

The amount of hydrogen extracted also increases with temperature (see Table 2 and Fig. 2), apparently due to extraction from deeper-lying layers of the catalyst. In contrast with the nickel catalyst, the amount of hydrogen adsorbed on the platinum catalyst is almost independent of the concentration of alkali. The results obtained in the course of the extraction of hydrogen from 0.2 g of PtO_2 by o-nitrophenol are shown in Table 3 (temperature of experiment 20°.

As will be seen from Table 3, for all concentrations of alkali and acid (with the exception of 5.0 N NaOH) the amount of hydrogen extracted from a given weight of platinous oxide is approximately constant. This can apparently be explained as being due to the considerable energy of bonding between the hydrogen and the surface and also to a small amount of hydrogen dissolved in the platinum.

S. M. Kirov State University, Kazakh
Alma-Ata.

Received November 5, 1956

LITERATURE CITED

[1] A. I. Shlygin, A. N. Frumkin, Proc. Acad. Sci. USSR, 2, 173 (1934).

[2] D. V. Sokolsky, S. T. Bezverkhova, Ibid., 94, No. 3 (1954).

[3] V. L. Frampton, F. D. Edwards, H. K. Henze, J. Am. Chem. Soc., 73, 4432 (1951).

[4] D. V. Sokolsky, V. A. Druz, Proc. Acad. Sci. USSR, 73, 949, (1950).

[5] L. Kh. Freidlin, K. G. Rudneva, Ibid., 74, 955 (1950).

KINETICS OF DEHYDROGENATION OF ALCOHOLS OVER PRECIPITATED COPPER CATALYST

Academician A. A. Balandin and P. Teteni

The kinetics of dehydrogenation of alcohols of different structure over copper has been investigated by several authors [1-7]. These authors have shown that the rate and activation energy of dehydrogenation of alcohols does not depend on their structure [1, 2], or depends on it but little [4, 5]. It has also been established [7] that adsorption coefficients of ethyl, n-propl and isopropyl alcohols on the copper catalyst are the same.

In the present work we have investigated the kinetics of dehydrogenation of alcohols differing considerably with respect to their structure: ethyl, isopropyl and benzyl alcohols and cyclohexanol. In addition to the determination of the activation energy of these alcohols this investigation is also of interest with regard to adsorption of different alcohols on a given catalyst.

In contrast to previous work we have in the present investigation used a copper catalyst prepared by precipitating cupric hydroxide with ammonia from a 20% solution of cupric nitrate. The cupric hydroxide was decomposed at 400° in a current of air, and the cupric oxide obtained was reduced with electrolytic hydrogen at 150, 200, 250 and 300° for 6 hours at each temperature. After each experiment the catalyst was regenerated with hydrogen. The substances used had physical constants identical with those found in the literature. Hydrogen used for the preparation of mixtures required for the determination of adsorption coefficients was obtained by electrolysis of a 20% solution of KOH, after which it was freed from traces of oxygen by passing over copper at 380-400°, and dried over $CaCl_2$. The experiments were carried out in the usual flow apparatus used at the Laboratory of Organic Catalysis of the University of Moscow. The starting materials were fed automatically by means of an injector operated by a motor (accuracy of feed ± 0.005 ml/min). Collection and measurement of the volume of gas evolved during the reaction was by means of an automatic gasometer of the Patrikeev type. It was found that within the temperature interval investigated (180-280°) the catalyst used brought about dehydrogenation as the only reaction in the case of all the four alcohols mentioned. The gas formed was found to be pure hydrogen (the purity of the gas was checked by gas analysis). The catalyzate was found by distillation to contain unreacted alcohol and the corresponding aldehyde or ketone. Experiments with catalysts of different particle size showed that the reactions were being carried out in the kinetic region.

As was shown in [8, 9], dehydrogenation of alcohols is governed by the general kinetic equation deduced by one of us [10] for unimolecular catalytic reactions in a vapor stream. In the case of dehydrogenation of alcohols without admixtures this equation has the form

$$\frac{dm}{dl} = k\frac{A_1 - m}{A_1 + (z_2 + z_3 - 1)\,m}, \qquad (1)$$

where k is the velocity coefficient of the reaction, A_1 is the rate of delivery of the alcohol, and m the rate of evolution of hydrogen, the remaining symbols having the meanings specified in [8].

Integrating this equation we get:

$$k = (z_2 + z_3)\,A_1 \ln\frac{A_1}{A_1 - m} - (z_2 + z_3 - 1)\,m. \qquad (2)$$

The relative adsorption coefficients entering into Equation (2) were determined by a contact reaction method based on the lowering of the rate of reaction on addition to the starting substance of a determined amount of the product of reaction or of an extraneous substance. The decrease in the rate of reaction indicates the extent of adsorption of the added substance on the active sites of the catalyst.

The adsorption coefficient z was calculated by means of the formula [11]

$$z = [B_1 (2H - Y) - YH]/[(1 - B_1) Y], \tag{3}$$

where:

$$B_1 = A_1/\Sigma A_r; \quad Y = m/\Sigma A_r; \quad H = Y/2 - Y \text{ *}.$$

It may be noted that the adsorption coefficients calculated by means of Formula (3) do not differ greatly from those calculated by means of the more simple formula [12] deduced for lower orders of reaction:

$$z = \left(\frac{m_0}{m} - 1\right) \Big/ \left(\frac{100}{p} - 1\right), \tag{4}$$

where p is the percentage of alcohol in the mixture, and m_0 the value of m for the pure alcohol.

The relative adsorption coefficients were determined from the velocity of dehydrogenation of binary mixtures of the products of reaction with the original alcohol. The volume rate of flow of the alcohol in the experiment with the pure substance was equal to the sum of the volume rates of flow of the alcohol and the reaction product in experiments with the mixtures. In order to check the constancy of the activity of the catalyst, the experiments with the mixtures were alternated by experiments with the pure substance. It was confirmed that the relative adsorption coefficients were independent of the volume rate of feed. The results of determinations of the adsorption coefficients are given in Tables 1 and 2. The curves of adsorption displacement were of a form similar to that observed earlier for other substances [12].

The relative adsorption coefficients of acetaldehyde and hydrogen differ from those obtained in earlier investigations which were found to be close, respectively, to unity and zero. However, the catalyst used in the investigations mentioned was obtained by calcinating cupric nitrate and reducing the cupric oxide obtained with hydrogen. On the other hand, the results of these earlier investigations which showed that the relative adsorption coefficients were independent of the temperature (in the case of the copper catalyst), have been confirmed in the present experiments. The relative adsorption coefficients of acetone obtained here are close to those calculated from the data given in [2] and are equal to 0.77 ± 0.02. Adsorption coefficients for the other substances on copper have not been determined in previous investigations.

As will be seen from Table 2, the relative adsorption coefficients of hydrogen are independent of the temperature. From this it follows [13, 14], that the heats of adsorption of the corresponding alcohols are equal to the heat of adsorption of hydrogen and, consequently, equal to each other. As is known from the literature [15, 16], the heats of condensation of the alcohols investigated at this time differ considerably, varying from 9.3 kcal/mole for ethyl alcohol to 12.06 kcal/mole for benzyl alcohol. The heats of physical adsorption of the alcohols investigated by us might, in the case of their physical adsorption on the catalyst, be expected to differ from one another as heats of physical adsorption are usually close to the heats of condensation. The fact that the heats of adsorption of these alcohols on a catalytically active surface are

* In the expression for H, Y denotes the amount reacted in the experiment with the pure substance.

TABLE 1

Relative Adsorption Coefficients z_2 (ratio of adsorption coefficients of aldehydes and ketones to those of the corresponding alcohols) Precipitated Copper Catalyst

Substance	Temp. °C	z_2
CH_3CHO/C_2H_5OH	250	0.68±0.03
	275	0.67±0.005
$(CH_3)_2CO/-C_3H_7OH$	189	0.64±0.01
	212	0.57±0.01
	230	0.64±0.03
$C_6H_5CHO/C_6H_5CH_2OH$	244	1.33±0.07
	269	1.34±0.06
$C_6H_{10}O/C_6H_{11}OH$	212	1.23±0.07
	238	1.24±0.02
	244	1.16±0.08
	250	1.16±0.02

TABLE 2

Relative Adsorption Coefficients z_3 (ratio of the adsorption coefficient k to adsorption coefficients of different alcohols) Precipitated Copper Catalyst

Alcohol	Temp. °C	$z_3=a_{H_2}/a_{alc}$
C_2H_5OH	223	0.55±0.04
	239	0.50±0.03
	266	0.56±0.05
iso-C_3H_7OH	189	0.30±0.01
	212	0.30±0.02
	216	0.38±0.04
	230	0.37±0.02
$C_6H_5CH_2OH$	235	0.52±0.03
	265	0.54±0.02
$C_6H_{11}OH$	212	0.52±0.03
	238	0.48±0.03

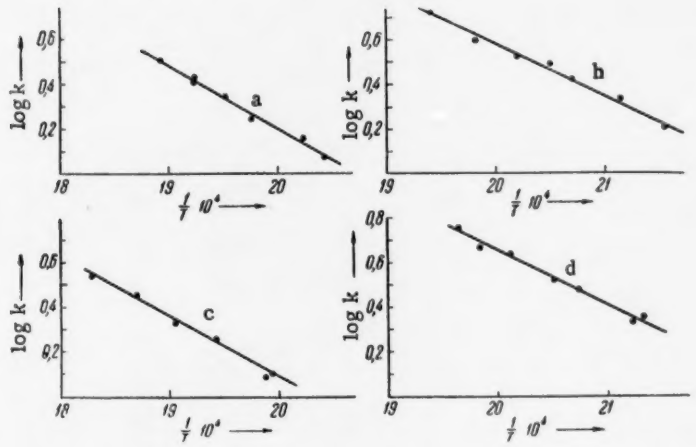

Fig. 1. Relationship between the logarithm of the velocity constant of reaction and the reciprocal temperature in the dehydrogenation of alcohols: a) ethyl alcohol, b) isopropyl alcohol, c) benzyl alcohol, d) cyclohexanol.

the same is evidence that chemical forces are taking part in the process of adsorption of alcohols during catalysis.

The determination of the relative adsorption coefficients of the products of dehydrogenation enabled us to determine the true energies of activation of dehydrogenation of the alcohols investigated. In order to determine the velocity constants, the corresponding adsorption coefficients from Tables 1 and 2, as well as the values of $\underline{m}$ (determined at different temperatures) and A_1 were substituted into Equation (2). The results obtained are given in Tables 3, 4, 5 and 6 and are plotted in Fig. 1. The true activation energies of dehydrogenation of alcohols on the given catalyst have been determined for the first time. In the previous work [4] on the copper catalyst which was prepared by a different method, the authors have determined the true activation energy of dehydrogenation of ethyl alcohol which was the same as the value now found by us (12.8 kcal/mole).

TABLE 3

Dehydrogenation of C_2H_5OH on Cu. Volume of Catalyst 4 ml; Flow Rate 0.126 ml/min; A_1 = = 11.25 ml/min · ml of Catalyst; $z_2 + z_3 = 1.21$; ϵ = 12,800 cal/mole; $k_0 = 6.65 \cdot 10^5$; ϵ /log $k_0 = 2.2 \cdot 10^3$

Expt. No.	T °C	V_{H_2} ml/min	m_{H_2} ml/min · ml cat.	k	k_{calc} for ϵ = 12800 cal/mole
6	217	4.40	1.10	1.18	1.22
7	222	5.23	1.31	1.44	1.50
2	231	6.36	1.59	1.79	1.77
3	240	7.87	1.97	1.23	1.97
1	247	9.37	2.34	2.67	2.67
5	247	9.14	2.28	2.58	2.67
4	256	11.00	2.75	3.23	3.28

TABLE 4

Dehydrogenation of Isopropyl Alcohol on Cu. Volume of Catalyst 4 ml; Flow Rate 0.164 ml/min; A_1 = 12.07 ml/min · ml of Catalyst; $z_2 + z_3 = 0.96$; ϵ = 10,700 cal/mole; $k_0 = 1.89 \cdot 10^5$, ϵ /log $k_0 = 2.03 \cdot 10^3$

Expt. No.	T °C	V_{H_2} ml/min	V_{H_2} ml/min · ml cat.	k	k_{calc} for ϵ = 10700 cal/mole
6	191	6.20	1.55	1.66	1.55
3	200	7.93	1.98	2.17	1.99
1	210	9.48	2.37	2.64	1.61
5	215	10.73	2.68	3.07	2.91
2	223	11.67	2.92	3.34	3.34
4	232	14.77	3.69	3.97	4.16
7	242	17.17	4.29	5.28	5.22

TABLE 5

Dehydrogenation of Benzyl Alcohol on Cu. Volume of Catalyst 4 ml; Flow Rate 0.21 ml/ min; A_1 = = 11.37 ml/min · ml of Catalyst; $z_2 + z_3 = 1.87$; ϵ = 12,300 cal/mole; $k_0 = 2.92 \cdot 10^5$; ϵ /log k_0 = = $2.25 \cdot 10^3$

Expt. no.	T °C	V_{H_2} ml/min	m_{H_2} ml/min · ml cat.	k	k_{calc} for ϵ=12300 cal/mole
6	229	4.60	1.15	1.27	1.27
1	230	4.43	1.11	1.24	1.33
3	242	6.30	1.58	1.79	1.73
4	252	7.36	1.84	2.17	2.17
5	262	9.24	2.32	2.83	2.70
4	274	10.90	2.73	3.43	3.42

TABLE 6

Dehydrogenation of Cyclohexanol on Cu. Volume of Catalyst 4 ml; Flow Rate 0.21 ml/min; A_1 = = 11.37 ml/min · ml of Catalyst; $z_2 + z_3 = 1.70$; ϵ = 11,100 cal/mole; $k_0 = 3.34 \cdot 10^5$; ϵ/log k_0 = = $2.01 \cdot 10^3$

Expt. no.	T °C	V_{H_2} ml/min	m_{H_2} ml/min · ml cat.	k	k_{calc} for ϵ = 11100 cal/mole
4	196	7.66	1.92	2.25	2.24
7	198	7.44	1.86	2.19	2.26
3	209	10.17	2.55	3.03	3.03
5	214	10.87	2.72	3.40	3.39
1	224	13.23	3.31	4.32	4.19
6	231	14.03	3.51	4.72	5.00
2	236	16.10	4.02	5.72	5.58

The data obtained indicate that the structure of the hydrocarbon radical of the alcohol has little effect on the value of the activation energy of dehydrogenation on the given metallic copper catalyst. Even radicals as different with respect to their nature as the phenyl and methyl radicals in ethyl and benzyl alcohols have no significant effect. The fact that the nature of the hydrocarbon radical has no little effect on the activation energy appears to provide a confirmation of the multiplet theory, the explanation being that the influence of the extraneous substituent manifests itself to a nearly equal extent [17] in the strength of the interatomic bond within the molecule, which is ruptured in the course of the reaction, as well as in the nature of the bond between the atoms of the reacting molecule and the atoms of the catalyst.

M. V. Lomonosov State University
Moscow

Received December 6, 1956

LITERATURE CITED

[1] W. G. Palmer, F. H. Constable, Proc. Roy. Soc. (A), 107, 225 (1925).

[2] A. A. Balandin, M. N. Marushkin and B. A. Ikonnikov, Sci. Records Moscow State Univ. Vol.22, 221 (1934).

[3] A. Bork, A. A. Balandin, Zs. phys. Chem., (B), 33, 54 (1936).

[4] A. Bork, A. A. Balandin, Zs. phys. Chem., (B), 33, 73 (1936).

[5] A. Bork, A. A. Balandin, Zs. phys. Chem., (B), 33, 435 (1936).

[6] A. Bork, Acta Physicochim. URSS, 1, 409 (1939).

[7] A. Bork, Acta Physicochim. URSS, 9, 697 (1938); J. Phys. Chem. 13, 421 (1939).

[8] A. E. Agronomov, Bull. Moscow State Univ. 6, No. 2, 109 (1951).

[9] A. A. Balandin and E. I. Klabunovsky, Proc. Acad. Sci. USSR, 98, No. 5, 783 (1954).

[10] A. A. Balandin, J. Gen. Chem., 12, 153 (1942).

[11] A. A. Balandin, Ibid., 12, 160 (1942).

[12] A. A. Balandin, O. K. Bogdanova and A. P. Shcheglova, Bull. Acad. Sci. USSR, Div. Chem. Sci., 1946, 5, 497.

[13] A. Kh. Bork, Collected Papers on Phys.-Chem. subjects (Acad. Sci. USSR Press, 1947) p.168.

[14] A. A. Balandin, Proc. Acad. Sci. USSR, 63, 33 (1948).

[15] J. H. Mathews, J. Am. Chem. Soc., 48, 562 (1926).

[16] N. Nagornow, L. Ratinjanz, Zs. phys. Chem., 77, 704 (1911).

[17] A. A. Balandin, J. Gen. Chem., 97, 667 (1954).*

* Original Russian pagination. See C. B. Translation.

ON CERTAIN REGULARITIES OF DIFFUSION BURNING OF LIQUIDS

V. I. Blinov and G. N. Khudyakov

(Presented by Academician G. M. Krzhizhanovsky, November 16, 1956)

An investigation of the burning of gasoline, kerosene, Diesel oil, solar oil and a number of other petroleum products in containers having different diameters enabled us to establish a number of important relationships for this type of diffusion burning of liquids.

1. In Fig. 1 are shown photographs of flames of gasoline burning in cylindrical containers having diameters of 1.1, 3, 15, 30 and 130 cm. From these photographs it is evident that with increasing diameter of the container the shape and structure of the flame undergo fundamental change. In the container with a diameter of 1.1 cm the gasoline flame has a conical shape which does not change with time. As the diameter of the burner increases, the flames of petroleum products begin to pulsate with a maximum frequency of approximately 18-20 cycles/sec. With further increase of the diameter the pulsation frequency of the flame decreases. For a diameter of d = 3 cm the upper part of the flame becomes unstable. With increasing d the boundary of the unstable part is displaced downwards. For d = 15 cm the whole flame assumes fanciful, rapidly changing contours. In the case of gasoline burning in the container with a diameter of 130 cm, irregular turbulent movements are clearly seen in the flame. A similar state of affairs can be observed in the burning of other liquids.

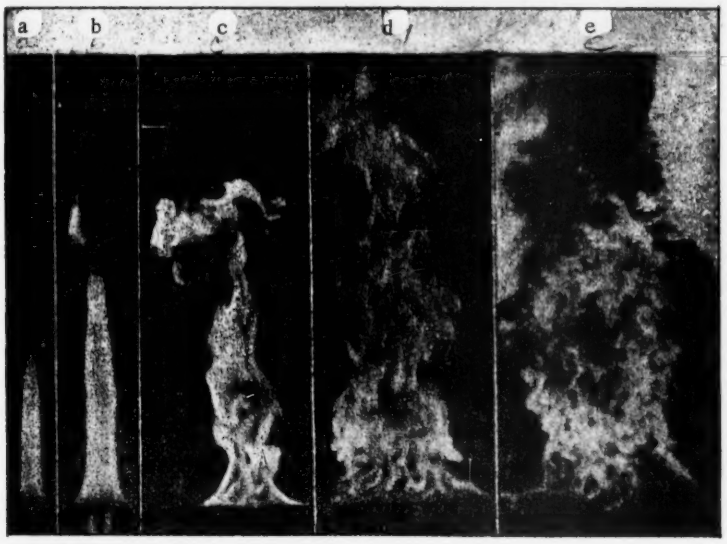

Fig. 1. Gasoline: a) d = 1.1 cm; b) 3.0 cm; c) 15 cm; d) 30.0 cm; e) 130.0 cm.

2. The burning of a liquid is, in fact, the combustion of the current of its vapor. In Table 1 are shown the Reynold's numbers (Re) for vapor currents of some of the petroleum products investigated. The values given have been calculated from the experimental data. It will be seen from the table that for containers having small diameters, the Reynold's numbers are small. Beginning with diameters d > 8 cm Re increases rapidly with increasing diameter, and for containers with diameters of 130 cm, Re is large and exceeds its critical value.

The photographs and the data in Table 1 show that the burning of liquids in containers is characterized by two regimes: the laminar regime – in the case of liquids burning in containers having small diameters, and the turbulent regime – for fuels burning in containers having diameters greater than 1 m.

3. From Table 1 it will be seen that for all the fuels investigated the relationship v(d) is the same, and is similar to that found for aviation gasoline and described in [1]. At first the velocity c decreases with increasing diameter of the container and tends toward a certain limiting value; for d > 10 cm, v increases with increasing diameter, and for values of d greater than 1 m it remains practically constant with varying d. Thus the entire range investigated can be divided into three regions each of which is characterized by a specific relationship v (d).

From the Reynold's numbers corresponding to different values of d and from the photographs of the flames it is possible to conclude that the first of these regions is the region of laminar burning, the third one is the region of turbulent burning, while the second region is one in which transition from the laminar to the turbulent regime takes place.

4. The variation of v as a function of d in the region of laminar burning can be expressed sufficiently accurately by the formula $v = a + bd^{-n}$, where a and b are constants depending on the nature of the liquid only. The constant a (a = v for d = ∞) is equal to 1.4 for aviation gas, 1.1 for tractor kerosene, 0.9 for household kerosene, 0.5 for solar oil, 0.8 for Diesel oil and 0.5 mm/min for transformer oil. The corresponding values of the index n are: 1.73, 1.61, 1.51, 1.54, 1.31 and 1.5.

Simple calculation shows that the decrease in the specific velocity of laminar burning of liquids with increasing diameter of the container is mainly due to a relative decrease in the amount of heat received by the fuel from the flame through the wall of the container.

5. The data in Table 1 show that in the case of laminar burning the ratio of the volume of fuel (Q) burnt per unit time, to the height of the flame (δ) is independent of the diameter of the container and, consequently, the quantity $u = Q/\delta d$ which characterizes the burning velocity, ascribed to unit surface area of the flame, varies directly as $1/d$.

These results are easily explained. In actual fact, during laminar burning of the unmixed gases the height of the flame [1, 2] $\delta \approx wd^2/D$, where w is the rate of flow of the burning gas and D the coefficient of diffusion of oxygen. If the densities of the vapor and of the liquid are denoted, respectively, by ρ_v and ρ, then $w\rho_v = v\rho$. Since $Q = \pi wd^2/4 = \pi v\rho d^2/4\rho_v$, we find, on substituting the latter result into the expression for δ that for laminar burning of a given fuel Q/δ = const, u = const/d.

6. From the experimental data given in Table 1 it follows that the specific turbulent burning velocity of liquids is practically independent of d: for an 18 fold increase (from 1.3 to 22.9 m) in the diameter of the container the burning velocity of aviation gas and kerosene hardly changed (the variations indicated are within the limits of experimental error). This fact leads us to an interesting conclusion.

It is obvious that the rate of vaporization and, therefore, the burning velocity, is determined by the amount of heat q received by the liquid from the flame per unit time [3]. But $q = q_1 + q_2 + q_3$ where q_1, q_2 and q_3 are the amounts of heat transferred to the liquid, respectively, through the wall, by conduction and by radiation from the flame. In the case of combustion in containers having diameters greater than 1 m the quantities q_1 and q_2 are small by comparison with q_3. Thus, the constancy of v in turbulent burning show that the amount of radiation energy received by 1 cm^2 of the surface of the liquid in unit time is independent of d.

7. The data in Table 1 show that the relative height of the flame δ/d in the turbulent regime is independent of the diameter of the container. This result is easy to explain, if we assume (as is often done)

TABLE 1

Petroleum product	Parameters	Diameter d, in cm																
		0.37	0.50	0.60	0.71	1.1	2.0	3.0	4.7	8.0	14.8	30	50	80	130	260	863	2290
Gasoline	v mm/min	—	—	18.0	13.2	5.5	3.4	2.2	1.8	1.4	1.6	2.5	4.1	—	4.1	—	3.8	3.4
	δ cm	—	—	9.5	9.7	11.9	20.3	24.2	31.4	—	—	100	—	—	300	440	—	3900
	$Q:\delta$	—	—	0.05	0.05	0.05	0.05	0.06	0.10	—	—	1.77	—	—	18.2	—	—	380
	$\delta:d$	—	—	16	13.5	10.4	10.3	8.1	6.7	—	—	3.3	—	—	2.3	1.7	—	1.7
	$Re\cdot10^3$	—	—	0.15	0.12	0.08	0.14	0.08	0,10	0.14	0.26	0.92	2.53	—	6.60	—	—	98
Tractor kerosene	v	12.0	7.5	6.4	4.8	3.2	1.9	1.4	1.4	0.9	1.2	1.8	3.0	3.4	4.0	4.2	—	3.6
	δ	3.6	5.4	6.3	6.3	9.6	15.3	20	29.5	41.3	68	—	—	—	208	—	—	—
	$Q:\delta$	0.03	0.03	0.03	0.03	0.03	0.4	0.05	0.08	0.11	0.31	—	—	—	25.5	—	—	—
	$Re\cdot10^3$	0.06	0.05	0.05	0.05	0.05	0.05	0.06	0.09	0.10	0.24	0.74	2.05	3.8	7.1	14.9	—	112
Diesel oil	v	6.9	5.0	4.2	3.5	2.5	1.7	1.3	1.1	0.6	0.7	—	—	2.7	3.3	3.5	—	—
	δ	3.0	3.9	4.3	5.0	7.8	13.0	19.0	27	40	—	—	—	—	220	312	—	—
	$Q:\delta$	0.025	0.03	0.03	0.03	0.03	0.04	0.05	0.07	0.07	—	—	—	—	20	60	—	—
	$\delta:d$	8.1	7.7	7.2	7.0	6.8	6.5	6.4	5.7	5.0	—	—	—	—	1.7	1.2	—	—
	$Re\cdot10^3$	0.04	0.04	0.04	0.03	0.04	0.05	0.05	0.07	0.07	0.14	—	—	3.0	6.0	12.7	—	—
Solar oil	v	9.3	5.1	4.1	3.3	2.4	1.1	0.6	0.6	0.6	0.6	0.8	1.7					
	δ	3.0	4.0	4.4	4.9	7.9	11.8	14.5	20.7	—	31	100	—					
	$Q:\delta$	0.03	0.03	0.03	0.03	0.03	0.03	0.03	0.05	—	0.31	0.56	—					

* The burning velocities for the reservoir with the diameter of 23 m are taken from data published by the Central Research Institute of Fire Fighting, while burning velocities for the reservoirs with diameters of 1.3 and 1.6 m were obtained in the course of experiments carried out in collaboration with a group of workers of the Central Research Institute of Fire Fighting.

that in the turbulent regime the coefficient of diffusion $D \approx wd \approx vd$. But $\delta \approx wd^2/D$, and therefore $\delta \approx d$.

In conclusion the authors wish to express their gratitude to L. A. Volodina and A. A. Koryakina for their assistance in the experimental work.

G. M. Krzhizhanovsky Power Institute
of the Academy of Sciences of the USSR

Received May 25, 1956

LITERATURE CITED

[1] V. I. Blinov, Bull. Acad. Sci. USSR, Div. Tech. Sci., No. 4, 115 (1956).

[2] D. A. Frank-Kamenetsky, Suppl. to Combustion, Flame and Explosions in Gases; By. B. Lewis and G. Elbe (I. L., 1948).

[3] G. N. Khudyakov, Bull. Acad. Sci. USSR, Div. Tech. Sci., No. 10-11, 1115 (1945); Ibid., No. 7, 1015 (1951).

* Russian Translation.

ZERO POINTS OF DILUTE SODIUM AMALGAMS

V. A. Smirnov and L. I. Antropov

(Communicated by Academician A. N. Frumkin, October 4, 1956)

During the last decade there has been growing recognition of the importance of the potential of zero charge, or the so-called zero point of metals ($_{Me}E_{q=0}$) in various electrochemical processes [1-6]. In this connection it appeared to us of interest to determine the zero points of dilute amalgams, many of which have found application in the reduction of inorganic and organic compounds [7-9]. Up to the present only amalgams of Thallium [10] and cadmium [11] in aqueous solutions have been investigated in this respect. In the present paper we describe the results of determinations of zero points of dilute sodium amalgams.

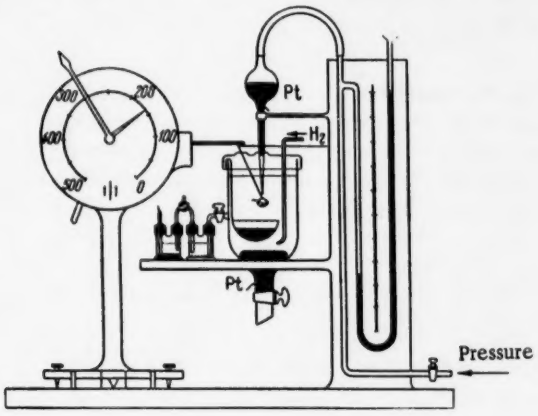

Fig. 1. Apparatus for the determination of zero points of amalgams by the drop-weight method.

The determination of zero points of amalgams of alkali metals is difficult because they undergo, comparatively easily, oxidation and rapid decomposition by aqueous solutions of electrolytes. In addition, exchange currents between the amalgams and solutions containing ions of the corresponding metal are usually large. In order to produce observable displacements of the potential from its equilibrium or stationary value, it is therefore necessary to use comparatively large currents which, however, may give rise to a change in the composition of the surface layer of the amalgam and to distorted results.

In the present investigation the amalgams were, immediately after their preparation, transferred into a special vessel filled with hydrogen* in order to reduce the possibility of their oxidation; samples of the amalgam required for the experiments were taken immediately prior to the actual determination.

In order to reduce errors due to aging and polarization resulting from high concentrations, the method chosen for recording the electrocapillary curves was the drop-weight method which ensures a continuous regeneration of the surface of the amalgam. The usual procedure adopted in drop-weight methods [12] was somewhat modified and the apparatus used was that shown diagrammatically in Fig. 1. For the sake of rapidity in each determination the drops were suspended directly in the solution by means of a torsion balance. The required dropping rate was fixed by means of capillaries having different diameters at the orifice and by setting the pressure to a suitable value controlled by means of a mercury monometer. The capillary and the reservoir above it, having a total capacity of about 10 ml, were filled with the amalgam to be investigated. Before the actual measurements were undertaken electrolytic hydrogen was passed through the solution of the electrolyte used for a period of 3-4 hours.

* The amalgams and the hydrogen were prepared by electrolysis.

The current was then switched on; mercury placed on the bottom of the electrolytic cell served as the second electrode.*

When the potential of the dropping electrode reached a given value the weight of the known number of drops was determined, the drops being collected in a small glass cup secured by means of a glass fiber to the wire of the torsion balance. The differences between the results of individual experiments carried out under these conditions did not exceed 0.5%. The control curves recorded for mercury in 1.0 N NaOH and in 1.0 N H_2SO_4 did not differ from the usual electrocapillary curves and thus provided a confirmation of the reliability of the method.

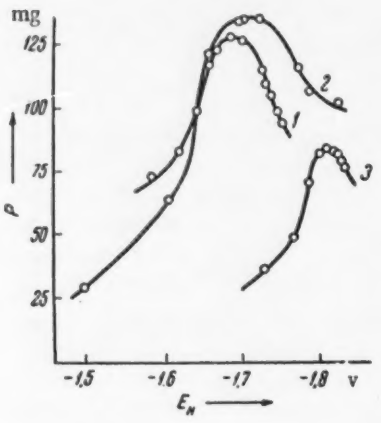

Fig. 2. Electrocapillary curves for sodium amalgams. Mole fraction Na: 1) 0.000126; 2) 0.000783; 3) 0.0174.

The electrocapillary curves recorded for amalgams in 1.0 N NaOH are plotted in Fig. 2. They exhibit a distinct maximum which should correspond to the potential of zero charge of the amalgams of the given composition.** The displacement of the maximum with changing composition of the amalgam is a regular one.

In Table 1 are given the zero points of all the amalgams investigated and the zero points of pure sodium, calculated by means of the electron work function [13, 14], as well as the values of the relative decrease of the surface tension of the amalgams by reference to that of mercury, calculated from the ratio of the weight of a known number of drops of the amalgam to the weight of the same number of drops of mercury.

From these data it follows that both the potential of zero charge of the amalgams and their surface tension vary most within the concentration limits of 0 and 0.0001 mole fractions Na in the amalgam; with further increase in the concentration of sodium up to the point where the composition corresponds to the transition from liquid to solid amalgams, these characteristics change little. A similar relationship was observed earlier by a number of authors for the boundaries amalgam-solution [15] and amalgam-vacuum [16, 17].

Within the concentration range investigated the potential of zero charge varies linearly with the logarithm of the mole fraction of sodium in the amalgam (Fig. 3). This relationship may be expressed by the empirical equation

$$_{\text{Na (Hg)}}E_{q=0} = a + b\log N_{\text{Na}}. \qquad (1)$$

On substituting numerical values we obtain the equation

$$_{\text{Na (Hg)}}E_{q=0} = -1.90 + 0.053\log N_{\text{Na}}. \qquad (1a)$$

* All the reagents used were purified beforehand: mercury – by the usual chemical method followed by two vacuum distillations; sulfuric acid – by electrolysis using a Hg-cathode and a Pt-anode; sodium hydroxide was prepared free from carbonates; the solutions were prepared with water purified by two disillations.

** The displacement of the potential from the zero point of the amalgam toward larger positive values at first gives rise to a decrease in the weight of the drops; subsequently it causes their weight to increase and pass through a second maximum at a potential close to the zero point of mercury.

TABLE 1

	Mole fraction Na in amalgam						
	0.00	0,000126	0,000783	0,00587	0.0174	0,0558	1.00
$E_{q=0}$, in	−0.21	−1.69	−1.73	−1.78	−1.81	−1.82	−2.25 −2.15
$\frac{P_{Na(Hg)}}{P_{Hg}}$	1.0	0.60	0,48	0.39	0.40	0.48	—

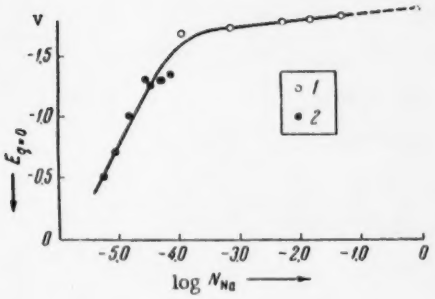

Fig. 3. Relationship between zero points and the logarithm of mole fraction Na in the amalgam. 1) experimental points; 2) points calculated from contact differences of potentials.

Amalgams with lower sodium concentrations have not been investigated in the present work, but data on differences of contact potentials obtained by O. Chaltykyan and M. Proskurnin [18] and plotted in Fig. 3 indicate that there is a sharp increase in the slope of the semilogarithmic curve in the range of lower concentrations.

The quantity a represents the zero point for $N_{Na} = 1$, and should, consequently, correspond to the potential of zero charge of sodium. The numerical value of a differs from the calculated zero point by 0.25-0.35 v. The extrapolated value of $_{Na}E_{q=0} = 0$ lies on the positive side of the calculated zero points of the pure metal. The reasons for these divergencies are not entirely clear and we can only limit ourselves to certain assumptions. In the first place it is improbable that the potential of zero charge varies uniformly over the whole range of concentrations in accordance with Equation (1), because mercury and sodium are capable of forming a number of binary compounds with each other [19] This circumstance is not accounted for in Equation (1). In addition, in the case of amalgams of high sodium content it is necessary to use activities, and not concentrations; the available values of the former are, however, not sufficiently reliable. Secondly, it must be borne in mind that the surface concentration of the metal may differ considerably from its bulk concentration, partly because it is impossible to overcome entirely the concentration gradient caused by the passage of the current. Since in the case of sodium amalgams the equilibrium or stationary potentials lie on the negative side of the corresponding zero points, the latter can be investigated only in the presence of anodic polarization. As a result of the impoverishment of the surface layer of the amalgam, the concentration of sodium in this layer is found to be lower than that in the starting amalgam. It is clear that in this case extrapolation of the relation $_{Na(Hg)}E_{q=0}$ − log N_{Na} to log $N_{Na} = 0$ the value of $_{Na}E_{q=0}$ obtained is slightly displaced to the positive with respect to its true value.

The variation of the zero points of sodium amalgams with their composition established above is of the same nature as the variation of the equilibrium potentials. For this reason the difference between the potential of zero charge and the equilibrium potential remains approximately constant throughout the process of decomposition of the amalgam. As this difference determines the conditions of adsorption or organic and inorganic substances on the surface of the amalgam, the fact that it remains constant in the course of the decomposition of the amalgam ensures that the surface concentration of substances undergoing reduction remains the same. This, apparently, is the reason why specific end products of reduction are obtained when using sodium amalgam, irrespective of variations in its composition and potential in the course of decomposition.

The sharp change of the zero point of mercury on passing to dilute sodium amalgams would lead us to assume that similar variations might be observed in the case of zero points of metals forming surface compounds with sodium (lead, tin etc.) [20] in the course of electrolysis in alkaline solutions. This circumstance may,

evidently, exert a definite influence on the course of electrochemical hydrogenation processes in alkaline solutions.

S. Ordzhonikidze Polytechnical Institute,
Novocherkassk

Received September 17, 1956

LITERATURE CITED

[1] L. I. Antropov, Trudy Erevansk. Politechn. Inst. 2, 97 (1946); J. Phys. Chem. 24, 1428 (1950).

[2] M. A. Loshkarev and A. A. Kryukova, J. Phys. Chem. 23, 209, 221, 1457 (1949).

[3] A. N. Frumkin and G. M. Florianovich, Proc. Acad. Sci. USSR. 79, 997 (1951).

[4] A. N. Frumkin, Vestn. Mosk. Gos. Univ., No. 9, Phys.-Math. and Nat. Sci. Series, Vol.5, 37 (1952).

[5] N. A. Isgaryshev and M. Ya. Fioshin, Proc. Acad. Sci. USSR., 90, 581 (1953).

[6] Ya. M. Kolotyrkin and L. A. Medvedeva, Tr. Soveshch. po electrokhim., 1953, page 369.

[7] V. V. Stender, Electrolytic Production of Chlorine and Alkalies, 1935.

[8] Sh. Sven, Electrochemical Methods of Preparation of Organic Compounds, 1951.

[9] N. D. Pryanishnikov, Practical Organic Chemistry, 1952.

[10] A. N. Frumkin and A. V. Gorodetskaya, Zs. phys. Chem., 136, 451 (1928).

[11] A. N. Frumkin and F. D. Servis, J. Phys. Chem., 1,52 (1930).

[12] G. Kucera, Ann. Phys., 11, 529, 698 (1909).

[13] R. M. Vasenin, J. Phys. Chem., 27, 878 (1953).

[14] L. I. Antropov, Trudy Novocherkassk. Politekhn. Inst., 25 (39), 1, 5 (1954).

[15] G. Meyer, Zs., phys. Chem., 70, 315 (1910).

[16] V. K. Semenchenko, J. Phys. Chem., 7, 501, (1936).

[17] A. M. Didenko, Uch. zap. Mosk. gor. ped. inst., 16 (1951).

[18] O. Chaltykyan and M. Proskurnin, Acta physicochim, URSS, 4, 263 (1936).

[19] Technical Encyclopedia, Handbook of Physical, Chemical and Technological Data, 2, 1929, page 194.

[20] O. Bredig, F. Haber, Ber., 31, 2741 (1898).

ON THE POSSIBILITY OF COMPLETE X-RAY PARTICLE SIZE ANALYSIS OF GRAPHITE POWDERS AND COLLOIDAL PREPARATIONS

L. A. Feigin and V. N. Rozhansky

(Presented by Academician P. A. Rebinder, November 6, 1956)

The development of x-ray methods of determination of the particle size distribution of solids has been going on for some 30 years. Using these methods it is possible, as a rule, to estimate only the mean dimensions of the monocrystal particle, the basis of the estimation being the so-called "width" of the diffraction line. In recent years some authors [1, 2, 7] have demonstrated the fundamental possibility of finding the distribution function of the dimensions of crystallites by making use of the shape of the diffraction line on x-ray powder photographs. This method is based on the harmonic analysis of the intensity of reflection of the diffracted rays and makes it possible to estimate separately lattice stresses and particle dimensions for crystals of any symmetry whatever [3].

If micro-stresses are absent from the crystal lattice, the intensity of the hkl reflection, $I(\theta)$, may be expressed in the form of the Fourier integral:

$$I(\theta) = \int_{-\infty}^{+\infty} h(n)\, e^{2\pi i n\omega(\theta)}\, dn, \tag{1}$$

where $\underline{n}$ is a parameter related linearly to the particle dimension, θ is the diffraction angle, and ω a variable in the mirror space.

The function h(n) is related to the particle size distribution curve g(M) by the expression:

$$h(n) = K \int_{|n|}^{\infty} (M - |n|)\, g(M)\, dM. \tag{2}$$

Differentiating (2) with respect to $\underline{n}$ we obtain:

$$-\frac{dh}{dn} = K \int_{|n|}^{\infty} g(M)\, dM; \quad \frac{d^2h}{dn^2} = Kg(n), \tag{3}$$

i.e., the first derivative, dh/dn, gives an integral, while the second derivative, d^2h/dn^2, gives a differential distribution function. In this way we obtain complete information on the particle size distribution of the sample.

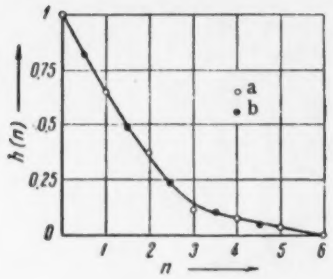

Fig. 1. The function h(n) of the line $(11\bar{2}2)$ for ground graphite powders: a) experimental points, b) points calculated by Formula (5).

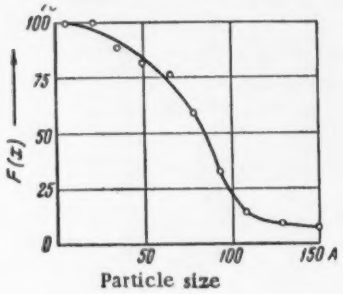

Fig. 2. Integral curve of particle size distribution in graphite after 15 hours' grinding in a vibration mill. The values plotted have been calculated for the line $(11\bar{2}2)$.

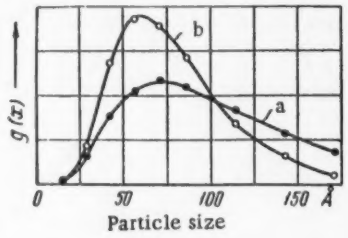

Fig. 3. Differential particle size distribution curves for graphic powders, a) 5 hours' grinding, b) 15 hours' grinding. The functions have been obtained assuming normal logarithmic distribution having the parameters determined from the experiment. The values plotted have been calculated for the line $(11\bar{2}2)$.

By investigating various other reflections we may obtain, in addition, information on the shape of the crystallites.

In actual practice, however, this method meets with considerable difficulties. Thus, in the case of metals – and it is in the analysis of metals that the method has been used up to the present – it becomes necessary to differentiate between the effect due to a given particle size distribution and that due to micro-stresses on the diffuse appearance of the lines, and this is not always possible. In practice it has thus far not been possible to establish the distribution function by this method. It may, however, be assumed that in the case of brittle solids diffusion of the lines due to micro-stresses should be absent. This assumption considerably simplifies the investigation of the particle size distribution of such samples.

We have made an attempt to determine the particle size distribution function for highly disperse graphitic systems. This problem arose in connection with the introduction into industrial practice of new types of colloidal graphite preparations prepared by mechanical dispersion of graphite powder in a vibration mill [4]. By varying the grinding time we were able to obtain graphite preparations of a very wide range of particle sizes. It is of interest to mention that after prolonged grinding, up to 30 hours, the usually inert graphite is obtained in a highly disperse state in which it resembles soot, and on being taken out of the vibration mill it undergoes spontaneous heating in air up to a temperature of about 700°.

As is well known, graphite can easily be broken up along the planes of cleavage without substantial distortion of the lattice. The forces of adhesion between atoms situated in the base plane are very large and for this reason graphite is often included among valence crystals (of the diamond type). Graphite can be flaked in the plane perpendicular to the base plane, the flakes being disrupted in a manner similar to that of brittle solids, but without serious distortion of the crystal structure. It is therefore natural to expect that mechanical dispersion of graphite will not give rise to the appearance of micro-stresses to any noticeable extent, and this result is borne out by experiment.

The true shape of the line was determined by the objective method of Stokes [5] which consists of comparing by harmonic analysis the intensities of lines obtained under identical conditions for a sample of sufficiently large crystal size (macrocrystalline etalon) with those obtained for the sample examined. The etalon used was unground graphite powder. This method furnishes directly the Fourier coefficients of the true profile of the line. Such a transformation can be effected with sufficient accuracy only when the line produced by the sample is considerably wider than that obtained for the etalon. In order to reduce the line width obtained by the instrument the prepared samples were thin (0.25 mm in diameter), the diaphragms used were narrow (0.2 to 0.25 mm in diameter), and the photographs were taken in cameras of fairly large diameters (86 or 114 mm); the wavelength of the x-rays chosen was such that the lines required were obtained at angles (θ) of approximately 45° (at these angles diffusion of the lines disappears as a result of the finite height of the sample). The subsequent treatment of the x-ray

photographs was carried out under strictly standard conditions. The photographs were carefully evaluated by a photometric method, taking into account the blackening curve.

Harmonic analysis was carried out for the lines $11\bar{2}0$ and $11\bar{2}2$ (these being most suitable for photometric evaluation and for determination of particle shape) of x-ray photographs of graphite powders of different degrees of dispersion. The curves representing the Fourier coefficients as functions of the parameter n which is proportional to the dimension of the crystallites, were found to be similar to the theoretical curves calculated for the case when lattice stresses are absent (Fig. 1). To find the integral particle size distribution function it is sufficient to differentiate the function h(n) determined by experiment (Fig. 2). The accuracy attained by such procedure cannot, of course, be very high and the curve can be plotted only within a narrow range of particle size (in our case for powders obtained after 15-20 hours' grinding in the vibration mill).

The accuracy can be increased, and the particle size range over which it is possible to determine the distribution curve can be widened only if we introduce specific assumptions regarding the nature of the given particle size distribution. A. N. Kolmogorov [6] showed that the distribution particle size of powders formed by the grinding process given obeys normal logarithmic law of the form

$$g(x) = \frac{1}{\sqrt{2\pi}\sigma x} \exp\left[-\frac{1}{2}\left(\frac{\ln x - \ln \xi}{\sigma}\right)^2\right], \tag{4}$$

where x is the particle size, ξ and σ are distribution constants. There are grounds to believe that the systems investigated by us do in fact follow such a normal logarithmic distribution. In this case the problem reduces to finding the median ξ and the dispersion σ from the experimental curve. Substituting the expression for the distribution function into Equation (2) we obtain:

$$h(x) = h(0)\,\Phi(\eta - \sigma) - \frac{h(0)\,x}{\xi e^{\sigma^2/2}}\,\Phi(\eta), \tag{5}$$

where

$$\eta = \frac{1}{\sigma}\ln\frac{x}{\xi}, \quad \Phi(z) = \int_z^\infty \frac{1}{\sqrt{2\pi}} e^{-z^2/2}\,dz.$$

In the case of a normal logarithmic distribution the following relationships hold good:

$$\bar{x} = \xi e^{\sigma^2/2}, \quad \overline{x^2} = \xi^2 e^{2\sigma^2}, \tag{6}$$

where $\bar{x}$ is the mean dimension and $\overline{x^2}$ the mean square dimension.

The values of $\bar{x}$ and $\overline{x^2}$ are easily found from the experimental curve h(x) [1]. The values of the median ξ and of the dispersion σ are then found from the relations (6). The curves h(n) calculated with these parameters using Formula (5) are sufficiently close to those obtained by experiment (see Fig.1); this result may be taken as an experimental confirmation of the possibility of using the normal logarithmic law to describe the particle size distribution of graphite. By introducing this assumption it was possible to extend the range of particle size distributions for which full distribution curve can be obtained, to larger particle dimensions (Fig.3).

Examination of lines with other indices makes it possible, in addition, to estimate the shape of the crystallites. Proceeding in this way it was found that the graphite particles could be represented in the shape of discs having heights several times smaller than their diameters.

Determinations of the specific surface by low-temperature adsorption of nitrogen by the method of Brunnauer, Emmet and Teller are in satisfactory agreement with data obtained by means of x-ray photographs. This appears to indicate that in our samples the regions of coherent dispersion are apparently identified with those graphite particles the size of which is determined by nitrogen adsorption.

The authors wish to express their sincere gratitude to Academician P. A. Rebinder and Prof. A. I. Kitaigorodsky for their criticisms and valuable advice.

All-Union Central Research Institute for Production Problems in High-Dispersion Structural Materials, M. V. Lomonosov State University, Moscow

Received October 17, 1956

LITERATURE CITED

[1] E. F. Bertaut, Acta Cryst., 3, 14 (1950).

[2] B. E. Warren, B. L. Averbach, J. Appl. Phys., 21, 595 (1950).

[3] B. E. Warren, Acta Cryst., 8, 483 (1955).

[4] L. A. Feigin, Chemical Knowledge and Industry, 1, 1956, p. 210.

[5] A. R. Stokes, Proc. Phys. Soc., 61, 382 (1948).

[6] A. N. Kolmogorov, Proc. Acad. Sci. USSR, 31, No. 2, 99 (1941).

[7] B. Ya. Pines and N. G. Bereznyak, J. Tech. Phys., 24, 329 (1954).

KINETICS OF THE PHYSICAL ADSORPTION OF ETHYLENE FROM MIXTURES

A. V. Alekseeva and K. A. Golbert

(Presented by Academician M. M. Dubinin, November 5, 1956)

Recently, processes whose rates are determined by diffusion inside granules have acquired more and more significance. However, the field of internal diffusion kinetics has been insufficiently developed, both theoretically and experimentally. Only in the last two years has there appeared systematic work on the internal diffusion kinetics of the adsorption of a single substance [1-3].* In particular, there are no data in the literature on the rate of absorption of ethylene from a mixed gas stream in spite of the fact that such data are very important for the development of adsorption methods for the separation and analysis of hydrocarbon gases.

In the present work was studied the rate of adsorption of ethylene from its mixtures with H_2, N_2 and CH_4 on AG-2 brand industrial carbon. The selection of the system was made in connection with the development of the technology of the separation of ethylene from gas mixtures with a low content of the desired component; however, the method developed and the results of the investigation have a more general value.

For this investigation, a differential method for measuring the kinetics of the adsorption of mixtures was specially developed,** since use of earlier methods would not permit obtaining data in a form convenient for treatment owing to the dependence of the internal diffusion coefficient on composition of the adsorbate. The principle of this method consists of passing a mixture of a given composition through an adsorption cell containing a thin layer of adsorbent until equilibrium is established. Then, a second mixture differing, but close in composition to the first, is passed through the cell over a precisely fixed time. The change in the amounts of adsorption of the components is calculated from data from chemical analysis of the mixture desorbed from the carbon. Desorption is carried out by pumping the adsorbent, heated to 200°, with a Teoppler pump. Such an experimental arrangement involves only a small change in the internal diffusion coefficient during the course of the adsorption and a practically linear relationship between the changes in the amounts of adsorption, $\underline{a}$, and the concentration, $\underline{c}$, in the gas phase.

The value of the degree of exhaustion of the granule is calculated from the equation

$$F = \frac{a - a_0}{a_\infty - a_0}, \qquad (1)$$

where a_0 and a_∞ are the amounts of ethylene adsorbed at equilibriium with mixtures over the concentration interval investigated; $\underline{a}$ is the amount of ethylene adsorbed during a given contact time with the mixture of higher ethylene content.

---

* References to previous work are given in these articles.

** This method was developed in 1953, prior to the publication of the article by Carman [1], in which was described a method for measuring the adsorption kinetics of a single substance, this method being based on an analogous principle.

For the measurements of the adsorption kinetics of the mixtures, we constructed a special apparatus having a low dead space in the adsorption cell, which guaranteed identical flow conditions around the granules of short and long layers of adsorbent. The basic part of the apparatus – the adsorption cell – consisted of two large-bore stopcocks joined by a short glass tube not longer than 1.5 cm. This tube and the stopcock bore were of almost equal internal diameter, 1.4 cm. Perpendicular to the main passage in each stopcock, there was a unilateral bore of small diameter for pumping off the mixture from the main bores with the stopcocks closed. The adsorbent was placed in the tube of the cell between two screens and layers of inert packing, the granules of which were identical in form and dimensions with those of the adsorbent. There was an electric coil on the tube of the cell. The use of a special grease, blended from lithium stearate and high-boiling distillates from aviation oils, together with the passage of cold water through the stopcock plugs prevented softening and dropping of the grease on the adsorbent. The mixtures used in the work were prepared from gases purified with carbon and by two-fold recondensation. The narrow intervals of adsorption, Δa, and concentration, Δc, of ethylene over which the measurements were carried out varied from 0.7 to 4.5 std. cc/g and from 0.1 to 6.4% C_2H_4, respectively.

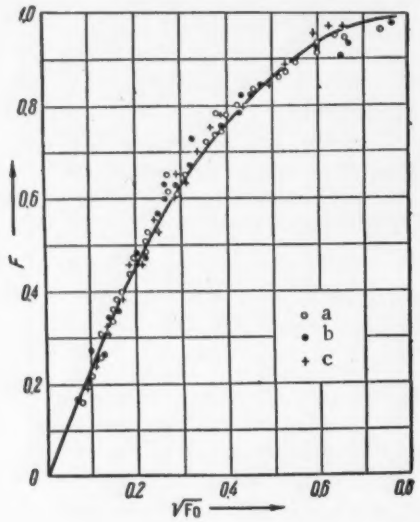

Fig. 1. a) $C_2H_4 - H_2$; b) $C_2H_4 - CH_4$; c) C_2H_4 c) $C_2H_4 - N_2$; curve – theoretical data.

The usual equation for the internal diffusion kinetics of the adsorption of a single substance with a constant diffusion coefficient was used for processing the data. That this equation could be used followed from the entire aggregate of data obtained in the present work. In particular, it was found that: 1) the rate of ethylene adsorption did not depend on gas flow rate (the rate was varied by a factor of two, from 1.85 to 3.70 liters/minute·sq. cm.; 2) in the initial stages of the adsorption process, there was a linear/ relationship between the degree of exhaustion of the granule and the square root of the time of contact of the gas mixture with the adsorbent; 3) the adsorption and desorption rate curves agreed, with indicates that the diffusion coefficient was practically constant within the interval investated; 4) the presence of the second component did not appreciably lower the ethylene adsorption, and the amount of the second component displaced by the ethylene was insignificant in comparison to the amount of ethylene adsorption.

Calculation of the internal diffusion coefficients, D, was carried out by means of a theoretical curve showing the degree of exhaustion of the granule, F, as a function of the Fourier number, $Fo = Dt/R^2$, which we calculated for the case of diffusion in cylindrical granules of radius R and length $2\underline{l}$ for a fixed value of the simplex of the form $s = R/\underline{l}$ of 0.308. Deviations of the experimental values of D for various contact times from the average values were not systematic and did not exceed the error of the measurements (10%). Then, from the average values of D were calculated values of the Fourier number at various loadings of the adsorption volume. Figure 1 shows that the experimental data for all systems satisfactorily fitted the theoretical dimensionless curve of F – Fo. Values of the Biot number, $Bi = \beta R/DG$, calculated from the experimental data, were in the range of 60 to 190 for all systems investigated. All this confirms the internal diffusion character of the kinetics of the adsorption of ethylene from the systems investigated and the applicability of the simple internal diffusion equation with constant coefficient for describing the experimental data. The data obtained on the dependence of the internal diffusion coefficient on amount of ethylene adsorbed, the nature of the second component, the porosity of the adsorbent, and temperature are presented in Figure 2.

In all of the systems investigated, the values of the internal diffusion coefficients increased sharply with an increase in the amount of adsorbed ethylene. For the systems nitrogen-ethylene and methane-ethylene, there was a linear dependence over the entire range of amounts adsorbed; for the system hydrogen-ethylene, the linear nature of the relationship was retained if the curve was divided into two parts.

The strong dependence of the coefficient of internal diffusion on composition can occur with any kind of transport of the substance into the granule. Actually, for surface diffusion, $D = D^0 \exp(-\alpha A/RT)$, where D^0 is a preexponential constant; α is a constant; A is the adsorption potential, which depends considerably on the amount of adsorption. On migration of the substance into the pore volume, $D = \bar{D}/G$, where $\bar{D}$ is the coefficient of volume or molecular diffusion; $G = \bar{\partial}\, a/\partial c$, a variable parameter usually greatly dependent on the amount of adsorption. Moreover, in the case of molecular diffusion, $\bar{D}$ also depends on the degree of filling of the surface, since pores of different dimensions are responsible for a different amount of adsorption. Hence, it follows that only for the case of volume diffusion is the product DG independent of the amount of adsorption. Calculations showed that, in the region investigated, DG decreased with 35-40% filling of the surface. Thus, although DG is variable, it changes more slowly than D. This indicates that in the process of transport of ethylene into the carbon granule, along with volume diffusion, there is also a substantial amount of molecular and/or surface diffusion.

Activation energies of the diffusion process calculated from experimental data in the temperature ranges 25-50° and 25-75° at adsorptions of 5.10 and 6.78 std. cc/g were 5100 and 5500 cal /mole, respectively, while the heats of adsorption were 5600 and 5200 cal /mole. The closeness of these values indicates the significant role of volume and/or molecular diffusion in the process of transfer of ethylene into the adsorbent. The slight dependence of DG on temperature also indicates the essential role of volume and/or molecular diffusion in this process. Actually, in the ranges of 25-75° and 25-50° DG only changed from $0.78 \cdot 10^{-2}$ to $0.67 \cdot 10^{-2}$ sq. cm./second.

It was found that the value of the internal diffusion coefficient materially depended on porosity. For samples of AG-2 carbon with bulk densities of 0.675 (A) and 0.540 (B), which differed from each other in total pore volume by 30% and in the volumes of macro-, micro-, and transitional pores by 22.44 and 34%, the diffusion coefficients were, respectively, $3.70 \cdot 10^{-5}$ and $8.9 \cdot 10^{-5}$ cm²/second. This difference in the values of the internal diffusion coefficient cannot be explained by a change in the coefficient G, since the product DG also changes from $0.46 \cdot 10^{-2}$ to $1.37 \cdot 10^{-2}$ cm²/second. Such a strong dependence on porosity can occur if molecular diffusion plays a basic role in the transport of the substance inside the granule.

The effect of the second component on the internal diffusion coefficient is clearly apparent over the entire range of ethylene adsorption investigated. Only at low filling of the adsorption volume (2.5 std. cc/g) was there no essential difference in the internal diffusion coefficients. But even in a region of average filling of the surface (12.6 std. cc/g), the ratio of D in the H_2 system to D in the N_2, CH_4, and A systems was, respectively, 1.5, 1.6, and 3.5, while the ratio for these systems was, respectively, 2.8, 3.7, and 4.5. This shows that volume diffusion, along with one or both of the other forms of transport, plays an essential role in the transport of ethylene.

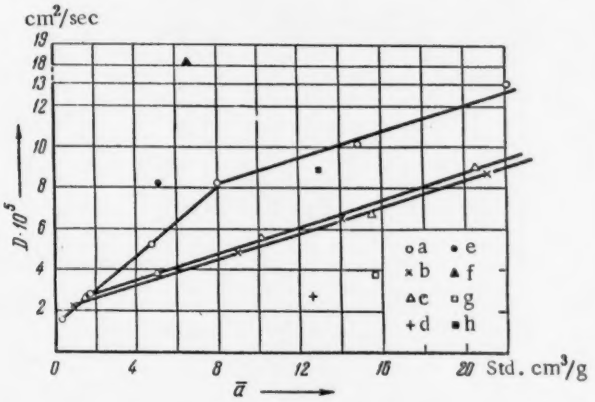

Fig. 2. a) $C_2H_4 - H_2$; b) $C_2H_4 - N_2$; c) $C_2H_4 - CH_4$; d) $C_2H_4 - Ar$ at 25°; e) and f) $C_2H_4 - CH_4$ at 50 and 75°, respectively; g) and h) $C_2H_4 - N_2$ at 25° oven carbon A and carbon B, respectively.

From the material presented above it follows that, within the frameworks of the usual representations of the process of the migration of ethylene inside a granule, there is a superimposing of three forms of transfer: volume, molecular, and surface diffusion, with the latter playing a secondary role. However, it should be noted that the process of ethylene migration inside a granule cannot be completely described only on the basis of the usual concepts of volume and molecular diffusion since analysis of the absolute values of the experimental coefficients of internal diffusion ($\sim 10^{-4}-10^{-5}$ cm^2/second) and of the DG products ($\sim 5\cdot10^{-3}-10^{-2}$ cm^2/second) leads either to improbably small values of the effective cross section and coefficient of winding (in the case of the assumption of volume diffusion) or to values of the pore radius comparable to molecular dimensions – of the order of tens of angstroms (in the case of molecular diffusion).

From the internal diffusion nature of adsorption kinetics, established in this work, flows a number of important practical conclusions relative to the effect of different parameters on separation processes in moving or stationary layers and also relative to the requirements of the adsorbent. The numerical characteristics obtained in the present work permit the carrying out of calculations on the dynamics of the adsorption of ethylene.

Research Institute for Synthetic Alcohols
and Organic Products

Received October 17, 1956

LITERATURE CITED

[1] P.C.Carman, F. A. Raal, Trans. Farad. Soc., 50, 842 (1954).

[2] P. C. C rman, R. A. W. Haul, Proc. Roy. Soc., A 222, 109 (1954).

[3] R. A. W. Haul, Zs. Phys. Chem. (Frankfurt), 1, 153 (1954).

KINETICS OF THE THERMAL DECOMPOSITION AND STRUCTURAL TRANSFORMATIONS OF FOSSIL COALS

V. I. Kasatochkin and Z. S. Smutkina

(Presented by Academician V. A. Kargin, November 24, 1956)

The process of the thermal decomposition of fossil coals is characterized by a number of distinguishing traits which can be attributed to peculiarities of the chemical structure of the organic material of the coal. The coal material, which we visualize as aromatic carbon lattices spatially interconnected by side chains [1], combine in their structure a relatively inert, nuclear (carbon lattice) part and a reactive, peripherial (side chain) part [2]. This peculiarity of structure could explain the generally observed two stages of primary and secondary decomposition which differ sharply in nature. In the primary decomposition stage, which takes place rapidly at a relatively low temperature, the bulk of the volatile matter is liberated, chiefly by reactions in which the side chains are destroyed. Chemical change of the nuclear part of the structure is observed in the later stage of secondary decomposition. During this, intense growth of the carbon lattice takes place, as is well illustrated by x-ray methods (see Figure 2). According to this picture of the decomposition, the carbon lattices of the original coal material remain in the solid product (coke), and are centers of two-dimensional crystallization of the carbon during carbonization of the organic material of the coal.

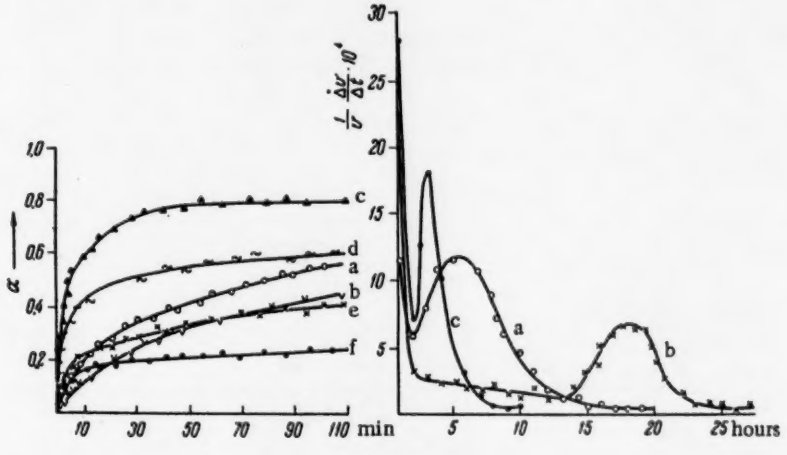

Fig. 1. Kinetic curves of the decomposition. Left figure – yield of volatile matter: a) shale, b) boghead, c) brown coal, d) long-flame, e) gas, f) coking. Right figure – rate of yield of volatile matter: a) 500°, coking coal; b) 450°, long-flame coal; c) 500°, long-flame coal.

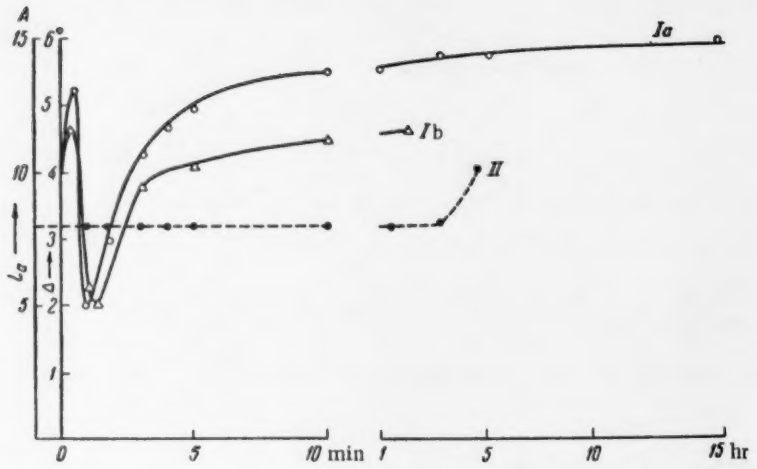

Fig. 2. Ia and Ib – interplanar regularity curves a) 500°, b) 425°; II – growth of the carbon lattice, 500°

In the present work, a comparative study was made of the kinetics of the thermal decomposition of the vitrainized material of Donets coals of different metamorphic states, the structure of which is characterized by an atomic carbon lattice, and of the organic material of bituminous shales (Estonian) and boghead (Olenek), which do not have carbon lattices [3]. The structural transformations of the coal material were also studied using x-rays and infrared spectroscopy.

TABLE 1

Sample	300–350°		350–400°	
	α	E, kcal./mole	α	E, cal./mole
Boghead	0.05	14679.2	0.20	28276.8
	0.10	14352.8	0.30	37170.4
	0.15	23488.4	0.40	41002.4
Shale	0.05	16962.4	0.15	13795.2
	0.10	21855.4	0.20	14561.6
	0.15	31967.6	0.30	22225.6
	0.20	39470.2	0.40	33338.4
			0.50	39469.6
Brown coal	0.10	5300.0*	0.30	6897.6
	0.30	20224.4	0.40	9346.4
	0.40	32620.0	0.50	13038.8
Long-flame coal	0.15	7176.4	0.20	7664.0
	0.20	18267.2	0.30	8813.6
	0.30	37513.0	0.40	9963.2
			0.50	18776.8
Gas coal	0.15	3914.4	0.20	3832.0
	0.20	15331.4	0.30	14944.8
			0.35	29889.6

* According to the data of E. A. Shapatina, V. V. Kalyuzhny and Z. F. Chukhanov [4].

The decompositions were carried out in a stream of nitrogen at constant temperature using small, weighed portions, and the kinetics were measured by means of the loss in mass. In order to introduce a correction for the nonisothermal conditions at the beginning of the decomposition, special experiments were carried out in which the course of the temperature during heating was measured by means of a thermocouple buried in the samples.

In Figure 1 are presented curves showing the yield of volatile matter, v/v_0, and the rate of elimination of volatile matter, $\frac{1}{v_0}\frac{\Delta_v}{\Delta_t}$, as functions of the time in the furnace where v_0 is the limiting yield of volatile matter determined by the standard method). With respect to the primary decomposition process, the metamorphic series of coals can be arranged in a regular succession depending on v_0, which reflects the change in the chemical nature of the side chains in the structure of the coal material during metamorphism (Figure 1). Brown coal is a member of this succession. Shales and boghead are exceptions, and this is connected with qualitative differences existing between the chemical structure of their organic material and that of coal. At long holding times in the furnace, maximum rates of elimination of volatile matter are

observed in the kinetic curves, these maxima corresponding to the secondary decomposition process (Figure 1). The distribution of the maxima with time depends on the stage of metamorphism of the coal and on the temperature. At relatively low temperatures (300-350°), the unimolecular specific rates of liberation of volatile matter for the fossil coals, calculated taking into account the non-isothermal condition at the beginning of the decomposition, in contrast to those for shales and boghead, have a high value and decrease sharply with an increase in the degree of decomposition, $\alpha = v/v_0$. Values of the apparent activation energies (Table 1) for the fossil coals are very low, 4000-7000 cal /mole, at low degrees of decomposition, which indicates the catalytic nature of the process. The observed rapid increase in activation energy in relation to α for the low temperature decomposition of coals is connected, as might be supposed, with the selectivity of the process of the primary destruction of the coal material, during which are successively split off the different atomic groupings according to increasing thermal stability. With an increase in the decomposition temperature, there is observed a more sloping course of the increase in activation energy in relation to α, which can be attributed to less selectivity of the processes of primary destruction in accordance with the concept of the inclusion of parallel reactions with higher activation energies [5].

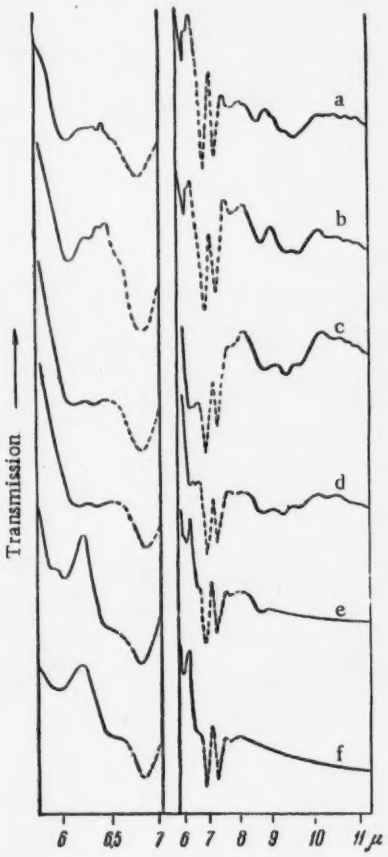

Fig. 3. Infrared absorption spectra of the solid products of the decomposition of long-flame coal: a) original coal; b) $\alpha = 0.024$; c) $\alpha = 0.13$; d) $\alpha = 0.29$; e) $\alpha = 0.79$; f) $\alpha = 0.97$

An x-ray investigation of the structural transformations of the coal material during thermal decomposition was carried out on a series of solid decomposition residues from coking coal which were obtained at different furnace times under the conditions described above. The x-ray powder photographs were taken with filtered iron radiation using a cylindrical camera of ordinary radius. In Figure 2 is shown the dependence of the angular half breadth of the (002) interference band (Curves Ia and Ib) on the degree of decomposition of coking coal at constant temperature, which expresses the change in interlattice regularity [1]. The observed changes in regularity are connected with processes of the primary destruction of side chains and with the freeing of structural units, individual carbon lattices with side chains, which, acquiring mobility during the transition into the liquid-flowing state, attempt to decompose parallel to each other under the influence of the molecular force field. Curve II depicts the course of the changes in linear dimensions of the carbon lattices, calculated from the half breadth of the second interference band from the (100) plane. The sharp increase in lattice dimensions observed at high degrees of decomposition corresponds to the secondary decomposition process and serves as a kinetic characteristic of the structural transformations of the nuclear part of the solid decomposition residue. The x-ray curves of lattice regularity and growth illustrate the differentiation with respect to time of the processes of destruction and joining in the peripheral part of the structure of the coal material and also of the processes of chemical change of the nuclear part of the structure.

The infrared absorption spectra of the solid decomposition residues at varying stages of decomposition under isothermal conditions were obtained by us in the region from 5.7 to 10 μ with an IKS-11 infrared spectrograph with an NaCl prism; these curves characterize the essential changes in the atomic groupings of the coal material. The samples for spectroscopic investigation were prepared as pastes in paraffin oil. In Figure 3 are presented the transmission curves for the solid decomposition residues from long-flame coal. The regular changes in the position and intensity of the absorption bands in relation to the degree of decomposition indicate the relatively low thermal stability of the aromatic ethers (9.7 μ band) in comparison

with aliphatic (8.5 μ) and cyclic (9.2 μ) ethers. Oxygen connected directly with the carbon lattice in the form of phenoxy groups is eliminated only during secondary decomposition, which is accompanied by the disappearance of the 6.2 μ band. The appearance of a band at 6.4 μ at relatively low degrees of decomposition is apparently a consequence of the destruction of radicals existing as links between the carbon lattices in the coal material.

The appearance of a band at 6.0 μ indicates the accumulation of unsaturated C = C bonds in the solid residues. It is possible that the accumulation of unsaturated bonds at high degrees of decomposition is connected with processes providing for subsequent intense growth of the carbon lattices through their union.

Institute of Fossil Fuels, Academy of Sciences USSR

Received November 21, 1956

LITERATURE CITED

[1] V. I. Kasatochkin, Bull. Acad. Sci. USSR, Div. Tech. Sci., No. 9 (1951); No. 10 (1953); Proc. Acad. Sci. USSR, 86, 759 (1952).

[2] W. Fuchs, A. G. Sandhoff, Ind. and Eng. Chem., 34, No. 5, 567 (1942).

[3] V. I. Kasatochkin and O. I. Zilberbrand, Proc. Acad. Sci. USSR, 111, No. 5 (1956).

[4] E. A. Shapatina, V. V. Kalyuzhny and Z. F. Chukhanov, Proc. Acad. Sci. USSR, 72, No. 5 (1950).

[5] Z. F. Chukhanov, Bull. Acad. Sci. USSR, Div. Tech. Sci., No. 8 (1954).

THERMODYNAMICS OF THE HYDROCHLORINATION OF PROPYLENE

S. G. Entelis and N. M. Chirkov

(Presented by Academician V. N. Kondratyev, November 24, 1956)

The hydrochlorination of propylene

$$C_3H_6 + HCl \rightleftarrows \text{iso-}C_3H_7Cl$$

is a reversible reaction, but direct determinations of the equilibrium constant and the heat of reaction have not been made.

From various tables of data, the heats of formation, $\Delta H^0_{f\,298.2}$ of propylene, hydrogen chloride, and isopropyl chloride are, respectively, +4879 cal /mole [1], −22063 cal /mole [2], and −31000 cal /mole [3], and the entropies, $S^0_{298.2}$, are, respectively, +63.8 cal /mole degree [1], 44.62 cal /mole·degree [2], and 72.4 cal /mole·degree [3]. Hence the heat of reaction and entropy change are ΔH_R = 13816 cal./ mole and ΔS_R = −36.02 cal. /mole/degree.

Consequently:

$$C_3H_6 + HCl \rightleftarrows u\text{-}C_3H_7Cl \qquad (1)$$

is a reversible reaction, but direct determination of the equilibrium constant and the heat of reaction have not been made.

TABLE 1

Values of α_p and α_{ac} in Experiments on the Hydrochlorination of Propylene in the Presence of H_3PO_4 with 72% P_2O_5

T, °C	$P_{(C_3H_6)_0}$, mm Hg	P_{HCl_0}, mm Hg	α_p	α_c
70	50	50	0.380	0.380
70	100	100	0.322	0.350
70	200	200	0.512	0.523
70	300	300	0.788	0.787
100	200	200	0.326	0.322
160	200	200	0.475	0.480
180	200	200	0.456	0.441

The heat of reaction was found experimentally by Tomsen [4] to be ΔH_R = −11960 cal/mole.

In our experiments, the equilibrium was studied by means of pressure in a static apparatus (we used the same apparatus as in our previous work [5]) at temperatures of 100, 120, 140, 160, and 180°C; the catalyst was orthophosphoric acid with 72% P_2O_5. Equilibrium was approached both from the HCl and C_3H_6 side and from the i-C_3H_7Cl side. Attainment of equilibrium by the system was determined by the complete cessation of pressure change. In those cases where the reaction did not go to completion, the equilibrium pressure was found by extrapolation to zero rate of the pressure-reaction rate curve. Generally, the error introduced was very small.

Before carrying out the measurements, it was found that, under our conditions, i-C_3H_7Cl was the only product of the reaction. For this purpose, a quantity of the product of the reaction between HCl and C_3H_6 sufficient for distillation was obtained in a flow apparatus in the presence of the catalyst—phosphoric acid—at 100°C. Distillation of the dry product in a column with 16 theoretical plates showed that all of the product

distilled in the range 33.3–34.5° C and had n_D^{15} 1.3810 (according to the literature n_D^{15} 1.3811 and b.p. 34.8°C).

Since the observations on the course of the reaction were carried out by the change in pressure of the system, Δ_p, it was necessary to establish preliminarily the relationship between Δ_p and the extent of the reaction, α. A series of experiments was carried out in which, along with Δ_p, the change in the amount of HCl (ΔN) in the system was analyzed acidimetrically. In Table 1 are presented values of $\alpha_p = \Delta_p/p_0$ and $\alpha_c = \Delta N/N_0$, where p_0 and N_0 are, respectively, the initial pressure and the initial amount of HCl in the system.

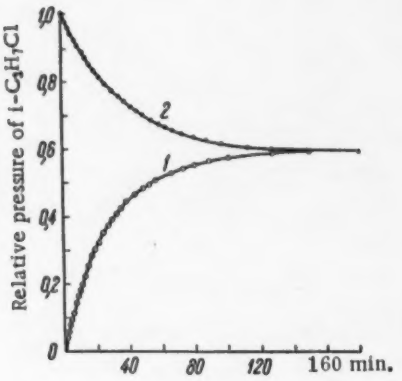

Fig. 1. Kinetic curves of the synthesis (1) and decomposition (2) of isopropyl chloride in the presence of orthophosphoric acid (72% P_2O_5). Amount of acid 1.2 g (based on 100% H_3PO_4), reactor volume 404.2 cc.

TABLE 2

Equilibrium Constants, K_p, for the Reaction $C_3H_6 + HCl = i\text{-}C_3H_7Cl$

T, °C	K_p, atm^{-1}	Avg. value of K_p	T, °C	K_p, atm^{-1}	Avg. value of K_p
100	151.0	151.0		14.6	
				13.8	
120	57.0	58.8		6.5	
	60.5		160	13.5	
	25.4			14.3	12.6
140	27.4	25.8		13.8*	
	24.4			10.7	
180	6.1	5.9		13.5*	
	5.6			13.1	
				12.6	

As seen from Table 1, in all of the cases cited there was satisfactory agreement between α_p and α_c.

In order to show that the equilibrium studied is a true equilibrium and did not involve the existence of a kinetically limited phenomenon, it was necessary to approach the equilibrium from both the synthesis and the decomposition sides.

In Figure 1 are presented the kinetic curves of the synthesis (1) and the decomposition (2) of isopropyl chloride at 160° C, the coordinates being the pressure of the $i\text{-}C_3H_7Cl$ in the reaction mixture and time. For convenience in comparing Curves 1 and 2, the pressure is expressed in relative units based on the initial pressure of the $i\text{-}C_3H_7Cl$ in the decomposition reaction.

The initial pressure of the $i\text{-}C_3H_7Cl$ in the decomposition reaction was 200 mm Hg, while in the synthesis reaction the HCl and C_3H_6, taken in a 1:1 ratio, had a total pressure of 400 mm Hg. It is obvious that with the attainment of true thermodynamic equilibrium, in both cases the composition of the equilibrium mixtures must be the same. As seen from Figure 1, both curves reach equilibrium at the same composition of the $HCl - C_3H_6 - i\text{-}C_3H_7Cl$ mixture.

The equilibrium constants of the reactions, plotted as Curves 1 and 2 in Figure 1, were of nearly the same value, 13.1 and 13.5 atm^{-1}, respectively. In Table 2 are presented the experimentally obtained values of

$$K_p = \frac{P_{i\text{-}C_3H_7Cl}}{P_{HCl}\,P_{C_3H_6}}.$$

The data of Table 2 are plotted in Figure 2 as log K_p vs. 1/T. From the slope of the curve, the heat of the reaction is $\Delta H_R = -13800 \pm 300$ cal /mole. Knowing ΔH_R and K_p, it is possible to find the change in entropy for the reaction: $\Delta S_R = -27.0 \pm 0.7$ cal/mole/degree; where, for the equilibrium constant in the temperature range 100-180°C we obtain the equation:

$$2.3R \lg K_p = 13800/T - 27.0. \qquad (2)$$

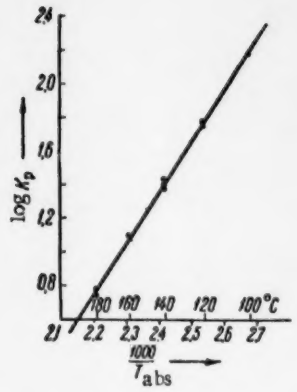

Fig. 2. Temperature dependence of the equilibrium constant K_p atm^{-1}, for the reaction C_3H_6 + + HCl = i-C_3H_7Cl.

As seen, the heat of reaction found by us agrees well with the value $\Delta H_{R_{298.2}} = -13816$ cal /mole calculated from the literature data; however, ΔS_R differs considerably from the calculated value $\Delta S_{R_{298.2}} = -36.02$ cal/mole/degree. The difference in temperature cannot explain the discrepancy of 9 entropy units in the value of ΔS_R. Although the values of c_p are unknown for the substances participating in the reaction of interest to us, the order of the change in entropy with temperature can be seen from the hydrochlorination of ethylene. The change in heat capacity during the reaction is

$$\Delta c_p = c_{p_{C_3H_6Cl}} - c_{p\ C_3H_6} - c_{p\ HCl} = \\ = -2.37 \text{ cal./mole} \cdot \text{degree}$$

(calculated from the data of [2]); whence from the well-known formula,

$$\Delta S_{R_T} = \Delta S_{R\ 298,2} - 2.3 \cdot 2.37 \cdot \log \frac{T}{298,2} .$$

As seen from the equation, a change in temperature from 298.2 to 453° K causes a change in ΔS_R of only 0.98 cal /mole/degree.

TABLE 3

Values of α_∞ for the Hydrochlorination of Propylene

	$T = 70°$ C, $K_p = 775$ atm^{-1}*				$T = 100°$ C, $K_p = 151$ atm^{-1}				$T = 120°$ C, $K_p = 50.5$ atm^{-1}			
p_0 мм	50	100	200	250	50	100	200	500	50	100	200	500
α_∞	0.88	0.94	0.93	0.94	0.63	0.80	0.84	0.90	0.61	0.70	0.77	0.84

For clarity, we present in Table 3 the values of the maximum depths of conversion $\alpha_\infty = \Delta p_\infty / p_0$, where Δp_∞ is the maximum change in pressure during the reaction in mm Hg, and p_0 is the initial partial pressure of one of the components in a 1:1 mixture in Hg. The values of α_∞ were calculated by the equation:

$$\alpha_\infty = \left(1 + \frac{A}{2}\right) - \sqrt{\left(1 + \frac{A}{2}\right)^2 - 1}, \text{ where } A = \frac{760}{K_p\, p_0} .$$

It is seen from Table 3 that reversibility begins to be substantial only at 120° C; at 100° C and, even more, at 70° C, the reversibility is small.

Institute of Chemical Physics
Academy of Sciences USSR

Received November 6, 1956

* The value of K_p at 70° C was calculated by Equation (2).

LITERATURE CITED

[1] E. J. Prosen, F. D. Rossini, J. Res. Bur. Stand., 36, 296 (1946).

[2] Select. Val. Chem., Thermodyn. Prop. Circ. Nat. Bur. Stand., 500 (1952).

[3] J. L. Franklin, Trans. Farad. Soc., 48, 443 (1952).

[4] J. Tomsen, Termochem. Untersuch., 4, 372.

[5] S. G. Entelis and N. M. Chirkov, J. Phys. Chem., 30, No. 11, (1956).

PROCEEDINGS OF THE ACADEMY OF SCIENCES OF THE USSR

Physical Chemistry Section

Volume 113, Issues 1-6

March-April, 1957

TABLE OF CONTENTS

TABLE OF CONTENTS (continued)